UNIVERSITÀ
DEGLI STUDI
DI PADOVA

Sede Amministrativa: Università degli Studi di Padova

Dipartimento di Scienze Chimiche

SCUOLA DI DOTTORATO DI RICERCA IN: SCIENZE MOLECOLARI

INDIRIZZO: SCIENZE CHIMICHE

CICLO XXV

Atmospheric plasma processes for environmental applications

Direttore della Scuola: Ch.mo Prof. Antonino Polimeno

Coordinatore di Indirizzo: Ch.mo Prof. Antonino Polimeno

Supervisore: Dr.ssa Ester Marotta

Dottorando: Volodymyr Shapoval

INDEX

SUMMARY

Plasma chemistry is a rapidly growing field which covers applications ranging from technological processing of materials, including biological tissues, to environmental remediation and energy production. The so called *atmospheric plasma*, produced by electric corona or dielectric barrier discharges in a gas and atmospheric pressure, is particularly attractive for the low costs and ease of operation and maintenance involved. The high concentrations of energetic and chemically active species (e.g. electrons, ions, atoms and radicals, excited states, photons) present in such plasmas can promote chemical reactions which are otherwise hardly possible under such mild temperature conditions. This thesis deals with the use of atmospheric plasma to activate two different processes: water purification from organic pollutants and carbon dioxide reforming of methane to produce syngas. Both address major environmental issues, specifically the ever growing demand for drinking water and the need to control carbon emissions in the atmosphere. Due to the very different nature of the two investigated processes, different plasma sources, types of discharge, reactors, experimental conditions and analytical procedures had to be developed and adopted. Despite such differences, however, both lines of research stem from a common background and share a common goal: to understand and exploit the great chemical potential of atmospheric plasma. Thus, a common research approach was used, based on extensive investigation of the discharge and plasma features, notably of its reactive species, and of the process efficiency, products and intermediates. The mechanistic investigations involved quantitative product and kinetic studies, spectroscopic determinations and some modeling.

An already available prototype reactor was used for water treatment, in which dielectric barrier discharges (DBD) are generated in the air above the liquid. The strong oxidants formed in humid air plasma (OH radicals, atomic oxygen, ozone) interact with the aqueous solution and induce the oxidation of even the most resistant organic pollutants. Phenol was used as a model organic pollutant and found to be decomposed quite efficiently, especially in dilute solutions, the rate of reaction increasing linearly with the reciprocal of phenol initial concentration. Despite its high reactivity air plasma displays some selectivity.

The rate of oxidation of monosubstituted phenols (m-$(CH_3)_2N$-, m-Cl-, p-NO_2- and m-NO_2-) depends linearly on the Hammett substituents constant yielding a ρ value of -0.48 which is characteristic of electrophilic attack by the OH radical. The main products and intermediates of phenol decomposition were determined quantitatively. The behavior of two such intermediates, maleic acid and fumaric acid, was investigated in detail since they are very common water secondary pollutants formed in the oxidative degradation of most aromatic compounds. The reaction mechanisms and the role of the major oxidizing species – hydroxyl radical and ozone – were investigated in experiments in which the two acids were treated separately and also in mixture under different pH conditions. Most interesting and useful was also the comparison with the results obtained in experiments of ozonation conducted under the same experimental conditions except for the fact that ozone was produced *ex situ*. These experiments show that under any conditions plasma treatment is more efficient due to the contribution of short lived highly reactive species. As for the oxidation mechanism of the two acids in the plasma system, it is concluded that due to their high reactivity with ozone, the decomposition process of maleic and fumaric acids is mainly due to this species. Depending on the pH of the solution, ozone reacts directly with the organic molecules or is converted to OH radicals. However, additional OH radicals produced directly by the electrical discharge also contribute to the oxidation of maleic and fumaric acids in the air-liquid plasma system, independently on the pH used. Thus, the direct formation of $^{\bullet}OH$ by the discharge *in situ* constitutes a big advantage of plasma treatment over reaction with ozone produced *ex-situ*, in particular at acidic pH values for compounds which do not react with ozone itself. In fact, contrary to ozone, OH radicals react efficiently with any organic compound and when directly produced by the discharge their concentration is independent on pH. The obtained results are also very useful to show the importance of ozone mass transfer from the gas phase to the solution. Both in plasma treatment and in ozonation ozone is not accumulated into the solution but reacts as it is transferred in water or directly on its surface. However, comparing the behavior of maleic and fumaric acids in plasma treatment and in ozonation, it was demonstrated that the ion wind present in the DBD reactor, due to the charged species formed by the discharge, plays an important role in mixing the solution. In fact, when ozone produced *ex-situ* is used magnetic stirring of the solution is required to allow the reaction to take place also in the bulk and not only on the

surface of water, while in the case of plasma treatment magnetic stirring increases the rate of the reaction but does not change significantly the shape of the oxidation curves.

The reactor and experimental apparatus for performing plasma driven carbon dioxide reforming of methane and product analysis had to be designed and developed from scratch since this line of research started with this Thesis. To allow emission spectroscopy measurements and in view of future investigations on the combination of plasma with heterogeneous catalysis, the reactor was made of quartz: two flanges are welded on the extremities of a tube of 570 mm of length and 37 mm of diameter, while a ring is welded in the middle of the tube to support a stainless steel tip which constitutes the high voltage electrode. The grounded counter electrode has the shape of a funnel and is covered by a stainless steel mesh. Most of the quartz tube is filled with ceramic cylinders, while the plasma zone occupies a volume of about 40 cm^3 in the middle of the tube for allowing its heating in a vertical furnace for future investigations with heterogeneous catalysts. The setting-up of the experimental apparatus was a major task which was followed by preliminary tests with different types of discharge for determining the most efficient regime for transformation of methane and carbon dioxide to the mixture of hydrogen and CO. The best results in terms of efficiency and product selectivity were obtained with a spark discharge, self-triggered by a simple and efficient power supplying. The average electron density of the plasma, 5.7 x 10^{14} cm^{-3}, was measured by emission spectroscopy techniques and the temperature of the bulk gas, approaching 100°C, by a thermocouple. However, the main characteristic of spark is the development of discharge filaments, in which the electron density and the temperature of the species, such as electrons, radicals, ions, but also atoms and molecules, are significantly higher than those of the bulk. In the present reactor these filaments fill completely the plasma zone. Thus, it is assumed that the elementary processes of the reaction between methane and carbon dioxide take place inside the discharge filaments. The major products, hydrogen and carbon monoxide were determined quantitatively by GC/FID/TCD. A few byproducts were also detected in low percentages and identified by means of GC/MS analysis. These include ethane, ethylene and acetylene. Based on quantitative product data and on precise measurements of the input and output flows, the reagents conversion, the products yield and selectivity and the energy efficiency of the process were calculated. The quite high conversion of CH_4 (74%) and CO_2 (69%), the high

selectivity for the desired products (78% H_2 and 86% CO) and the good energy efficiency (2.4 mmol/kJ) obtained make this system competitive with other reactors/processes described in the literature. Moreover, no carbon deposition was observed and CO_2/CH_4 ratios between 0.5 and 1.5 could be used without significant changes in the characteristics of the process. Easy power control and self-triggering of the system eliminate the need for expensive high-voltage switches, making this setup attractive for scaling up and further development.

RIASSUNTO

La chimica dei plasmi è un settore in rapida espansione che conta un gran numero di applicazioni, dal trattamento di materiali, inclusi materiali biologici, alla decomposizione di inquinanti e produzione di energia. Il cosiddetto *plasma atmosferico*, prodotto da scariche elettriche corona o a barriera di dielettrico in un gas a pressione atmosferica, è particolarmente attraente grazie ai costi contenuti e alla facilità di impiego e manutenzione. L'elevata concentrazione di specie ad alta energia chimicamente attive (ad esempio elettroni, ioni, atomi, radicali, specie eccitate, fotoni) presenti in questi plasmi può promuovere reazioni chimiche che in condizioni più blande sarebbero difficilmente realizzabili. La Tesi riguarda l'impiego del plasma atmosferico per attivare due diversi processi: la purificazione dell'acqua da inquinanti organici e il reforming di metano con anidride carbonica per produrre gas di sintesi. Entrambi i processi mirano a dare un contributo nella risoluzione di un problema ambientale, la crescente domanda di acqua potabile in un caso, la necessità di limitare le emissioni di carbonio nell'atmosfera nell'altro. A causa della natura molto diversa dei due processi indagati, essi richiedono lo sviluppo e l'impiego di sorgenti di plasma, tipi di scarica, reattori, condizioni e procedure sperimentali diversi. Tuttavia, nonostante queste differenze, entrambe le linee di ricerca derivano da conoscenze comuni e condividono lo stesso obiettivo: comprendere e sfruttare l'enorme potenziale chimico dei plasmi atmosferici. Anche nella ricerca è stato quindi applicato un approccio comune, basato su uno studio approfondito delle caratteristiche della scarica elettrica e del plasma, in particolare per quanto riguarda le specie reattive, dell'efficienza del processo e dei prodotti e degli intermedi che si formano nel processo. Gli studi meccanicistici sono basati sull'analisi quantitativa dei prodotti, sulla cinetica del processo, su misure spettroscopiche e su simulazioni.

Il reattore impiegato per il trattamento delle acque è un prototipo realizzato in precedenza, in cui vengono generate scariche a barriera di dielettrico (DBD) nell'aria sovrastante la soluzione. I potenti ossidanti formati nel plasma in aria umida (radicale OH, ossigeno atomico, ozono) interagiscono con la soluzione acquosa e inducono l'ossidazione anche dei più resistenti inquinanti organici. Il fenolo, usato come inquinante organico modello, viene decomposto efficacemente, soprattutto in soluzioni diluite. La sua velocità di scomparsa aumenta linearmente con il reciproco della sua concentrazione iniziale.

Nonostante l'elevata reattività, il plasma in aria mostra una certa selettività. La velocità di ossidazione di fenoli monosostituiti m-($(CH_3)_2N$-, m-Cl-, p-NO_2- and m-NO_2-) dipende linearmente dalle costanti di Hammett. Il valore di ρ ottenuto, pari a -0.48, è caratteristico dell'attacco elettrofilo da parte del radicale OH. I principali prodotti ed intermedi della decomposizione del fenolo sono stati determinati quantitativamente. Il comportamento di due di questi intermedi, l'acido maleico e l'acido fumarico, è stato analizzato in dettaglio poiché si tratta di comuni inquinanti secondari delle acque derivanti dalla degradazione ossidativa della maggior parte dei composti aromatici. Esperimenti in cui i due acidi sono stati trattati separatamente e in miscela a diversi pH hanno permesso di indagare i meccanismi di reazione e il ruolo delle principali specie ossidanti – radicale ossidrile e ozono – nella decomposizione dei due acidi. Molto interessante ed utile è stato anche il confronto con i risultati ottenuti in esperimenti di ozonizzazione realizzati nelle stesse condizioni sperimentali ma in cui l'ozono veniva prodotto *ex situ*. Questi esperimenti dimostrano che in tutte le condizioni sperimentali il trattamento al plasma è più efficiente del trattamento con solo ozono grazie al contributo aggiuntivo da parte di specie a vita breve altamente reattive. Per quanto riguarda il meccanismo di ossidazione dei due acidi nel plasma, è stato concluso che a causa dell'elevata reattività con ozono, il processo di decomposizione degli acidi maleico e fumarico è dovuto principalmente a questa specie. A seconda del pH della soluzione, l'ozono reagisce con le molecole organiche come tale oppure viene convertito in radicali OH. Nel sistema al plasma, radicali OH vengono prodotti anche direttamente dalla scarica elettrica e contribuiscono anch'essi all'ossidazione degli acidi maleico e fumarico, indipendentemente dal pH della soluzione. E' quindi evidente che la formazione diretta di $^{\bullet}$OH *in situ* da parte della scarica costituisce un enorme vantaggio del trattamento al plasma rispetto al caso in cui l'ozono venga prodotto *ex-situ*, in particolare nel caso di composti che a pH acidi non siano in grado di reagire direttamente con l'ozono. Infatti, contrariamente all'ozono, il radicale OH reagisce in modo efficiente con qualsiasi composto organico, inoltre, quando viene prodotto direttamente dalla scarica la sua concentrazione è indipendente dal pH. I risultati ottenuti si sono rivelati molto utili anche per dimostrare l'importanza del trasferimento di massa dell'ozono dalla fase gas alla soluzione. Sia nel trattamento al plasma che nell'ozonizzazione l'ozono non si accumula nella soluzione ma reagisce non appena viene trasferito in acqua o direttamente sulla superficie dell'acqua. Comunque,

confrontando il comportamento degli acidi maleico e fumarico nel trattamento al plasma e nell'ozonizzazione, è stato dimostrato che il vento ionico attivo nel reattore DBD e dovuto al trasferimento di specie cariche generate dalla scarica, svolge un ruolo importante nel mescolamento della soluzione. Infatti, quando l'ozono viene prodotto *ex-situ* è necessario agitare la soluzione con un'ancoretta magnetica perché la reazione abbia luogo nell'intera massa di acqua e non solo sulla sua superficie; al contrario, nel caso del trattamento al plasma il mescolamento magnetico aumenta la velocità della reazione ma non cambia significativamente la forma dell'andamento dell'ossidazione in funzione del tempo.

Nel caso del processo di reforming di metano con CO_2 attivato da plasma è stato necessario progettare e sviluppare il reattore e l'intero sistema sperimentale da zero poiché questa linea di ricerca è stata iniziata con questa Tesi. Per poter realizzare misure di spettroscopia di emissione e in vista di studi futuri sulla combinazione del plasma con la catalisi eterogenea, il reattore è stato realizzato in quarzo: due flange sono saldate alle estremità di un tubo lungo 570 mm e largo 37 mm (diametro interno), mentre un anello è saldato nel mezzo del tubo per supportare una punta di acciaio inossidabile che costituisce l'elettrodo ad alto voltaggio. Il controelettrodo, posto al potenziale di terra, ha la forma di un imbuto ed è ricoperto da una retina di acciaio. Il tubo è in buona parte riempito con cilindri di ceramica forati, mentre la zona del plasma occupa un volume di circa 40 cm^3 nel mezzo del tubo, soluzione che ne permetterebbe il riscaldamento in una fornace verticale in eventuali studi futuri con catalizzatori eterogenei. La realizzazione dell'apparato sperimentale ha richiesto un grosso impegno. Il passo successivo è stato l'esecuzione di esperimenti di prova con diversi tipi di scarica per determinare il regime più efficiente per realizzare la trasformazione di metano e anidride carbonica in una miscela di idrogeno e monossido di carbonio. I risultati migliori in termini di efficienza e selettività dei prodotti sono stati ottenuti con una scarica di tipo spark, auto-innescante grazie ad un sistema di alimentazione elettrica semplice ed efficiente. La densità elettronica media del plasma, pari a 5.7×10^{14} cm^{-3}, è stata misurata tramite tecniche di spettroscopia di emissione e la temperatura del gas, poco inferiore a 100°C, tramite una termocoppia. La caratteristica principale della scarica di tipo spark è lo sviluppo di canali filamentari di scarica, in cui la densità degli elettroni e la temperatura delle specie, vale a dire elettroni, radicali, ioni, ma anche atomi e molecole, sono significativamente maggiori di quelle della massa del gas. Nel

reattore in questione questi canali filamentari di scarica occupano interamente la regione in cui si sviluppa il plasma. Di conseguenza, si può assumere che i processi elementari della reazione tra metano e anidride carbonica si verifichino all'interno di tali canali. I prodotti principali della reazione, idrogeno e monossido di carbonio, sono stati determinati quantitativamente tramite GC/FID/TCD. Alcuni sottoprodotti sono stati rivelati in basse percentuali e identificati tramite analisi GC/MS: si tratta di etano, etilene ed acetilene. Sulla base dei dati quantitativi relativi alla formazione dei prodotti e delle misure precise dei flussi di entrata ed uscita del gas nel e dal reattore, sono state calcolate le percentuali di conversione dei reagenti e di resa e selettività dei prodotti. I risultati di conversione di CH_4 (74%) e CO_2 (69%), di selettività per i prodotti desiderati (78% H_2 and 86% CO) e di efficienza energetica sono risultati molto buoni e rendono il sistema competitivo con altri reattori e processi descritti nella letteratura. Non viene inoltre osservata deposizione di carbone e il rapporto CO_2/CH_4 può essere variato tra 0.5 e 1.5 senza variazioni significative delle caratteristiche del processo. La facilità di controllo della potenza e la caratteristica di auto-innesco del sistema fanno sì che non siano necessari costosi sistemi di controllo che lavorano ad alto voltaggio e rendono promettente il ridimensionamento dell'apparato sperimentale e interessante il suo impiego in ricerche future.

1. INTRODUCTION

Today the world community is strongly concerned with the state of the environment. Its global deterioration negatively influences human health, human security and prospects of sustainable economic development.

The Thesis deals with the study of two processes of environmental interest driven by plasma: water purification and carbon dioxide reforming of methane.

The first part of this chapter gives a brief account on water pollution. The removal of hazardous organic pollutants from groundwater and wastewater is one of the most critical and urgent topics in environmental research. Since many of these pollutants are biologically resistant, the application of common water treatment methods is often not sufficient. Great attention is focused on so-called advanced oxidation processes (AOPs) that are based on generation of highly reactive species such as ozone, hydrogen peroxide and hydroxyl radicals, which are capable of oxidizing almost any organic compound in solution [1].

The second part of the chapter deals with carbon dioxide reforming of methane, also called methane dry reforming (MDR), to produce synthesis gas, the mixture of CO and hydrogen. This reaction is very interesting due to the possibility to achieve a desirable product in the utilization of the two major greenhouse gases or of a natural gas feedstock containing CO_2. MDR reaction allows obtaining a lower H_2/CO ratio compared to other reforming processes like steam reforming or partial oxidation of methane. The lower H_2/CO ratio is desirable for further synthesis of methanol or hydrocarbons in the Fischer-Tropsch process. However, MDR reaction is extremely endothermic (standard enthalpy is 247 kJ/mol) and requires high temperatures and heterogenous catalysis. This leads to strong energetic requirements and possible carbon deposition which deactivates the catalyst. In the case of plasma driven MDR the plasma provides the energy to activate the extremely endothermic reaction allowing to perform this process at near room temperature without necessity of a catalyst.

In paragraph 1.3 an introduction on plasma is provided leading to a more detailed description of the types of electrical discharges used in the Thesis, notably corona and dielectric barrier discharges to produce non-thermal plasma (NTP) in air at room temperature and atmospheric pressure for water decontamination and spark discharges to perform the carbon dioxide reforming of methane. The elementary reactions taking place in air plasma and in the MDR process are described. Finally, a brief account is given on the state-of-the art of organic pollutant NTP processing in air and in aqueous solution and of plasma driven dry reforming techniques with particular focus on MDR.

1.4 Water pollution

Water is vital for the survival of our planet and the proper management of water resources is a major challenge in the new millennium. The steady growth of world population, together with a development model primarily focused on profit with scarce attention to the proper use and management of resources of the planet, has already led to dramatic consequences. About 1 billion people currently cannot rely on a continuous supply of potable water and, with the increasing world population it is expected that within 2025 this number could go up to 3.5 billion [2-7].

In March 2007 the first European Water Conference was held at the European Parliament in Brussels. On March 22 of each year the world celebrates World Water Day, proclaimed for the first time in 1993 by United Nations General Assembly. The main issue of that conference was scarcity of water in the world and the importance of a cooperative approach in the management of water resources, both at the international and local levels. In fact, the amount of water actually used for human use is really negligible and equal to about 0.01% of the total water supplies on Earth. Like other resources, distribution of water on the planet is unequal and only human activity driven by principles of economic solidarity and intelligent technology can promote equitable access of populations to the resource. The growth in industry and agriculture which has taken place with economic development led to the over-exploitation of water resources. Alongside civil activities which exploit 10% of all available water, agricultural and industrial activities use more substantial amounts of the resource, 70% and 20% respectively.

In this context, the development of new technologies for water decontamination polluted by agricultural and industrial applications is a fundamental part of an integrated approach that will lead to greater availability of water for all [2-7].

Water contamination may be due to natural or anthropogenic causes. Among the natural causes are the activity of volcanoes, fires and decomposition of biomass. The sources of anthropogenic pollution are distinguished in point and diffuse sources. Examples of point sources are: factories, discharge of waste water, mines and oil wells. Among the diffuse sources we mention the deposition from acid rains, traffic and agriculture.

1.1.1 Organic pollutants of water

Organic compounds, which are among the most dangerous pollutants, derive from anthropogenic sources such as agriculture (widespread use of pesticides, herbicides and insecticides), incinerators, landfills and industry. In addition to surface water (rivers, lakes), pollution also affects groundwater. In particular, among the most common organic contaminants in water, listed below, the first three classes also exist in groundwater [8]:

- Chlorinated solvents, in particular trichloroethylene ($HClC=CCl_2$), perchloroethylene ($Cl_2C=CCl_2$), chloroform ($CHCl_3$);
- Aromatic hydrocarbons coming from petrol (benzene, toluene, xylenes) and other petroleum products;
- Methyl-terbutyl ether (MTBE) from petrol;
- Polycyclic aromatic hydrocarbons (benzo-[a]-pyrene, dibenzoanthracene, etc.) from soot, coal and from incomplete combustion of hydrocarbons;
- Fertilizers and pesticides (DDT, Chepone, Lindane, etc.);
- Compounds belonging to different chemical classes used as solvents or precursors in synthetic processes (benzene, nitrobenzene, phenol, p-dichlorobenzene, o-diaminobenzene, acrylonitrile, vinylchloride, urethane), dyes, explosives (TNT, picric acid, nitroaniline).

A very dangerous characteristic for some classes of compounds widely used in the past (PCBs, PBBs, DDTs and others) is persistence due to their low reactivity.

Among the various organic pollutants of water phenol occupies a prominent place. It is a compound used in many industrial processes as an intermediate or feedstock in the production of pesticides, insecticides, wood preservatives, glues, tar, drugs, cosmetics, dyes and polymers. An example of phenol-based polymer is bakelite obtained by reaction of phenol with formaldehyde. For its antiseptic property phenol is used also as a disinfectant.

Given the great variety and use of its derivatives, phenol is not only present in industrial effluents, but also in soil and surface and ground water.

Phenol is toxic by ingestion, inhalation and skin contact, causing digestive disorders, nervous system disorders, headaches, fatigue, and rashes on the skin. Also causes burns if it comes into contact with the throat. The ingestion of 1 gram of phenol is lethal to humans. In water has a negative effect already at ppb concentrations. In concentrations between 0.01 and 0.1 ppb gives a bad smell and taste to water. It is toxic to some aquatic life in concentrations above 50 ppb. It also has a high demand for oxygen, 2.4 mg O_2/mg.

Another serious effect of phenol in water is the ability to combine with chlorine used to disinfect drinking water producing chlorophenols that are compounds even more toxic and difficult to remove than phenol itself.

1.1.2 Technologies for the removal of organic pollutants from water

There are numerous techniques for the removal of organic pollutants from waste water. The methods are divided into destructive (pointing to the elimination of the pollutant) or non-destructive (favoring the pollutant recovery). The destructive methods are often adopted with high concentrations of pollutants, while for low concentrations methods of recovery are usually applied. All methods require pre-treatments such as coarse/fine screening, grit removal, flocculation, sedimentation.

The most important methods for water purification are the following:

- **Incineration**: useful for small volumes of wastewater with high concentrations of pollutants, it requires substantial investment and energy costs. Another problem is that

the combustion of organic waste may generate highly toxic compounds such as dioxins and furans. Therefore, a final combustion chamber for treatment of the exhaust gases must be present before they are released into the atmosphere.

- **Air Stripping**: it involves the transfer of volatile organic compounds from liquid to gas phase through injection of air. Typical methods use spray atomizers. Alternatively, wastewater is passed through porous materials upstream with respect to the air flow.

- **Absorption on Activated Carbon**, a separation technology in which the contaminant is absorbed from the aqueous phase on activated carbon by pumping pressurized water to be treated into the column containing the adsorbent material. Activated charcoal is carbon treated to substantially increase the specific surface area up to 500-1500 m^2/g. The pollutants retained by the adsorbent material are then extracted or destructed by oxidation. This will regenerate the adsorbent. The efficiency of the absorption depends on concentration, polarity and molecular weight of the pollutant, and temperature.

- **Chemical Oxidation** is a very effective method for removing organic pollutants, which can meet the strict legal limits on emissions. It can also be an excellent preparation for the next stage of biological oxidation. However, it is convenient only for small concentrations of pollutants and low COD (Chemical Oxygen Demand), otherwise the amount of oxidizer to be used becomes high with the consequent increase in the cost of disposal.

- **Electrochemical Oxidation**: it is not widely used because of the high operating costs. The conductivity of the solution to be treated has to be sufficiently high, otherwise salts must be added. The process involves three stages: electro-coagulation, electro-flotation, and electro-oxidation.

- **Biological Oxidation**: it usually takes place through the use of activated sludge. It is applicable only to limited ranges of pollutant concentration (for example, for phenol only up to a maximum concentration of 100 mg/L). It also requires careful adjustment of parameters such as pH, temperature, humidity. It can be implemented under aerobic or anaerobic conditions, the first being generally more effective.

- **Photochemical Oxidation**: it consists in irradiation of water with UV light beams. Hydroxyl radicals are thus formed by photolysis of water. UV low pressure mercury

lamps were used in the past. However production of UV light is very expensive; absorption occurs only in specific wavelengths, and its interaction with other molecules present in the reaction medium generates many intermediates that slow down the process.

- **Plasma treatment**; one of the most promising novel AOPs (Advanced Oxidation Process) and one of the objects of this thesis. The plasma can be generated above or within the wastewater.

1.2 Greenhouse gases

Carbon dioxide and methane are the two major greenhouse gases, with CO_2 being generally perceived as the more worrisome of the two because it is released in much larger amounts. However, increasing attention is dedicated also to the uncontrolled release of methane in the atmosphere due to its high global warming potential. Methane is the main component of natural gas and its presence in the atmosphere is due to different sources ranging from the oil wells to agriculture. Once into the atmosphere, the main sink of methane is due to its oxidation by OH radical, which determines an atmospheric lifetime for this compound of about 10 years [9, 10].

Annually about 6.3 Gt of carbon, equivalent to 23 Gt of carbon dioxide, are released into the atmosphere from the combustion of fossil fuels. Unlike other polluting gases, such as methane, carbon dioxide is not decomposed photochemically or chemically in the atmosphere. The natural mechanisms which could eliminate this gas from the air are photosynthesis in plants (a *temporary sink* since the plant death and decomposition will return most carbon to the atmosphere) and absorption by ocean waters and soil. However, these mechanisms are not able to efficiently balance the processes, like combustion, which release this gas. Indeed, CO_2 concentration in atmosphere increased from near 280 ppm in the beginning of the XIX century to more than 380 ppm nowadays [11].

In the next paragraph the major available methods for limiting CO_2 emissions are briefly described.

1.2.1 Strategies for limiting CO_2 emissions

In addition to the implementation of much needed policies to save energy and develop technologies based on renewable energy sources and on hydrogen, different strategies are being pursued to contain CO_2 emissions in the atmosphere. The first consists in the exploitation of the natural mechanisms for CO_2 removal by way of different approaches including afforestation, reforestation, agricultural practices to increase CO_2 fixation in soil and ocean fertilization. Such measures must be flanked by other means since by themselves they cannot possibly succeed in containing the load of atmospheric carbon.

An alternative strategy consists in capturing and sequestering carbon dioxide in appropriate storage areas (paragraph 1.2.1.1).

Finally, the most attractive solution, but also a great challenge due to the high thermodynamic stability of carbon dioxide, is conversion of CO_2 into useful materials. This can be obtained through biological processes, in which CO_2 is converted into biomass by means of photosynthetic processes which promote the growth of rapidly growing algae within especially biophotoreactors. The biomass is then gasified to produce hydrogen or fermented to produce alcohol. Alternatively the conversion of CO_2 can be obtained through chemical processes (paragraph 1.2.1.2).

1.2.1.1 CO_2 capturing and sequestration

This strategy is named Carbon Capture and Storage (CCS) and involves the capture of carbon dioxide contained in the exhaust gas of power plants, refineries and industrial plants and its subsequent sequestration in a way which prevents its release into the atmosphere. Two types of sequestrations are used: geological sequestration and mineral sequestration. Storage areas considered for geological sequestration are the oceans, saline aquifers, oil fields and natural gas and coal reservoirs. Since several decades in the United States and in other parts of the world CO_2 is pumped into oilfields to enhance the oil recovery. The carbon dioxide introduced keeps the reservoir under pressure to help the oil spill. Moreover, it acts as a solvent which washes the rock favoring the separation of the oil. Exhausted oilfields are also used to confine carbon dioxide. The gas introduced into the

reservoir fills the available space in the porous rocks that had previously hosted the fossil fuels. The escape of carbon dioxide is prevented by impermeable layers that limit the field and had previously confined fossil fuels for millions of years. It is estimated that the storage capacity of depleted oil and natural gas fields is near 920 GT of CO_2.

In *mineral sequestration* CO_2 is converted into stable carbonates by way of reactions like the following ones:

$$½\ Mg_2SiO_4 + CO_2 \rightarrow MgCO_3 + ½\ SiO_2 + 95\ kJ/mol$$

$$⅓\ Mg_3Si_2O_5(OH)_4 + CO_2 \rightarrow MgCO_3 + ⅔\ SiO_2 + ⅔\ H_2O + 64\ kJ/mol$$

which can be performed within natural sites (mines) or in special reactors. Contrary to geological sequestration, mineral sequestration does not involve either the risk of undesired abrupt releases of CO_2 or any impact on the environment. The problem is that these reactions, although thermodynamically favored are kinetically very slow so that costly pretreatments of the minerals are required.

Before sequestration, carbon dioxide must be “captured”. Usually carbon dioxide is present in the fume emissions by thermoelectric power plants or industrial settlements diluted in air, so it has to be separated and concentrated (post-combustion capture). This is usually achieved by flowing the exhaust gas through a filter in contact with an amine which reacts with CO_2 to trap it as a dialkylcarbamate

$$R_2NH + CO_2 \rightarrow R_2NCO_2^- + H^+$$

The reaction is reversible, so it is possible to free all the captured carbon dioxide and generate a concentrated stream of CO_2 to be channeled into the storage site. The drawback of this method is that it is quite expensive.

An alternative to post-combustion capture is the process of pre-combustion capture, which consists in the removal of CO_2 prior to combustion and is addressed to the production of hydrogen. The capture process consists of three stages: firstly the hydrocarbon fuel (typically methane, or gasified coal) is converted into synthesis gas. The fuel can be coal, which is converted by gasification, or natural gas and light hydrocarbons, which can be converted via steam reforming.

Gasification:

$C + H_2O \rightarrow CO + H_2$

Steam reforming (in the presence of a catalyst):

$C_nH_m + nH_2O \rightarrow (m/2 + n)H_2 + nCO$

The second step consists in the conversion of CO into CO_2 by the water gas shift reaction (in the presence of a catalyst):

$CO + H_2O \rightarrow CO_2 + H_2$

Finally, the CO_2 is separated from the hydrogen which can then be combusted cleanly. On the contrary, CO_2 can be compressed into liquid and transported to a storage site [12].

Another approach consists in heating biomass without oxygen, thus performing a low-temperature pyrolysis [13], which allows converting the carbon into biochar, which can be stored in soils. There biochar is stable for hundreds or thousands of years, thus it could be considered as a long term sink of carbon.

All of the main methods of capturing CO_2, being very complex and expensive, are feasible only in the case of large centralized plants, while are not usable to separate carbon dioxide from vehicle exhaust or from domestic heating systems. Up to now, there are no valid alternative methods to be applied in these cases. The only possibility is to use centralized plants equipped with CO_2 capture systems for producing hydrogen from fossil fuels and using it as fuel in vehicles and in heating systems. This solution would keep the production of carbon dioxide limited to large systems in which the capture methods can be used.

1.2.1.2 Chemical conversion of CO_2

An alternative to CO_2 sequestration is given by the possibility to chemically convert it. The major obstacle to this solution is the high thermodynamic stability of the CO_2 molecule, but the research on this topic is very active and many promising approaches are nowadays proposed.

One of the most important processes investigated is the chemical reduction of CO_2 to fuels. This would offer not only a way of recycling carbon dioxide, but also a means to increase the sustainability of oil reserves for other purposes. Chemical reduction of CO_2 can be achieved by electrocatalysis, photocatalysis and thermocatalysis. These approaches have also been combined with biochemical techniques to utilize enzymes or mimic their active sites [14]. For example, Grimes et al proposed a process to convert the captured CO_2 into methane [15] using a photocatalyst constituted by arrays of nitrogen-doped titania nanotubes sputter-coated with an ultrathin layer of platinum and/or copper as co-catalyst. The titania captures high energy ultraviolet wavelengths, while the copper shifts the bandgap into the visible wavelengths to better utilize the part of the solar spectrum where most of the energy lies. In addition, the thin-walled nanotubes increase the transport ability of the charge carriers by reducing the chance for recombination of the electron with the hole.

GoNano Technologies, Inc's Carbon Capture & Recycle allows through a photocatalytic process selectively convert CO_2 into useful and valuable feedstock chemicals like formic acid, formaldehyde, and/or methanol [16].

Another approach consists in the reaction of CO_2 with compounds with a relatively high free energy, thus providing a thermodynamically favourable process. Among the reactions employing this strategy, there is the addition of carbon dioxide to epoxides, a process which can generate useful classes of compounds as cyclic carbonates and polycarbonates. The catalysts more are applied in this case are metal complexes [17-19].

1.2.2 Methane reforming and partial oxidation

Methane is the main component of natural gas. Remarkably, while oil reservoirs are extensively used to produce increasing quantities of fuels, natural gas was not similarly exploited for a long time as it is found in locations far from consumption sites and its transportation is expensive (as a gas) and hazardous (as a liquid or compressed gas) [20]. Only in the last decades, as a consequence of the increasing energy demand, decreasing oil resources and consequent increasing oil price, natural gas valorization has become a major target.

The best solution for exploiting natural gas as an energy source is to convert it to something safer, easier and cheaper to transport, such as methanol or syngas. Syngas, or synthesis gas, is a mixture of H_2 and CO which serves as a most useful feedstock in chemical industry. In fact it can be catalytically converted into hydrocarbons, through the Fischer-Tropsch process ($nCO + 2nH_2 \rightarrow (CH_2)n$), or into valuable oxygenated compounds, such as methanol ($CO + 2H_2 \rightarrow CH_3OH$) [21].

The process generally used to produce syngas from methane is steam reforming (MSR)

$$CH_4 + H_2O \rightarrow CO + 3H_2 + 206\ kJ/mol$$

However, as the syngas obtained by steam reforming has a H_2/CO ratio too high to be directly employed in subsequent synthetic processes,. steam reforming is generally coupled with water gas shift (WGS) reaction

$$CO + H_2O \rightarrow CO_2 + H_2 - 41\ kJ/mol$$

to achieve a 2:1 H_2/CO mixture or to produce hydrogen [21] which can be used in fuel cells. While the MSR reaction is strongly endothermic, the WGS reaction is mildly exothermic. [22].

Thus, at the end of the process, CO_2 is formed as a byproduct which has to be eliminated, either via sequestration and storage or via other processes. Although natural gas is a “cleaner” energy source with respect to higher hydrocarbons, since its combustion produces less carbon dioxide per unit of energy released, it contributes significantly to global

carbon emission due to its extensive use and applications. Furthermore to improve the heating value of the gas and to meet pipeline specifications the percentage of CO_2 present as a common impurity in natural gas must be removed [23].

Another possibility to convert methane into synthesis gas is partial oxidation (MPO):

$CH_4 + 1/2O_2 \rightarrow CO + 2H_2 – 36$ kJ/mol

This process is mildly exothermic, has a greater selectivity to syngas than MSR and gives a more desirable H_2/CO ratio with respect to it. However, it needs high temperatures and pressures to be performed or the use of a catalyst. Moreover, the process is difficult to control due to the competition with the complete oxidation of methane and hazardous for the risk of concentrating large amounts of heat in a small zone of the catalyst [24].

Finally, methane can be subjected to thermocatalytic decomposition (TCD). In this process it is directly converted to hydrogen and solid carbon

$CH_4 \rightarrow C + 2H_2 + 75.6$ kJ/mol

The carbon produced can be completely isolated and used as filler or construction material. However, this reaction requires high temperature, near 1200 °C, without catalyst. Different sources of heat could be used: microwave plasma, molten-metal bath of concentrated solar energy [25].

1.2.3 Dry reforming of methane

Dry reforming of methane,

$CH_4 + CO_2 \rightarrow 2CO + 2H_2$,

is the solution which would allow the use of natural gas without any release of CO_2 but on the contrary recycling CO_2 in a useful process . Additional advantages of this process are the production of a syngas with a lower H_2/CO ratio with respect to steam reforming, therefore more suitable for the following synthetic processes, and the possibility to use biogas as the starting material as its main components are just CH_4 and CO_2. Unfortunately,

dry reforming is a highly endothermic reaction (247 kJ/mol) which requires activation by heterogeneous catalysis and is favored by low pressure and high temperature. Three main processes can occur as side reactions, reverse water-gas shift ($CO_2 + H_2 \rightarrow H_2O + CO$), the Boudouard reaction ($2CO \rightarrow CO_2 + C$) and methane cracking ($CH_4 \rightarrow C + 2H_2$). The last two reactions are responsible for carbon deposition which can theoretically be prevented by operating at very high temperatures but which in practice is the main reason for the lack of any established industrial application of CO_2 reforming of CH_4 [26]. This is however a target of today's scientific research, which is very active in exploiting methane dry reforming by developing new catalysts and new methods for the catalysts preparation [27] and/or new experimental devices, such as, for example, membrane reactors [28] or plasma reactors based on both thermal and non-thermal plasma [29].

The catalysts which show high activity and stability in dry reforming are nickel-based and noble metal-supported catalysts (Rh, Ru, Pd, Pt, Ir). Nickel-based ones are generally considered the most convenient from an industrial point of view because of their lower cost and higher availability as compared to noble metals. However, they are more sensitive to carbon deposition, which blocks pores and active sites, leading to catalyst deactivation [26, 27, 30]. Moreover, since nickel is a toxic metal its replacement would be highly desirable. This aspect is highly considered in EU, while in the USA, due to its low cost, the use of nickel is still widespread: therefore the development of nickel-based catalysts is currently the object of many scientific investigations. In particular, different preparation methods, supports and pretreatments, addition of promoters and doping with small amounts of noble metals are tested to affect, not only the activity and stability of the catalyst, but also, and with particular attention, carbon formation [27, 31 - 35]. On the other hand, noble metal-based supported catalysts are highly active and less prone to carbon deposition, but their applicability is limited by high costs and low availability. However, convenient supports and preparation methods favor metal dispersion and prevent sinterization allowing using very small quantity of the metal [36, 38].

1.3. Plasma: definition and generation

Plasma is an ionized gas, which means that at least one electron is not bounded to an atom or molecule and the atoms or molecules are present as positively charged ions. With increasing the temperature, matter transforms in the sequence: solid, liquid, gas and finally plasma, so the expression “fourth state of matter” is justified. The majority of the universe, solar corona, solar wind, nebula, and Earth’s ionosphere – are all plasmas. The best known natural plasma phenomenon is lightning.

The term *plasma* was first introduced by Irving Langmuir (1928). Langmuir wrote: “Except near the electrodes, where there are sheaths containing very few electrons, the ionized gas contains ions and electrons in about equal numbers so that the resultant space charge is very small. We shall use the name *plasma* to describe this region containing balanced charges of ions and electrons” [39].

The plasma can be efficiently produced in laboratory and in industry through the application of electrical discharges which are widely used in practice. Plasma offers three major features that are attractive for applications in chemistry and related disciplines [40]:

1. Temperature of at least some plasma components and energy density can significantly exceed those in conventional chemical processes.
2. Plasmas are able to produce very high concentrations of energetic and chemically active species (e.g. electrons, ions, atoms and radicals, excited states, and different wavelength photons).
3. Plasma systems can be far from thermodynamic equilibrium: the high concentrations of the active species are present in plasma region while the bulk temperature of system remains at near-room value.

These plasma features favors traditional chemical processes increasing their efficiency, and often are successful stimulation of chemical reactions which are hardly realizable in conventional chemistry.

Plasma chemistry is a rapidly expanding area of science and engineering. Its applications covers micro-fabrication in electronics, protective coatings for aircrafts,

polymers surface modification and functionalization, medical cauterization and wound treatment, ozone production, plasma TVs, etc.

Most plasmas of practical significance have the electron temperatures of 1-20 eV, with electron densities in the range 10^6–10^{18} cm^{-3} [40] (1 eV approximately equals 11600 K.)

The plasma is quasi-neutral, which means that the concentrations of positively charged particles (positive ions) and negatively charged particles (electrons and negative ions) are well balanced. A first parameter which characterizes the plasma is the ionization degree, i.e. the ratio of density of charged species over that of neutrals. If this parameter approaches to unity, such plasma is called completely ionized. Completely ionized plasma studies are presented by thermonuclear fusion systems [41, 42]. In case the ionization degree is low such plasma is called weakly ionized. The ionization degree in the plasma of conventional plasma–chemical systems lies in the range of 10^{-7}–10^{-4} [40].

The plasma is a multi-component system, that's why each component (neutral or charged) has its own average energy and relevant degree of freedom (translational, rotational, vibrational, and those related to electronic excitation). In another words, the plasma is characterized by a multiple temperatures. In case the electric discharge is used to generate the plasma, the energy from the electric field is first acquired by the electrons between collisions (on the mean free path) and then is transferred from the electrons to the heavy component. Due to the fact that the electrons are much lighter than the heavy particles, the electron energy loss in collisions is small. That's why the electron temperature is higher than that of heavy components. Finally, collisions of electrons with heavy particles (Joule heating) can equilibrate their temperatures. If time or energy are not sufficient for the equilibration (like in coronas and pulsed discharges) or an intensive cooling mechanism of the entire gas is present (like in wall-cooled low-pressure discharges), such plasma remains far from the thermal equilibrium.

The temperature difference between electrons and heavy neutral particles due to Joule heating in the collisional weakly ionized plasma is proportional to the square of the ratio of the electric field (E) to the pressure (p). This means that in the case of small values of E/p the temperatures of electrons and heavy particles approaches each other which is a basic requirement for so called *Local Thermodynamic Equilibrium* (LTE). Additionally, LTE

condition requires chemical equilibrium as well as restrictions on the gradients. LTE allows to apply the major laws of equilibrium thermodynamics and plasma can be characterized by a single temperature in the volume. Ionization and chemical processes in such plasmas are determined by temperature. The quasi-equilibrium plasma of this kind is usually called thermal plasma and is presented in nature by the plasma of the stars. [40].

If plasma is produced by the application of an electric field the breakdown voltage (or ignition voltage) depends on the type and pressure of the gas and on the distance between the electrodes (gap). This was first investigated in 1889 by F. Paschen [43]. He investigated the minimum potential necessary to create a spark between two electrodes. The dependence of the breakdown voltage on the pressure and the distance between the electrodes is known as Paschen's curve. This dependence is usually represented by a nonlinear function V= f(pd), where p is the pressure and d is the gap distance. As the pressure is reduced below several torr·cm (Fig. 1.3.1.) the curve of breakdown voltage versus pressure times gap distance reaches a minimum, and then, as pressure times gap distance is further reduced, rises again.

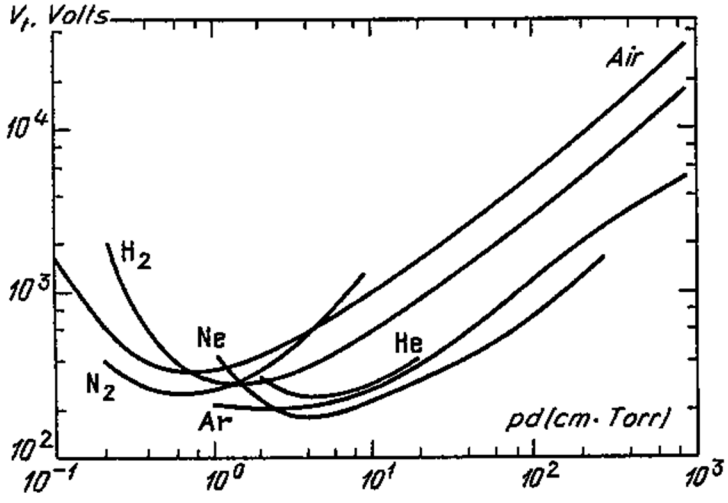

Fig. 1.3.1. The Paschen's curves for different gases [44].

First this behaviour was not well understood, but later Townsend proposed a theory that explained this phenomenon. The Townsend theory is based on the description of the

microscopic processes taking place in a gas, which include electron acceleration in the electric field, electron impact ionization of neutral gas molecules producing electron avalanches, secondary electron emission at the cathode due to its bombardment by the positively charged ions. This theory allowed to analytically describe the dependence of the breakdown voltage on p and d (Paschen's law):

$$V = f(pd) = \frac{Bpd}{C + \ln(pd)}$$

where the constants B and C mainly depends on the type of gas.

1.3.1. Atmospheric plasma

The plasma developed at atmospheric (or normal) pressure is called atmospheric pressure (AP) plasma or simply atmospheric plasma. The pressure of about 760 torr is considered high compared to the pressure at which the minimum of the Paschen's curve is generally reached (at the same distance between the electrodes). At atmospheric pressure the working point of the discharge is situated in the far right part of the Paschen's curve and thus the breakdown voltage is much higher than that at the Paschen's minimum. This could be explained by the fact that when the product between the pressure and the gap is high the electrons will collide with many gas molecules during their movement from the cathode to the anode. Collisions reduce the electrons energy and under such conditions the electron impact ionization becomes more difficult. To compensate for the energy losses due to the greater number of collisions and higher voltage (acceleration field) is required so the avalanche breakdown becomes possible.

The Townsend theory describes well the low pressure plasma, while at high pressures significant deviations from the Townsend theory occur. An example is given by the fact that at high pressures and long distances between the electrodes the breakdown develops much faster than it is predicted by the Townsend theory. In this case the mechanism described by the streamer theory has to be considered. As it will be explained in

the following paragraphs, this theory takes into account the development of narrow ionized channels.

Atmospheric plasma is very attractive for applications because it does not need vacuum systems and the related costly equipment. It can be generated in open air and with large gaps. Its applications include for example activation of chemical processes, ozone production, water and gas purification, surface modification and functionalization.

Atmospheric plasma can be produced by different types of electrical discharges which give rise to plasma with different features, as is described in the next paragraphs.

1.3.2. Non-thermalizing electrical discharges

The application of non-thermalizing discharges produces plasmas very far from the thermodynamic equilibrium, characterized by multiple different temperatures related to different plasma particles and to their different degrees of freedom. Typically, the electron temperature significantly exceeds that of heavy particles ($T_e >> T_0$) and is that which directly determines ionization and chemical processes in such systems, which, therefore, are not so sensitive to thermal processes and to the temperature of the gas. The non-equilibrium plasma of this kind are usually called non-thermal plasma. An example of non-thermal plasmas in nature is the aurora borealis.

The relationship between different plasma temperatures in collisional weakly ionized non-thermal plasma can be conventionally presented as $T_e > T_v > T_r \approx T_i \approx T_0$. Electron temperature ($T_e$) is the highest one in the system, followed by the temperature of vibrational excitation of molecules (T_v). The lowest temperature is usually shared in plasma by heavy neutrals (T_0, temperature of translational degrees of freedom or simply gas temperature), ions (T_i), as well as rotational degrees of freedom of molecules (T_r). In many non-thermal plasma systems, electron temperature is about 1 eV, whereas the gas temperature is close to room temperature [40].

The main types of non-thermalizing electrical discharges applied in the Thesis are corona discharge and dielectric barrier discharge, which are described in the following sections.

1.3.2.1 Corona discharges

A corona discharge occurs in a gas between an electrode with a small radius of curvature, called active electrode, and a large surface external electrode, between which is applied a voltage of several kV. The electrode configurations which are commonly used to obtain the corona effect, are wire-to-cylinder, point-to-plate and wire-to-plate. The terms DC, AC and Pulsed corona indicate that the discharge is driven respectively by a DC, AC and Pulsed high voltage. The active electrode generates an electric field high enough to produce free charges, while the external electrode also called passive electrode acts primarily as a collector of charges. A positive or negative corona can be distinguished depending on whether the active electrode is at a voltage higher or lower, respectively, than that of the earth. The electrical discharge is the passage of current through a gas due to production, multiplication and movement of free charges, ions or electrons. Under the action of a sufficiently strong electric field the free electrons in the gas may undergo a significant acceleration and cause ionization of neutral molecules of the gas and, through the production of secondary electrons, lead to electronic avalanches. The free electrons originally present in the gas are formed by cosmic radiation at a rate of about one electron per mm^3 per second. The free charges that are generated by the corona, heading towards the electrode of opposite charge, create local electric fields that modify the applied field. As a consequence of this influence the current intensity does not vary linearly with the applied voltage, but follows a pattern which is determined by the presence of space charges. The electrical discharge depends not only by the electric field applied but also by the nature of the gas used and by its pressure. The ionization of the gas is described quantitatively by the coefficient α, which indicates the number of electrons produced, both by electron ionization of neutral molecules and by electron detachment from anions, when an electron moving toward the electrode of positive potential travels a path of unit length. The energy acquired by electrons not only increases with increasing electric field E but also with their mean free

path, which in turn decreases with increasing pressure p. Therefore, the production of ions via electron molecule collisions increases with the term E/p. [1]. During the discharge there are also processes that lead to the reduction in the number of electrons, such as recombination and electron attachment. Electron attachment greatly reduces the mobility of charges. The process is described quantitatively by the coefficient η, which represents the average number of attachments of an electron in a path of unit length. This coefficient depends on the nature of the gas and on the energy of the electrons. Electron attachment is very important in air discharges for the presence of oxygen, due to its high electronegativity. The corona discharge has the characteristics of a Townsend's discharge, since the applied voltage is high enough to produce electron impact ionization and extraction of electrons from the cathode, which trigger a process which is capable of self-sustaining. [1]

The area surrounding the active electrode is called ionization region, as the ionization process prevails over electric attachment, while the remaining space is the drift region, where electronic attachment prevails and transport of charged species occurs.

In negative DC corona, the space charge does not change appreciably the original electric field in the ionization region, where mostly radicals and positive ions are concentrated. At a distance of a few millimetres from the corona electrode there is the boundary between the ionization and the drift region. In the drift region electron attachment occurs, negative ions form and negatively charged species move towards the ground electrode. The discharge current is influenced by the mobility of charged species in the drift region and is lowered if a gas that favors electron attachment is used, since it reduces the number of free electrons.

In positive DC corona, the ionization region has a high density of electrons that move toward the positive electrode. Dissociative attachment prevails, leading to the formation, for example, of O^- ions. The drift region is dominated by the transport of positive ions and secondary electrons will be produced as a result of extraction processes from cathode, photoemission and photo-ionization. Following electron attachment negatively charged species such as O_2^- and O_3^- are produced, which together with the free electrons move towards the active electrode. [1]

The two most important forms of corona regime are the so-called *glow corona* and *streamer corona* (channel or filamentary discharge). The establishment of one of these two discharge regimes depends essentially on the distance between the electrodes and on the evolution in time of the applied voltage.

The streamers are filamentary discharge channels which, thanks to the electric field generated by their electric charge, extend where the value of the geometrical electric field is lower than required for ionization. The development of streamers is different depending on whether the active electrode is positively or negatively charged.

In the case of positive polarity streamers begin to develop when the voltage is high enough for free electrons to acquire sufficient energy to ionize neutral molecules and produce an electron avalanche. Given the large difference in mobility, positive ions can be considered stationary compared to the electrons in motion. The avalanche then spreads like a cloud of electrons, rapidly increasing in number, which moves towards the anode, leaving behind a positive space charge. The geometrical electric field, due to electrodes geometry and to the applied voltage, is increased by the field produced by spatial charge. The ionization activity at the avalanche head is accompanied by emission of photons consequent production of photo-electrons. These photo-electrons under the action of the resulting field give rise to secondary avalanches that can neutralize, with their electrons, the positive spatial charge. Positive ions, left behind by secondary avalanches, create a spatial charge more advanced toward the cathode. For the formation of the streamers, it is necessary that the first avalanche reaches a critical size, due to a number of charges sufficient to create an electric field due to spatial charge which, added to the geometrical field, is capable of generating a further electron avalanche.

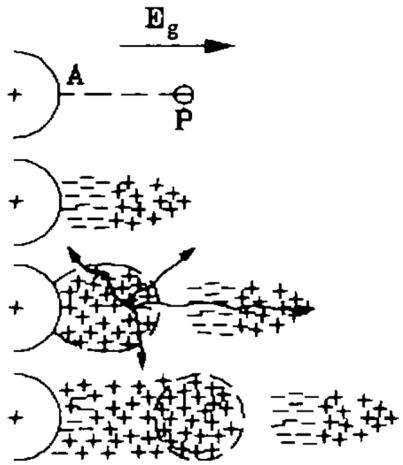

Fig. 1.3.2. Schematic representation of positive streamer formation.

A schematic representation of the formation and propagation of a positive streamer is shown in Fig. 1.3.2. The development of a positive streamer only roughly follows the lines of the applied field due to the major effect due to spatial charges present at its head. In case two secondary avalanches of sufficient size come simultaneously from different directions at the head of the streamer, branches of the filament will occur. As the phenomenon repeats itself, the streamer develops into a highly branched structure.

In the case of negative polarity there is a discharge mechanism which is somewhat different from that for positive polarity. This mechanism is illustrated in Fig. 1.3.3. When the primary avalanche, created by a free electron near the cathode, has reached the appropriate size, the electric field is greatly increased both in the vicinity of its tail and of its head. From point A in Fig. 1.3.3 a positive streamer is developed (reverse streamer) towards the cathode, while a photo-electron produced at a point B, under the action of the resulting field, generates a secondary avalanche. When the secondary avalanche has developed sufficiently, an opposite streamer moves from its tail to the head of the primary avalanche. The phenomenon is repeated and the negative filament moves towards the anode. The streamer propagates in areas where the applied field is reduced, leaving behind a partially ionized channel that has an excess of negative charges inside. Due to photo-ionization and bombardment by positive ions (accelerated by a strongly increasing field) there is a continuous extraction of electrons from the electrode. The neutralization of positive ions at

the cathode and the extraction of new electrons determine the negative charge excess of the streamer.

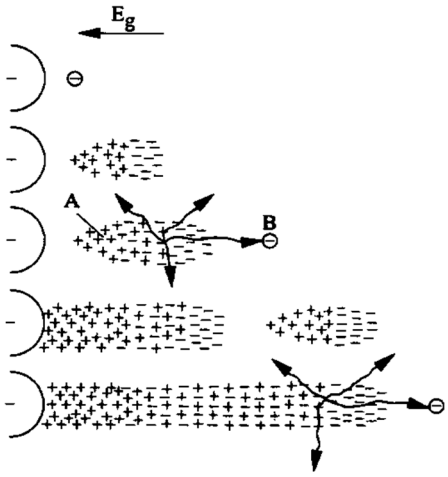

Fig. 1.3.3. Schematic representation of negative streamer formation.

The photo-electrons that give rise to secondary avalanches are accelerated in rapidly decreasing fields due to the rapid decrease of the field component generated by spatial charge. The applied field then, in this case, has a more pronounced influence, so the negative streamers have a development closer to the lines of the applied field and fewer branches. Moreover, they have a more limited extension than the positive streamers. It should also be noted that electron attachment reduces the mobility of negative charges where the field is lower, which corresponds to the final stages of the development of the avalanche [45].

A *glow corona* is established when the distance between the electrodes is short enough so that the electric field is sufficiently high for the occurrence of ionization processes in a uniform manner in space and time. A stable corona discharge is obtained, consisting of a series of small electron avalanches that surround the active electrode. Visually, the glow corona appears as a faintly luminous sheath surrounding the electrode, whose intensity increases with increasing applied voltage. In the case of positive glow corona, the positive spatial charge is distributed uniformly around the positive electrode, with an effect comparable to an increase in the diameter of the electrode. The decrease of the electric field thus produced inhibits ionization avalanches induced by photo-electrons present beyond the positive space charge region. The result is a very stable discharge in which the ionization

region is restricted around the active electrode. With this corona regime the discharge current remains constant in time. In contrast, for streamer corona, the discharge current is formed by a DC component which is overlapped with current pulses.

1.3.2.2 Dielectric barrier discharges (DBD)

Dielectric barrier discharges (DBDs), or simply barrier discharges, take place when at least one electrode is covered by a dielectric material, which can be for example glass, quartz, ceramics, a polymer. DBDs have been known for more than a century. First experimental investigations were reported by Siemens in 1857 and concern the generation of ozone [46]. This was achieved by subjecting a flow of oxygen or air to the influence of a dielectric barrier discharge (DBD) maintained in a narrow annular between two coaxial glass tubes by an alternating electric field of sufficient amplitude. The novel feature of this discharge apparatus was that the electrodes were positioned outside the discharge chamber and were not in contact with the plasma. A few years after Siemens' original publication, Andrews and Tait, [47] in 1860, proposed the name "silent discharge", which still is frequently used in the English, German, and French scientific literature. Ozone and nitrogen oxide formation in DBDs became an important research issue for many decades [48, 49]. In 1943 Manley [50] proposed a method for determining the dissipated power in DBDs by using closed voltage/charge Lissajous figures and derived an equation which became known as the power formula for Ozonizers. Occasionally, also the term corona discharge is used in connection with DBDs, although most authors prefer to use this term only for discharges between bare metal electrodes without dielectric. Both discharge types have common features: the generation of "cold" non-equilibrium plasmas at atmospheric pressure and the strong influence of the local field distortions caused by space charge accumulation.

Typical planar DBD configurations are sketched in Fig. 1.3.4. As a consequence of the presence of at least one dielectric barrier these discharges require alternating voltages for their operation. The dielectric, being an insulator, cannot pass a DC current. Its dielectric constant and thickness, in combination with the time derivative of the applied voltage, dU/dt, determine the amount of displacement current that can be passed through the dielectric(s). To transport current (other than capacitive) in the discharge gap the electric field has to be high enough to cause breakdown in the gas. In most applications the

dielectric limits the average current density in the gas space. Preferred materials for the dielectric barrier are glass or silica glass, in special cases also ceramic materials, and thin enamel or polymer layers.

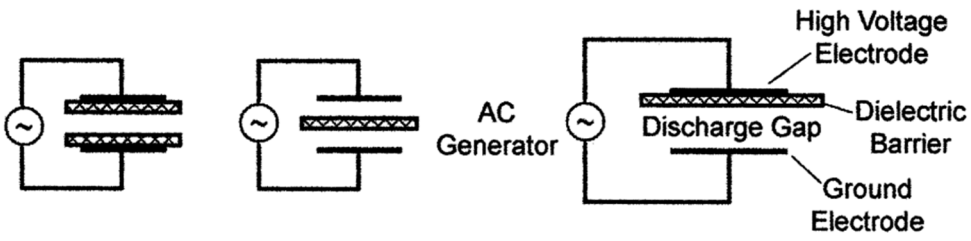

Fig. 1.3.4. Basic DBD configurations [51].

Besides the planar configuration showed above also annular discharge gaps between cylindrical electrodes and dielectrics are used in many technical applications. The discharge gap itself has a typical width ranging from less than 0.1 mm to several centimetres, depending on the application. The gas can either flow through the DBD (ozone generation, surface treatment, pollution control) or it can be re-circulated (CO_2 lasers) or fully encapsulated (excimer lamps, excimer based fluorescent lamps and light panels, plasma display panels).

At atmospheric pressure electrical breakdown in a large number of microdischarges is the normal situation for most gases in DBD configurations. Under certain circumstances also apparently homogeneous, diffuse discharges [52-54] can be obtained, or also regularly spaced glow discharge patterns [55-58]. The most common appearance of dielectric barrier discharge at elevated pressure is that shown in Fig. 1.3.5. It is characterized by a large number of short-lived microdischarges. Each microdischarge has an almost cylindrical plasma channel, typically of about 100 µm of radius, and spreads into a larger surface discharge at the dielectric surface(s). Fig. 1.3.5 shows a schematic diagram of a single microdischarge and a simple equivalent circuit.

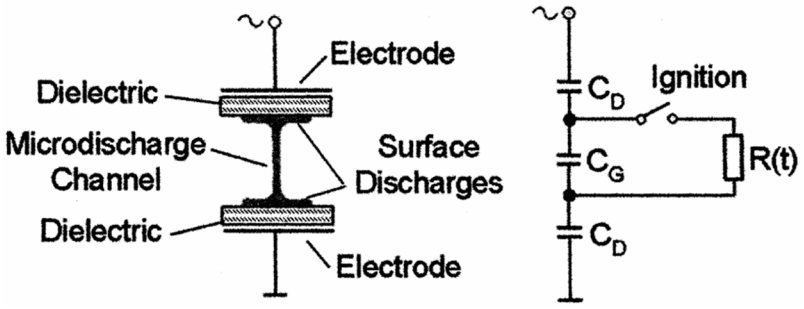

Fig. 1.3.5. The microdischarge and the simplified equivalent circuit [51].

By applying an electric field larger than the breakdown field local breakdown in the gap is initiated. In the equivalent circuit this is symbolized by closing a switch and forcing some of the current through the plasma filament, whose resistance *R(t)* rapidly changes with time. In reality, growing electron avalanches quickly produce such a high space charge that self-propagating streamers are formed [58-60]. A space-charge induced field enhancement at the streamer head, moving much faster than the electron drift velocity, is reflected at the anode and travels back to the cathode where, within a fraction of nanosecond, an extremely thin cathode layer is formed. At this moment the current flow through the conductive channel bridging the electrode gap peaks. Subsequently charge accumulation at the dielectric surface(s) reduces the local electric field to such an extent that ionization stops within a few nanoseconds and the microdischarge is choked.

Research on DBDs has focused on tailoring microdischarge characteristics by making use of special gas properties, adjusting pressure and temperature, and optimizing the electrode geometry as well as the properties of the dielectric(s).

The total charge Q transferred in a microdischarge depends on the gas properties and can be influenced by the gap spacing and by the properties of the dielectric. Q is proportional to the width of the discharge gap d, and to the quantity e/g (e: relative permittivity, g: thickness of dielectric). The latter relation was experimentally checked to hold up to extreme e-values of about 1000 [61, 62]. Contrary to what one might expect, Q does not depend on gas density [59].

Recent advances in spectroscopic measuring techniques and in laser diagnostics provided important additional information by in situ determinations of electron, atom, free radicals and excited species concentrations in individual microdischarges [63-65]. The gas temperature inside microdischarge filaments was derived from rotational band structures [66-68] as it was done for corona discharges.

The early phases of microdischarge formation are characterized by electron multiplication, by excitation and dissociation processes initiated by energetic electrons, and by ionization processes and space charge accumulation. The ionic and excited atomic and molecular species initiate chemical reactions that finally result in the synthesis of a desired species (e.g. ozone, excimers) or the destruction of pollutants (e.g. VOCs, nerve gases, odors, NH_3, H_2S, NO_x, SO_2, etc.). In many low-pressure discharges the major reaction paths are dominated by charged particle reactions. In the majority of DBD applications, however, most charged particles disappear before any major changes occur and reactions primarily involve neutral species like atoms, molecular fragments and excited molecules (free-radical chemistry). In any case, discharge activity and energy dissipation occur mainly within the small volume fraction occupied by microdischarges. The generated active species set the initial conditions for the ensuing chemical reactions. An adequate picture of the physical processes during breakdown and microdischarge formation is a prerequisite for a detailed understanding of DBD chemical reactor. Each individual microdischarge can be regarded as a miniature plasma chemical reactor. Scaling up or increasing the power density just means that more microdischarges are initiated per unit of time and per unit of electrode area. In principle, individual microdischarge properties are not altered during up-scaling.

1.3.3 Spark discharges

The spark discharge is a transient process in the gas which occurs at voltages above the breakdown level at pressures near atmospheric or above in gaps of about 1 cm and longer (*pd > 1000 Torr cm*) [44]. The voltages required for the breakdown at such high values of *pd* are quite high, running to tens and hundreds of kV.

Lightning is a huge scaled spark discharge: it may be several kilometers long being the electrical breakdown of the gap between a cloud and the ground, or between two clouds. The sound (thunder) is caused by the shock wave which is a sharp rising in pressure due to an intensive releasing of heat in the spark channel when a high discharge current passes through it.

The spark discharge is formed in strongly nonuniform fields: between a point and a plane, between a thin wire and a concentric cylinder, etc. In these cases, the corona discharge usually precedes the spark phenomena.

In contrast to the corona discharge, which is a weakly luminous and is confined in the neighborhood of the active electrode, the spark discharge is of transient type and develops between electrodes crossing the entire discharge zone.

The complete physical phenomena of the spark are rather complex. Due to high *pd* values the Townsend quasi-homogeneous breakdown mechanism cannot be applied. In conditions of high pressure and distance between the electrodes the mechanism of breakdown can be described in terms of streamers formation. The spark breakdown at high pd and considerable overvoltage develops much faster than the time necessary for ions to cross the gap and provide the secondary emission [40].

The foundation of the streamer theory was laid by the work of Loeb, Meek and Raether [70, 71] in the 1940s and later studies [72, 73]. The streamer develops from an electrode of large curvature and propagates in low electric fields by reproducing high field at the streamer head. Ionization processes take place only in this region, whereas the plasma in the streamer channels is in a decay regime. Streamers can be as large as 1–10 m in length and electron density in the streamer channel is assumed to lie in the range of 10^{14}–10^{15} cm^{-3}. During the streamer propagation the electron temperature T_e in the streamer channel rises to around 1 eV whereas the gas temperature T_0 does not change [74].

After bridging a gaseous gap the streamer channel can spontaneously decay or transform into a streamer breakdown. For a streamer breakdown to be developed the gas temperature in the streamer channel after bridging the gap has to rise greatly (up to 5000–6000K for air). Also, the streamer channel have to be heated for a time which is short

compared to the plasma decay time due to electron attachment or electron-ion recombination [74]. In this case a strong current flows through the highly conductive spark channel. The voltage in the insulation gap sharply drops down due to presence of the current limiting (the voltage drops across the external resistance) or as a result of the rapid discharge of the charge storage capacitor, thus the discharge burns out. In case the voltage across the electrodes rises up again after the quenching of the discharge (renewing the insulation properties of the gas), the spark discharge repeats. If the power supply is sufficiently high for sustaining a large current for a considerable time, the cathode spot can be formed and the spark will be transformed into an arc discharge [44].

1.3.4 Chemical processes in atmospheric plasma

The energetic electrons produced in atmospheric plasma may transfer their energy to the molecules in the gas through inelastic collisions, giving rise to a whole series of reactions, from which charged species, molecules and metastable excited neutral fragments (atoms and radicals) originate. The probability for such species to form is related to the amount of energy that is released in the collision and therefore the plasma capacity to provide enough energy to induce the specific reaction to occur. The energy barriers to be overcome for the occurrence of various processes are: ionization energy for the formation of an X^+ species from an X neutral species, electronic excitation energy for the formation of the excited species X*), vibrational and rotational excitation energy of molecular and atomic species to form metastable states and bond dissociation energies. Below are summarized the main reactions that may occur between the electrons and the species present in the gaseous medium, considering the molecules of air as examples [40].

- Ionization of an atomic species, X, or of a molecular species XY, with consequent formation of secondary free electrons

$$X + e^- \rightarrow X^{+\bullet} + 2\ e^-$$

$$XY + e^- \rightarrow XY^{+\bullet} + 2\ e^-$$

Example: $O_2 + e^- \rightarrow O_2^{+\bullet} + 2\ e^-$ (E_a = 12.5 eV)

$$N_2 + e^- \rightarrow N_2^{+\bullet} + 2\ e^- \qquad (E_a = 15.6\ eV)$$

The ionization may be accompanied by processes of fragmentation with formation of free radicals:

$$XY^{+\bullet} \rightarrow X^{\bullet} + Y^+$$

- Electron attachment:

$$X + e^- \rightarrow X^-$$

$$XY + e^- \rightarrow XY^-$$

The electron attachment can cause dissociation into ionic and radical fragments (dissociative electron attachment)

$$XY + e^- \rightarrow X^{\bullet} + Y^-$$

Example: $O_2 + e^- \rightarrow O^{-\bullet} + O \qquad (E_a = 3.5\ eV)$

- Excitation of atomic and molecular species:

$$X + e^- \rightarrow X^* + e^-$$

$$XY + e^- \rightarrow XY^* + e^-$$

Example: $O_2 + e^- \rightarrow O_2^* + e^- \qquad (E_a = 1\ eV)$

which can be followed by dissociation into radical species

$$XY^* + e^- \rightarrow X^{\bullet} + Y^{\bullet} + e^-$$

- Simple dissociation:

$$XY + e^- \rightarrow X^{\bullet} + Y^{\bullet} + e^-$$

Example: $O_2 + e^- \rightarrow 2\ O + e^-$

- Recombination:

$$XY^{+\bullet} + e^- \rightarrow XY$$

1.4 Application of air plasma to organic pollutants decomposition

1.4.1 Chemical processes in air atmospheric plasma

The main reactive species produced in air atmospheric plasma are the following:

- The ions $O_2^{+\bullet}$, $N_2^{+\bullet}$, NO^+, H_3O^+, $O^{-\bullet}$, $O_2^{-\bullet}$, $O_3^{-\bullet}$;
- The atomic species O and the $^\bullet$OH radical;
- Excited species of atomic and molecular oxygen and nitrogen;
- The neutral species O_3 and NO_x.

As described in the previous paragraph, $O_2^{+\bullet}$, $N_2^{+\bullet}$, $O_2^{-\bullet}$, $O^{-\bullet}$ and O are formed by the direct interaction of air molecules with electrons. On the contrary, the formation of NO^+, H_3O^+, $O_3^{-\bullet}$, $^\bullet$OH, O_3 and NO_x takes place following further processes as described below.

The hydroxyl radicals are formed from water molecules, generally present in traces also in dry air, through different possible channels: the reactions of excited species of atomic oxygen and nitrogen with water [75]

$$O(^1D) + H_2O \rightarrow 2\ ^\bullet OH$$

$$N(^2D) + H_2O \rightarrow {}^\bullet OH + NH$$

and an ionic path, which constitutes also the via of formation of the H_3O^+ ion [75, 76]

$$O_2^{+\bullet} + H_2O + M \rightarrow O_2(H_2O)^{+\bullet} + M$$

$$O_2(H_2O)^{+\bullet} + H_2O \rightarrow H_3O^+ + O_2 + {}^\bullet OH$$

$$O_2(H_2O)^{+\bullet} + 2\ H_2O \rightarrow H_3O^+ + H_2O + O_2 + {}^\bullet OH$$

where M is a different gas species, such as N_2, that can dissipate the energy of the reaction [78, 79].

NO^+ is formed by the following reactions

$O^+ + N_2 \rightarrow NO^+ + N$

$N^+ + O_2 \rightarrow NO^+ + O$

Ozone formation is due to the recombination of atomic oxygen in the ground state with molecular oxygen

$O(^3P) + O_2 + M \rightarrow O_3 + M$

In the discharges applied in air the formation of nitrogen oxides is often observed, due to the reactions reported below

$N + O_2 \rightarrow NO + O$

$O + N_2 \rightarrow NO + N$

$NO + O + M \rightarrow NO_2 + M$

$NO + O_3 \rightarrow NO_2 + O_2$

$NO_2 + O_3 \rightarrow NO_3 + O_2$

$NO_2 + {}^{\bullet}OH + M \rightarrow HNO_3 + M$

$NO_2 + N \rightarrow N_2O + O$

As it can be noted, some of these reactions entail a decrease in ozone concentration [78, 80].

1.4.2 Air plasma for the removal of organic pollutants

1.4.2.1 Air plasma for the removal of volatile organic compounds (VOCs)

Air atmospheric plasma is nowadays already applied for the decomposition of volatile organic compounds (VOCs); two examples are plants for the treatment of dioxins-containing effluents from municipal waste incinerators and devices for air purification in closed environments. Recognized merits of such treatments include mild operation conditions (room temperature and pressure), high efficiency in the decomposition of VOCs present in low concentration, easy operation and maintenance [1]. In these systems VOCs are oxidized by reactions with the ions and radicals produced in the air discharge. The main processes are summarized below; these can act as potential early stages of the degradation of the volatile organic compounds (indicated as RY):

- Decomposition induced by charge exchange reactions with cations:

$$X^{+\bullet} + R\text{-}Y \rightarrow R\text{-}Y^{+\bullet} + X \qquad X^{+\bullet} = O_2^{+\bullet},\ N_2^{+\bullet},\ \text{etc.}$$

The species $R\text{-}Y^{+\bullet}$ may dissociate through elimination of radicals:

$$R\text{-}Y^{+\bullet} \rightarrow R^{\bullet} + Y^{+}$$

- Decomposition induced by electron attachment or charge exchange with anions:

$$e^{-} + R\text{-}Y \rightarrow R^{\bullet} + Y^{-}$$

$$X^{-\bullet} + R\text{-}Y \rightarrow R^{\bullet} + Y^{-} + X \qquad X^{\bullet -} = O_2^{\bullet -},\ O_3^{\bullet -},\ \text{etc.}$$

- Decomposition through the formation of an electronic excited state:

$$R\text{-}Y^{*} \rightarrow R^{\bullet} + Y^{\bullet}$$

- Decomposition induced by reactions with radicals and atoms ($OH^{\bullet}$, $Cl^{\bullet}$, $O^{\bullet}$, etc) which give addition, in the case of unsaturated compounds, or $H^{\bullet}$ extraction:

The reaction path for a specific compound depends on the concentration of various radicals and ions produced in plasma and on the chemical characteristics of the compound, which determine the thermodynamic and velocity constants of the various possible

reactions. In particular, the charge exchange reactions induced by cations are important for those organic compounds which have ionization potentials lower than O_2 and N_2. On the other hand charge exchange reactions involving anions are important for those compounds with high electron affinity. Since organic compounds generally have ionization potentials lower than the air molecules and have bigger cross sections for electronic attack, the energy of plasma is effectively transferred to VOCs molecules, even if the VOC is present in parts per million concentrations.

The decomposition of organic compounds in non-thermal plasma can be usefully compared with that which occurs in the troposphere and that has been and continues to be the subject of numerous studies. In non-thermal plasma, however, the concentration of electrons, ions and radicals is much greater than it is in the troposphere and these species, therefore, play in the corona treatment an important role in the initiation reactions. The four processes mentioned above as initiation stage of the decomposition of organic compounds in non-thermal plasma have in common the formation of radical R; in the presence of oxygen those radicals reasonably suffer the same reactions involved in tropospheric degradations of VOCs, schematized below [81, 82]:

$$R^{\bullet} + O_2 \rightarrow ROO^{\bullet}$$

$$ROO^{\bullet} + NO \rightarrow RO^{\bullet} + NO_2$$

$$2\ ROO^{\bullet} \rightarrow 2\ RO^{\bullet} + O_2$$

$$RO^{\bullet} \rightarrow \text{carbonyl-containing intermediate + radical } (Cl^{\bullet}, R'^{\bullet}, \text{etc.})$$

proceeding via peroxide and oxide radical intermediates. The carbonyl-containing intermediate products are in turn oxidized and the final products of VOCs decomposition in non-thermal plasma are CO, CO_2, and H_2O, and in the case of treatment of chlorinated compounds Cl_2 and HCl are also formed.

1.4.2.2 Air plasma for the removal of organic pollutants in the solution

Recently, the use of atmospheric plasma has been proposed also for the treatment of polluted waters. Actually, the application of DBD and corona discharges for the purification of water is a common technique if one considers the processes of ozonation, in which the electrical discharges at atmospheric pressure are used for the production of ozone. However, in these processes ozone is generally produced *ex situ* and then placed in contact with the solution to be treated [51, 83]. Otherwise, the idea of applying the discharge directly to the air above the solution, *in situ*, is born from the purpose to decompose the pollutants taking advantage not only of ozone but also of the other reactive species produced in the plasma, generally characterized by lifetimes much shorter than that of ozone and higher reactivities [83].

Electrical discharges considered for water treatment applications can be generated in the gas phase in contact with the liquid surface or directly into the liquid phase. In the first case different discharge regimes have been reported in the literature, including streamer corona, spark and arc with a variety of electrode geometries (e.g., point-point, point-plate, wire-plate and wire-cylinder) [84 - 92]. In these devices the reactive species formed in the air plasma are transferred into the water and react with the organic pollutants contained in it or produce secondary radicals, capable of decomposing the pollutants. Some reactions of formation of secondary radicals are shown below:

$$O\ (gas) + H_2O \rightarrow 2\ {}^{\bullet}OH(aq)$$

$$O^{-\bullet}(gas) + H_2O \rightarrow OH^{-}(aq) + {}^{\bullet}OH(aq)$$

$$O_2^{-\bullet}(gas) + H_2O \rightarrow OH^{-}(aq) + {}^{\bullet}O_2H(aq)$$

Ozone also is a precursor of OH radicals in water, in particular in solutions with basic pH [93, 83], as it is attacked by the hydroxide anion. The overall process of ozone decomposition in water is rather complex but can be summarized by reactions (1.4.1)-(1.4.6):

$$O_3 + {}^{-}OH \rightarrow O_2^{-\bullet} + HO_2^{\bullet} \qquad (1.4.1)$$

$$O_3 + HO_2^{\bullet} \rightarrow 2O_2 + {}^{\bullet}OH \qquad (1.4.2)$$

$O_3 + {}^{\bullet}OH \rightarrow O_2 + HO_2^{\bullet}$ (1.4.3)

$O_3 + O_2^{-\bullet} \rightarrow O_3^{-\bullet} + O_2$ (1.4.4)

At pH < 8:

$O_3^{-\bullet} + H^+ \rightarrow HO_3^{\bullet}$ (1.4.5)

$HO_3^{\bullet} \rightarrow O_2 + {}^{\bullet}OH$ (1.4.6)

[93, 94]

At pH > 8:

$O_3^{-\bullet} \rightarrow O^{-\bullet} + O_2$ (1.4.7)

$O^{-\bullet} + H_2O \rightarrow {}^{\bullet}OH + {}^{-}OH$ (1.4.8)

$OH^{\bullet} + O_3 \rightarrow HO_2^{\bullet} + O_2$ (1.4.9)

As shown in reactions (1.4.5)-(1.4.9), the ozone radical anion, $O_3^{-\bullet}$ reacts further depending on the pH of the solution, however, in all cases it gives rise to the formation of ${}^{\bullet}OH$ [94].

The main species which have been recognized to react with the organic pollutants in such air/water heterogeneous systems are hydroxyl radical, ozone and hydrogen peroxide.

When the discharges are applied directly into the water [95-101] an amount of energy sufficient to cause not only ionization, but also vaporization must be provided. Hybrid reactors, which employ both discharges above and into the solution have also been reported [102-104].

The mechanism of organic pollutants decomposition when the discharge is applied into the water can be summarized as follows [100, 105]: the discharge applied in water induces the formation of a plasma channel which can reach temperatures of 14000-50000 K, acting as a black body, i.e. a source of UV radiation. The plasma channel expands generating intense shock waves, which can indirectly induce pyrolysis reactions and formation of radicals through electrohydraulic cavitation. When the plasma cools down, in a time of about 1-3 ms, the thermal energy is absorbed by the surrounding water, causing the formation of vapor bubbles. The temperature and pressure of the bubbles are high enough

to instantaneously produce supercritical water. The removal of organic compounds is due to direct and indirect photolysis, pyrolysis and reactions with free radicals within the plasma channel which has a high temperature. However, while the plasma affects only a small volume of solution, the discharges induce extreme electromagnetic and mechanical conditions in the overall volume of the water, where the processes responsible for the oxidative degradation of organic compounds are UV photolysis, electrohydraulic cavitation and oxidation by supercritical water.

Contrary to what happens for the application of the discharge on the surface of the water, the initiation of the discharge in water requires a certain initial conductivity, generally of a few mS/cm, while a high conductivity (> 400 mS/cm) reduces the length of the plasma channels and makes the production of radicals less efficient [96, 97].

Moreover, the generation of discharges in water requires an amount of energy approximately ten times higher than that for the generation of discharges above the water surface. This is due to the fact that the production of vapor bubbles and plasma channels in water requires heating and vaporization, which subtract energy to the process of production of radical species [88, 91].

For these reasons, the research group in which the Thesis was carried out, preferred to develop an experimental system in which the discharge is applied above the aqueous solution.

The prototype dielectric barrier discharge reactor was tested using phenol as a model compound, and proved quite efficient in comparison with other systems reported in the literature [106]. It was found that phenol is removed from the aqueous solution according to an exponential decay as a function of treatment time at constant applied voltage. The effect of different experimental variables was investigated, including the active electrodes material and size and the flow rate of air above the solution. A few intermediates and CO_2, the final product of phenol decomposition, were detected and identified by LC/ESI-MS and FT/IR analysis. The major reactive species formed upon application of the discharge in air, the OH radical and ozone, were determined by means of specific chemical probes.

Using the same dielectric barrier discharge reactor the rates of phenol advanced oxidation in deionized (milliQ) and tap water were determined and compared. Interestingly, a significant rate increase was found in tap with respect to milliQ water [107]. Control

experiments proved that this was not the effect of conductivity or of traces of iron or of residual active chlorine from the depuration process operated in the aqueducts of Italian cities. The same increase in efficiency as observed in tap water was instead obtained when phenol was treated in solutions containing bicarbonate anions in the same concentration as present in tap water, an effect attributed to buffering of the solution pH. The role of pH has been investigated thoroughly by measuring the process efficiency over a wide pH range, from 2 to 10, by using different buffer systems to probe reactivity at near neutral pH, the most relevant for drinking water applications, and by testing the effect of different buffer concentrations. These latter experiments failed to detect any significant kinetic effect attributable to the well-known reactivity of bicarbonate as quencher of OH radicals.

1.4.3 Mechanisms of phenol oxidation

The plasma systems described so far proved to rapidly and efficiently degrade many organic compounds, including phenols, [99, 108, 109] polychlorinated byphenyls, [110] perchloroethylene and pentachlorophenol, [86, 111] and many others. However, phenol is the most studied compound and became the model commonly used to test and compare novel discharge-initiated advanced oxidation processes because it is an important and ubiquitous organic pollutant of waters and because its properties and oxidation pathways have been extensively studied and are well described in the literature.

Depending on the conditions and on the oxidant species used a large number of different products can be formed from phenol oxidation, among which there are polihydroxybenzenes and quinones, organic acids and aldehydes formed from the aromatic ring cleavage and polymerization products [112, 113].

In previous studies performed in our group it has been demonstrated that the major species responsible for the oxidative degradation of phenol in the experimental system used in this thesis are ozone and hydroxyl radical. The data reported in the literature on the reactions of these two species with phenol in aqueous solution are briefly resumed below.

Reaction with O_3

Ozone can react both with undissociated phenol and with its conjugate base which is the phenoxide ion ($C_6H_5O^-$). The rate of the reaction with phenoxide is six orders of magnitude greater than that with undissociated phenol:

$PhOH + O_3 \rightarrow$ products	$k = 1.3 \cdot 10^3$ dm^3 mol^{-1} s^{-1} [112, 114]
$PhO^- + O_3 \rightarrow$ products	$k = 1.4 \cdot 10^9$ dm^3 mol^{-1} s^{-1} [112, 115]

However, phenoxide is present in significant concentration only in solutions at very high pH (the pKa of the phenol is 9.95).

The reaction of ozone with the undissociated phenol proceeds through attack at positions 2,3 and 3,4, since attack at positions 1,2 is unfavorable for reasons of steric hindrance [89]. The first product that is obtained is a molozonide, which rearranges immediately to ozonide. The ozonide is very unstable and decomposes to give a zwitterionic intermediate by breaking the ring. Following the nucleophilic attack of a water molecule alpha-hydroxy peroxides are formed, highly reactive species, which can decompose as shown in the Fig. 1.4.1 [89]:

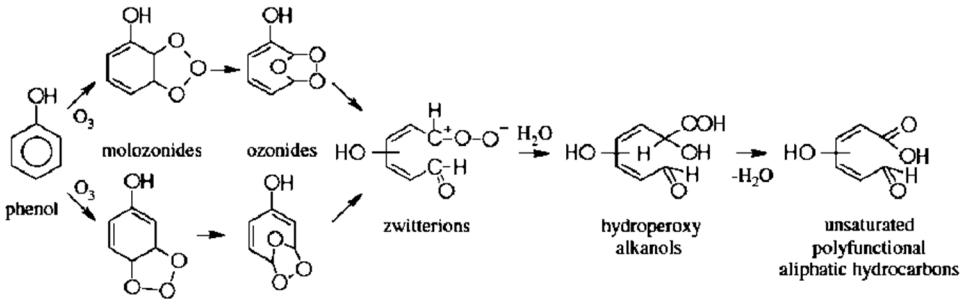

Fig. 1.4.1. Phenol ozonation schematic

The oxidative degradation chain continues through a subsequent reaction with ozone that results in the cleavage of the original molecule of phenol into two fragments, one containing 4 carbon atoms and the other 2.

The main products obtained are listed in Fig. 1.4.2.

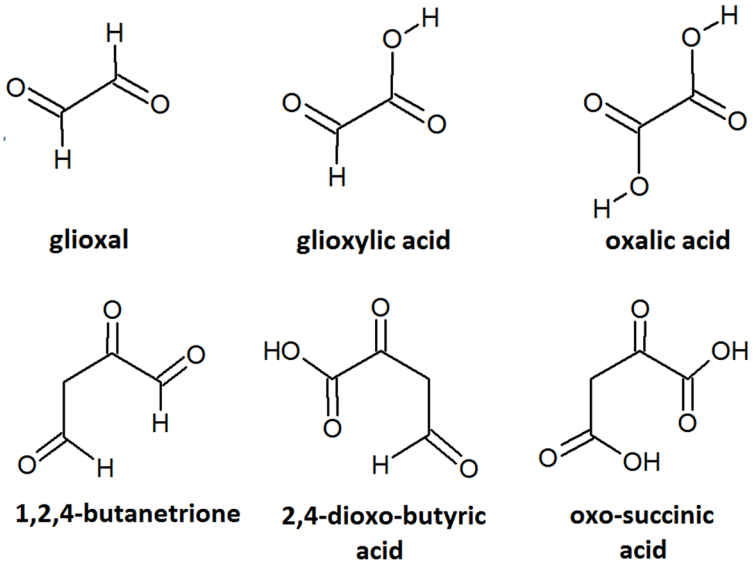

Fig. 1.4.2 The products of phenol decomposition

Reaction with $^{\bullet}OH$

The hydroxyl radical attacks the benzene ring of phenol preferentially at position 2 and 4 because the radical produced by attack at position 3 would be much less stable. In Fig. 1.4.3 the product of the attack at position 4, the 1,4-dihydroxy-cyclohexadienyl (DHCHD) radical, is shown as an example. This radical is subjected to attack by oxygen, which is very soluble in water (1.4 mM at 20°C), and is converted to 1,4-dihydroxy-ciclohexadienylperoxide (DHCHDP) radical.

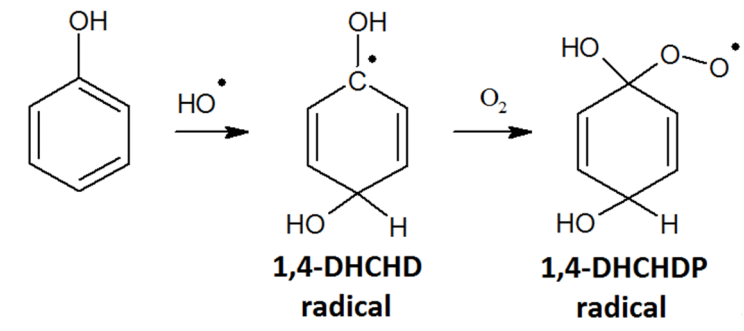

Fig. 1.4.3. OH attack on phenol and formation of 1,4-DHCHDP radical

The 1,4-DHCHDP radical can react to give hydroquinone. Another possibility is that the endoperoxyalkyl species (EPA), with which 1,4-DHCHDP is in equilibrium, adds another molecule of oxygen to form the peroxo radical EPAP, as shown in Fig. 1.4.4.

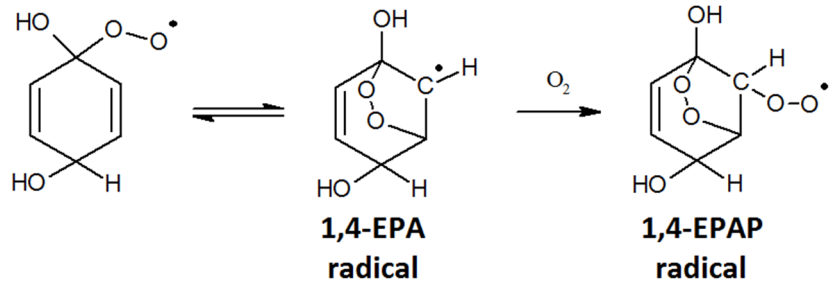

Fig. 1.4.4. The formation of 1,4-EPAP radical

Subsequent steps induce breaking of the ring with the possible loss of a moleculesof CO_2 or H_2O, leading to derivatives which have 5 or 6 atoms of carbon and contain a carbon-carbon double bond. Through a sequence of similar steps, these derivatives undergo degradation into smaller oxygenated fragments containing from 2 to 4 carbon atoms.

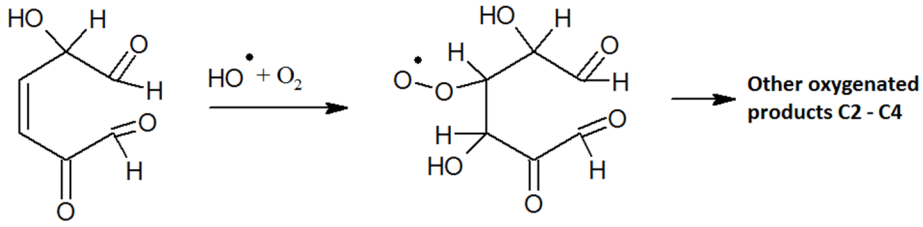

Fig. 1.4.5. The formation of light oxygenated products

The main ones are as follows: glyoxal, glyoxylic acid, ketomalonaldehyde, hydroxymalonaldehyde, 3-hydroxy-1,2-propanediol, 2-hydroxy-oxypropionic acid, 2-hydroxy-1,3,4-butantrione, 2,4-dihydroxy-1,3-butanedione.

1.5 Application of atmospheric plasma to dry reforming of methane

1.5.1 The processes in CO_2/CH_4 plasma

The first studies on the possibility to apply plasma technologies for the conversion of CH_4 and CO_2 to syngas date back to the second half of the eighties [116]. The first type of discharge employed was a controlled-arc. Later the same researchers applied a gliding arc discharge [117, 118], which is a particular type of discharge occurring between two or more diverging electrodes placed in a fast gas flow. This operates at atmospheric pressure or higher and generates regions of both thermal and non-thermal plasma [119]. The results of the first investigations were encouraging and from those years until now various studies on CO_2 reforming of methane with thermal and non-thermal plasma methods were reported in the literature. Among the experimental devices generating plasma at room temperature and atmospheric pressure developed so far there are systems energized by different types of electrical discharges, as for example continuous corona discharge (DC) of positive and negative polarity [120, 121], AC discharges [121], dielectric barrier discharges (DBD) [122] and pulsed discharges [123]. The main advantages of the application of plasma to the process of dry reforming of methane are the possibility to operate at low temperature and the consequent decrease of carbon deposition during the process.

The reactions which are generally considered responsible for the activation of CH_4 and CO_2 in the plasma driven process [124-127] are due to collisions of the gaseous molecules of the hydrocarbon and of carbon dioxide with electrons (eq. 1.5.1-1.5.2).

$$CH_4 + e^- \rightarrow CH_3 + H + e^- \qquad (1.5.1)$$

$$CO_2 + e^- \rightarrow CO + O + e^- \qquad (1.5.2)$$

The dissociation energies of CH_4 and CO_2 are equal to 4.5 and 5.5 eV, respectively [127]. Some researchers in describing the mechanism of the process consider also the collisions between electrons and the primary species originating from the dissociation of the precursor molecules, i.e. CH_3, CH_2, CH and CO (eq. 1.5.3-1.5.7) [125].

$CH_3 + e^- \rightarrow CH_2 + H + e^-$ (1.5.3)

$CH_2 + e^- \rightarrow CH + H + e^-$ (1.5.4)

$CH + e^- \rightarrow C + H + e^-$ (1.5.4)

$CO + e^- \rightarrow C + O + e^-$ (1.5.5)

Eq.s 4 and 5 justify possible coke formation from both CH_4 and CO_2. However, in competition with coke deposition, elementary carbon can also react with atomic oxygen to give CO (eq. 1.5.6).

$C + O \rightarrow CO$ (1.5.6)

CO can thus be formed by reaction (1.5.2) and (1.5.6), but not only, as there are different important pathways, which are initiated by the reaction of CH_3 with O and from which H_2 can also originate (eq. 1.5.7-1.5.11).

$CH_3 + O \rightarrow CH_2O + H$ (1.5.7)

$CH_2O + O \rightarrow CHO + OH$ (1.5.8)

$CH_2O + H \rightarrow CHO + H_2$ (1.5.9)

$CHO + O \rightarrow CO + OH$ (1.5.10)

$CHO + H \rightarrow CO + H_2$ (1.5.11)

$CHO + CHO \rightarrow CH_2O + CO$ (1.5.12)

Considering that OH radical is formed in eq.s (1.5.8) and (1.5.10) and that it can also be formed by the reaction of CH4 with O (eq. 1.5.13) and by the recombination of O and H (eq. 1.5.14), reactions (1.5.15)-(1.5.16) must also be considered, eq. (1.5.16) in particular for the formation of CO.

$CH_4 + O \rightarrow CH_3 + OH$ (1.5.13)

$O + H + M \rightarrow OH + M$ (1.5.14)

$CH_2O + OH \rightarrow CHO + H_2O$ (1.5.15)

$CHO + OH \rightarrow CO + H_2O$ (1.5.16)

Similarly, besides eq.s (1.5.9) and (1.5.11), molecular hydrogen can originate by recombination of two hydrogen atoms (eq. 1.5.17) and by reaction of atomic hydrogen with other radicals or with methane (eq. 1.5.18-1.5.20).

$$H + H \rightarrow H_2 \qquad (1.5.17)$$

$$H + HCO \rightarrow H_2 + CO \qquad (1.5.18)$$

$$H + OH \rightarrow H_2 + O \qquad (1.5.19)$$

$$H + CH_4 \rightarrow H_2 + CH_3 \qquad (1.5.20)$$

Eq.s 1.5.15 and 1.5.16 give rise to the formation of water, as do also the possible processes reported in eq. 1.5.21 and 1.5.22.

$$CH_4 + OH \rightarrow CH_3 + H_2O \qquad (1.5.21)$$

$$H_2 + OH \rightarrow H_2O + H \qquad (1.5.22)$$

In principle, water is not a desirable product. However, it has been reported that water can prevent carbon deposition (eq.s 1.5.23 and 1.5.24) [127].

$$C + H_2O \rightarrow CO + H_2 \qquad (1.5.23)$$

$$C + 2\,H_2O \rightarrow CO_2 + 2\,H_2 \qquad (1.5.24)$$

Other possible byproducts are hydrocarbons containing two or three atoms of carbon, saturated or not, formed mainly through radical recombination steps.

The mechanism for CH_4 and CO_2 activation considered in eq.s (1.5.1) and (1.5.2) is direct dissociation, in which the molecules of CH_4 or CO_2 collide with electrons having kinetic energies higher than the dissociation energy threshold of the ground-state molecules (eq. 1.5.1 and 1.5.2). However, depending on the energy of the electrons in the plasma, a second mechanism has to be considered, in which dissociation takes place through a

vibrational channel [126, 128]. This means that the reactant molecule is vibrationally excited and can therefore promote the occurrence of endothermic reactions (eq. 1.5.25).

$$A + BC^* \rightarrow AB + C \qquad (1.5.25)$$

Dissociation of vibrationally excited molecules has activation energy lower than that of direct dissociation from the ground state, resulting in enhancements of the dissociation rate constants of several orders of magnitude. Moreover, vibrational excitation can be achieved by collisions with electrons of low energy. For these reasons dissociation through vibrational excitation is considered the most important reaction mechanism in plasma characterized by mean electron energies between 1 and 3 eV. Dissociation through vibrational excitation is particularly favored for CO_2 as this molecule has a high rate of vibrational excitation and a relaxation time low enough to allow for the building up of high vibrational populations. On the contrary, the molecule of methane is characterized by a slow rate of vibrational excitation and by a high rate of relaxation, so its dissociation through the vibrational channel is rather difficult to achieve.

Under thermal conditions, a second initiation route of the process of dry reforming of methane is pyrolysis, which converts CH_4 into elementary carbon and hydrogen molecules and CO_2 into carbon monoxide and atomic oxygen, giving rise essentially to the same species produced by the interaction with electrons.

The occurrence and the relative contribution of all the reactions listed above as well as of those only mentioned, which lead to the production of hydrocarbons as secondary products, determine the reagents conversion, the product selectivity and the energy efficiency of the process. These are the key parameters to evaluate the process itself and depend on electron energy, electron density and temperature of the plasma, but also on the reactor configuration. Thus, the process of dry reforming of methane driven by plasma is strictly linked to the design of the reactor and to the type of discharge applied.

1.5.2. Studies of the atmospheric plasma assisted dry reforming of methane

The most attractive plasmas for the activation of chemical processes are those generated at room temperature and atmospheric pressure ("atmospheric non-thermal plasma"), usually by the application of electrical discharges. The first studies on the possibility to apply non-thermal plasma technologies for the conversion of CH_4 and CO_2 to syngas date back to the second half of the nineties [122]. From those years until now various studies on CO_2 reforming of methane with non-thermal plasma methods were reported in the literature.

The experimental devices developed so far are energized by different types of electrical discharges, as for example continuous corona discharge (DC) of positive and negative polarity [120, 121], AC discharges [121], dielectric barrier discharges (DBD) [122] and pulsed discharges [123]. In this case the local electron density is in the range of 10^{15} – 10^{20} m^{-3}. The results of these studies are encouraging and show that through non-thermalizing electrical discharges CO_2 and CH_4 can be converted to syngas operating at low temperature, thus decreasing the carbon deposition during the process.

The results obtained with corona discharge are good in terms of reagents conversion and products selectivity but the energy efficiency is rather low [129]. DBD was applied to dry reforming of methane by several researchers [130]. However, in most cases low conversion of reactants and low selectivity for syngas are reported, while ethane and other hydrocarbons are formed in significant amounts.

The experiments with thermal plasma reported so far are promising due to the high reagents conversion and products selectivity obtained. This is due in particular to the high electron density of thermal plasma. However, these systems require very high electrical powers, waste energy in the gas heating and need particular technical solutions as for example for cooling the reactor.

Gliding arc discharges in the reactors employed so far gave better energy efficiency than corona discharges and DBD but lower conversion and selectivity [131, 132].

Different types of pulsed discharges have also been applied to MDR: spark discharges [133], pulsed glow discharges [128] and pulsed arc [134]. It is reported that if very

short pulses are applied (duration of tens of nanoseconds) the plasma excitation time is much lower than the vibrational relaxation time (of the order of microseconds), thus this is the case in which [128] dissociation through vibrational excitation is much more efficient than direct dissociation from the ground state.

In order to increase the energy efficiency and the process selectivity of the plasma driven process of dry reforming of methane, various groups working on this subject have proposed the combination of plasma with a catalyst [135-150]. Different configurations have been investigated with regard to the reciprocal position of the two activations means. When the catalyst is placed in the discharge zone, the results in most cases demonstrate the occurrence of a synergy between plasma and heterogeneous catalysis which allows to work at lower temperatures with respect to those required if only the catalyst is used, to reduce byproduct formation with respect to the application of plasma alone and to decrease coke deposition. Due to its known activity, low cost and availability, the catalyst most used in these applications is Ni/γ-Al_2O_3 containing a percentage of nickel between 2 and 12% and prepared by wet impregnation [135, 139, 141, 143-145]. Other catalysts were however investigated [135, 136-138, 140, 146, 147]. The types of discharges which proved to be more suitable to combination with catalysts are corona and DBD.

2. CONTENTS, OBJECTIVES AND ORGANIZATION OF THE THESIS

As anticipated in the introduction chapter, this Thesis reports and discusses the results of studies on the application of atmospheric plasma to activate two processes of major environmental interest: advanced oxidation of organic pollutants for water remediation and carbon dioxide reforming of methane to produce syngas. Due to the very different nature of the two investigated processes, different plasma sources, types of discharge, reactors, experimental conditions and analytical procedures had to be developed and used. In spite of such differences, however, the two lines of research stem from a common background and share common objectives: to identify the chemical reactions and reactive intermediates leading to the desired products and to apply this knowledge for exploiting the great chemical potential of atmospheric plasma. Thus, a common research approach was used, based on extensive investigations of the discharge and plasma features, notably of its reactive species, and of the process efficiency, products and intermediates. Depending on the specific process studied, different experimental analytical techniques were used, including various types of chromatography (GC/FID, GC/TCD, GC/MS, HPLC/UV), TOC-analysis and spectroscopy (FT-IR and optical emission spectroscopy). All experimental results and observations were then combined and, in one case also integrated with the results of kinetic numerical modeling, to achieve a consistent mechanistic description of the process. A brief description of the contents of the following two chapters is given below.

Chapter 3 deals with water decontamination by air plasma treatment. It describes the apparatus used, a prototype barrier discharge reactor already available in the laboratory where the Thesis was carried out, and the experimental procedures adopted to obtain and analyze the results. The study focused initially on phenol, used as a model organic pollutant, but later extended to maleic acid and fumaric acid, two intermediates formed in the oxidation not only of phenol but also of the majority of aromatic compounds. Most useful insight was acquired from the comparison with results obtained in parallel experiments carried out under the same experimental conditions except for the fact that ozone was produced *ex situ*. Kinetic modeling supports the interpretation of experimental results obtained in these very complex heterogeneous reacting systems.

Chapter 4 deals with plasma driven dry reforming of methane. Since this was a new project initiated with this doctorate, a major task consisted in the design, development and testing of the experimental apparatus to identify the best discharge conditions. The new analytical protocols which had to be developed are also described as well as the procedures for the reduction and interpretation of the experimental results in terms of conversion, selectivity and efficiency. Specifically, in order to find the best regime the effects on conversion, yield and energy efficiency due to changes in the input flow at constant power were compared with those due to changes in input power at constant flow. The characterization of major plasma excited species achieved by optical emission spectroscopy is also described. The results obtained in this study under the best discharge conditions found, specifically a self-triggered spark discharge, are then compared with those reported in the literature. The outcome is very satisfactory and suggests the possibility for further development and scaling-up of the process.

3. DECOMPOSITION OF ORGANIC COMPOUNDS IN SOLUTION INDUCED BY AIR ATMOSPHERIC PLASMA

3.1 Experimental methods and procedures

This chapter describes the experimental set-up, the materials and the methods used for the research activity dealing with the decomposition of organic compounds in aqueous solution with air atmospheric plasma.

3.1.1 Chemicals

Pure air used in the experiments was a synthetic mixture of 80% nitrogen and 20% oxygen purchased from Air Liquide with specified impurities of H_2O (<3ppm$_v$) and C_nH_m (<0.5ppm$_v$). Phenol, 1,2-dihydroxybenzene, 1,4-dihydroxybenzene, maleic acid, fumaric acid, *cis,cis*-muconic acid were products of Sigma Aldrich and Fluka (purity > 99%). The inorganic salts $NaH_2PO_4 \cdot 12H_2O$, $Na_2HPO_4 \cdot 12H_2O$, $Na_3PO_4 \cdot 12H_2O$, Na_2CO_3 and $NaHCO_3$ were purchased from Carlo Erba Reagenti.

3.1.2 Instrumentation for chemical analysis

Liquid Chromatography

The samples were analyzed using an HPLC instrument which is manufactured by Thermo Separation Products and consists of the pump P2000 Spectra SYSTEM and the UV-VIS diode array detector UV6000LP. The column used was a Zorbax-SB Aq 4.6x150 mm (Agilent Technologies) column with particle size of 3.5 µm and an injection loop of 20 µL. A 20 mM phosphate buffer (pH = 2) containing 1% of acetonitrile was used as eluent. In the most experiments the isocratic elution was used at a flow rate of 1.0 mL/min. The chromatograms were recorded at the wavelengths of 210, 218 and 270 nm.

Infrared Spectroscopy

Infrared spectroscopy allows online monitoring the production of ozone in corona discharge, as well as the formation of the final product of mineralization, which is CO_2.

Analyses were carried out using a Fourier transform spectrometer (Nicolet 5700) equipped with a gas cell of 10 cm length. The gas cell is connected downstream to the reactor. Two types of window cells were used: windows of NaCl for the experiments under dry conditions and of CaF_2 for experiments in humid conditions. The acquired spectral window is from 4000 cm^{-1} to 650 cm^{-1} for the NaCl cell, and from 4200 cm^{-1} to 1000 cm^{-1} for the CaF_2 cell. The compartment where the cell houses was pre-evacuated with nitrogen in order to limit the interference on analysis due to the presence of ambient air, particularly as regards the signal produced by CO_2.

pH measurement

The pH of the water solution before, during and after the treatment was monitored using a pH meter (Metrohm 827). Before measurements, the instrument was calibrated using calibration buffer solutions (Merck).

Conductivity measurement

The conductivity of the water solution before and after the plasma treatment experiments was measured with a conductometer (Metrohm 660). Before measurements, the instrument was calibrated using a calibration solution of 0.2 mM KCl (30 µS).

Total organic carbon analysis

For determining the total organic carbon (TOC) in the solutions a Shimadzu TOC-VCSN was used. This is a standalone instrument with an autosampler and an automatic diluter. It performs the combustion with catalytic oxidation and is equipped with

nondispersive infrared sensor (NDIR) for CO_2 measurement. The range of the device is from 4 μg/L to 25 g/L.

3.1.3 The experimental set-up

To compare air plasma and ozone as oxidation means, two different experimental set-ups were employed, which however include the same reactor. In the case of plasma experiments the reactor was supplied with a high voltage, so non-thermal plasma was produced in the air above the aqueous solution. In the case of ozonation the power supply of the reactor was turned off and ozone was generated ex-situ by an ozonizer. Each experimental set-up includes a gas line for air circulation and analysis of the exhaust. The two experimental set-ups are described in detail in the following sections.

3.1.3.1 The reactor

Experiments were performed with the DBD-like corona reactor, developed previously [106] (Fig. 3.1.1). It consists of a glass vessel (internal dimensions 95x75 mm and 60 mm height) closed by a Teflon cover with four passing electrodes of stainless steel which support two parallel wires of 75 mm length and 0.15 mm diameter fixed upon their tips. The wires, made of stainless steel, are placed at a distance of 38 mm between each other and are kept above the aqueous solution.

The outside surface of the reactor base is covered with a film of colloidal silver and connected to a grounded plate. The cover is sealed by a Viton gasket to the glass vessel and is fixed to it and to the base by four screws.

On the cover there are two connectors for gas input and exhaust. In the middle of the Teflon cover a sampling port is placed. This is equipped with a septum which allows withdrawing of the solution samples during the decomposition experiments without disturbing the gas atmosphere inside the reactor.

The volume of treated solution was 70 mL, the thickness of liquid 9.8 mm, the gap between the surface and the electrodes 15 mm, and the volume of air inside the reactor was near 286 mL.

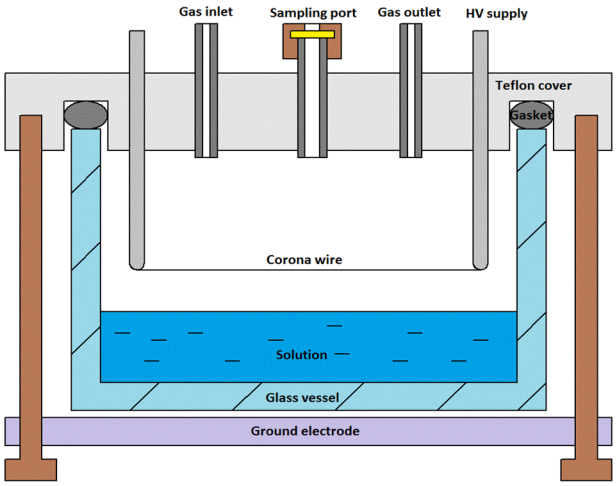

Fig. 3.1.1. Scheme of the DBD reactor

The discharge occurs in the gas phase above the liquid surface. During the experiments the high voltage applied to the wires was maintained constant (18 kV): voltage and current profiles were monitored with a digital oscilloscope (TDS5032B, bandwidth 350 MHz, maximum sample rate is 5 Gs/s) to assure the reproducibility of the electrical conditions.

To achieve an interaction of ozone with the organic compounds as similar as possible to that which takes place in the plasma-induced process, the same reactor used in the experiments with plasma was employed also in the ozonation experiments. The reactor works just as a hermetic vessel containing the solution (corona electrodes are not connected and left floating). All tubes and transmission lines are made of Teflon. The concentration of ozone was adjusted to be equal to that produced by the DBD discharge and ozone was simply flowed above the water surface at the same flow rate employed in the experiments with plasma. Initially the solution was not stirred as it is in the experiments with plasma. However, in the case of plasma treatment the discharge generates the so called “ion wind” which is a stream of ionized gas which moves the water surface. Thus, to better compare

ozonation with plasma treatment magnetic stirring was then applied in both types of experiments.

3.1.3.2 The gas feeding line

The reactor is connected to a gas feeding line (Fig. 3.1.2). Dry synthetic air comes from a high-pressure cylinder and is controlled by a flow meter (the flow is 30 mL/min). In the plasma experiments it passes through a bubbler filled with milliQ which is placed ahead of the reactor to be saturated with water and consequently to minimize evaporation from the solution.

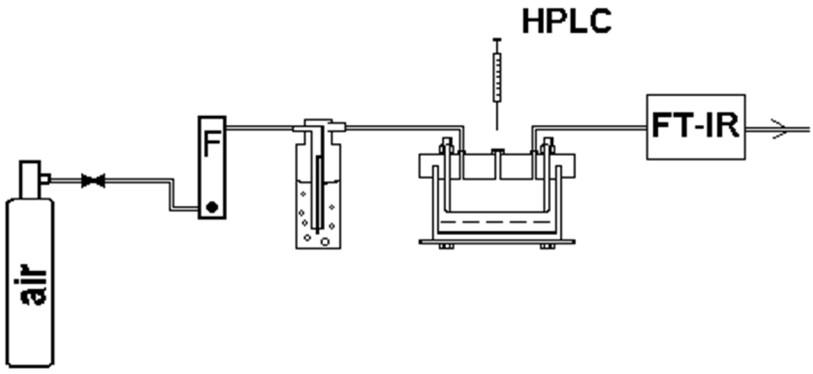

Fig. 3.1.2. Gas feeding line used for experiments of plasma treatment

To perform the ozonation experiments the setup described above was modified as shown in Fig. 3.1.3. The synthetic air pass through an ozonizer GAIOFISH 100, which is a compact industrial device based on a DBD discharge and produces 100 mg/h of O_3 at 1 L/min if air as a feeding gas. It is directly powered from the electricity network without any kind of power regulation. For this reason it is not possible to automatically adjust the ozone concentration, thus a particular feeding system was set up for this scope. It consists of three rotameters: the first (rotameter A, 800 mL/min full-scale) sets a general flow through the ozonizer, thus determining the ozone concentration. The other two rotameters split the ozone flow to obtain a flow of 30 mL/min (rotameter B) with a desired ozone concentration entering into the reactor, while the rest (rotameter C) goes into the exhaust.

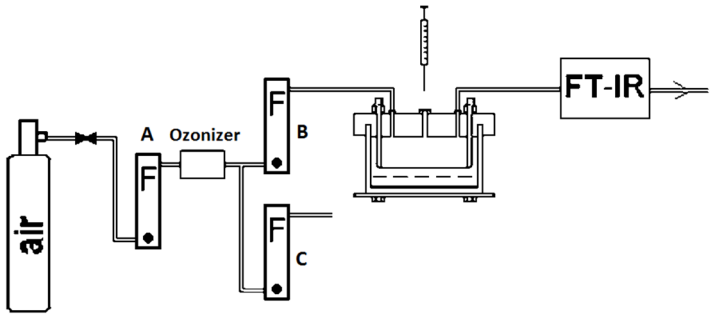

Fig. 3.1.3. Gas feeding line used for ozonation experiments

In both plasma and ozonation experiments the outlet from the reactor was connected to the gas cell placed inside the FT-IR apparatus to monitor the concentration of ozone and of CO_2 in the gas.

3.1.3.3 Power supply and electrical monitoring

The reactor is powered with an AC high voltage transformer with 18 kV and a frequency of 50 Hz and operated in a Dielectric Barrier Discharge (DBD) corona mode. It produces corona discharge due to recharging of its internal capacitance every half-cycle, producing negative and positive corona in every period of a sine wave. This topology helps to prevent breakdowns and spark discharges in the reactor. This also helps to operate safely with high voltage power transformer supply. The load is predominantly capacitive and has low active power consumption.

The schematic of the power supply is shown in Fig. 3.1.4. It includes a voltage regulator autotransformer TX1, an isolation transformer TX2, a voltage rising transformer TX3, a resistor R1 for current limiting and measurement systems such as a resistive-capacitive voltage divider and a shunt for current monitoring. The function of TX1 is to adjust the voltage from the wall plug (230 V) from 0 to 230 V (during the experiments the output of the transformer did not exceed 80 V). The transformers TX1 and TX2 are assembled together in a single module produced by F.M.T. Electric Technologies, Italy, which also contains voltage, current and frequency meters.

The transformer TX2 with transformation ratio of 1:1 is necessary to have the possibility to isolate the primary winding of the high voltage transformer TX3.

The whole system (the high voltage transformer, voltage divider and the reactor) is placed inside a shielded room to protect the system from external electromagnetic disturbances during electrical monitoring (especially, for current monitoring). The shielded room contains a multi-stage mains filter, gases inlets/outlets and BNC connectors for electrical monitoring.

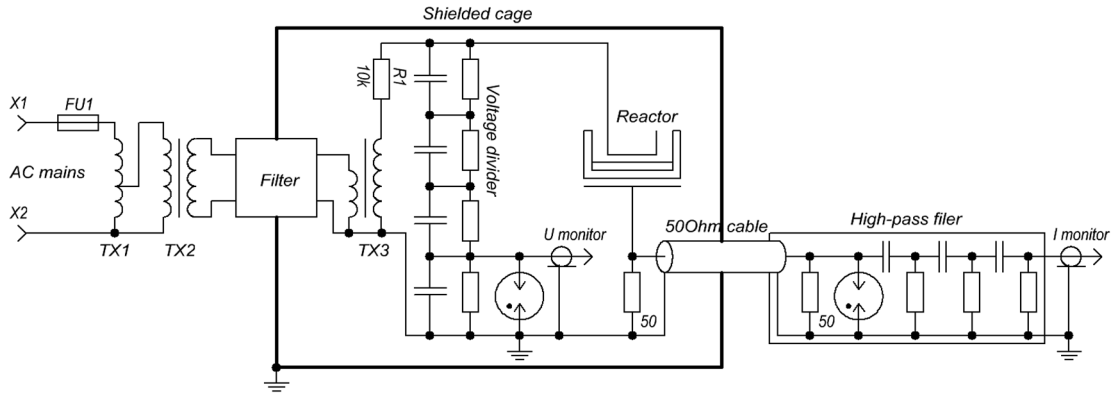

Fig. 3.1.4 Schematics of the power supply system

The voltage divider is of resistive-capacitive type and has a division factor of 1:1000. The values of its elements are chosen in such a way that the phase shift between the measured voltage and the output signal is minimized. The voltage divider works also like a capacitive buffer, thus the corona reactor is supplied from the voltage source.

The monitoring of the current requires the special precautions due to very short current patterns. Two low-inductance high-frequency resistors of the value of 50 Ohm are paced in the both sides of the cable with 50 Ohm impedance which is connected to three stage high pass filter which rejects mains 50Hz frequency and allows monitoring the fast transients which is a corona current patterns.

Both current and voltage monitors are protected with spark gaps.

Typical voltage and current profiles are presented in Fig. 3.1.5.

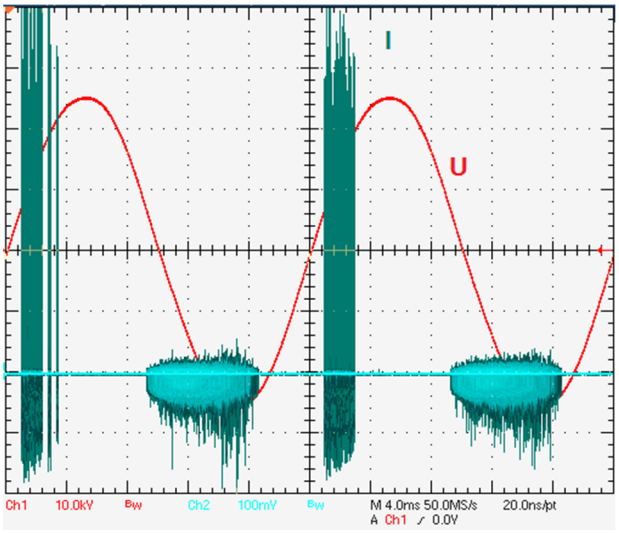

Fig. 3.1.5. Current and voltage oscillograms

A phase shift between voltage and current profiles is present (near 70°) due to the capacitive nature of the reactor. Current profile consists of many spikes. Positive corona needs higher threshold potential to start so current spikes are much stronger than for negative one. On the other hand, negative corona has much wider time range, so both kinds of discharges make a contribution to power consumption and chemical processes activation in the gas and liquid phases.

3.1.4 Experimental procedures

3.1.4.1 Determination of process efficiency and products in the liquid phase

The aqueous solutions to be subjected to plasma treatment or ozonation were prepared in milliQ pure or buffered water and contained the organic compound, typically at a concentration of $5 \cdot 10^{-4}$ M. The treated volume of the solutions was 70 mL. The efficiency of the decomposition process was determined by measuring conversion of the organic compound as a function of treatment time. To accomplish this, 0.5 mL aliquots of the treated solution were withdrawn at desired times (for example, 15, 30, 45, 60, 90, 120, 180, 240 min) and analyzed by HPLC instrument equipped with a diode array detector (DAD). The elution was followed at 210 and 270 nm in the case of phenol and substituted phenols, at

218 and 210 nm for maleic and fumaric acids. The fraction of the residual organic compound, C/C_0 was plotted against the treatment time and the data were fitted by the equation:

$$\frac{C}{C_0} = e^{-k \cdot t} \qquad (3.1.1)$$

where k is the rate constant of the process [151].

The intermediate products of phenol decomposition detected by HPLC were the following: 1,2-dihydroxybenzene, 1,4-dihydroxybenzene, *cis,cis*-muconic acid, *trans,trans*-muconic acid, fumaric and maleic acids. They were quantified by means of calibration curves built choosing the wavelength of maximum absorbance. The calibration curves were linear for concentrations up to $5 \cdot 10^{-4}$ M with correlation coefficients R^2 not less than 0.999.

When maleic and fumaric acids were subjected to plasma treatment and to ozonation on their own no decomposition products were detected by HPLC.

Most experiments were performed in buffered aqueous solutions to maintain the pH constant: the control of pH is critical in the case of plasma treatment because air plasma generates nitrous oxides, which in water are converted to nitric acid causing the pH to decrease. In the experiments the pH of the solution was varied from 1.8 to 11.3 using different pH modifiers or buffering systems. These must assure the stability of pH for at least 4 hours, which is the usual duration of the experiments. Moreover, they must be as much as possible inert with the organic compounds under investigation and with the reactive species present into the system. In Table 2.1 the four pH modifiers used are reported.

Table 3.1.1. pH modifiers and typical pH in experiments of plasma treatment

Buffer composition	initial pH	pH after plasma treatment (4 hours)
H_2SO_4 $1.7 \cdot 10^{-2}$ M	1.6 – 1.9	1.5 – 1.9
$NaHCO_3$ $4.4 \cdot 10^{-3}$ M	7.2 – 7.6	7.2 – 7.4
20% NaH_2PO_4 80% Na_2HPO_4 $4.4 \cdot 10^{-3}$ M total	7 – 7.1	6.9 – 7
Na_2CO_3 $4.4 \cdot 10^{-3}$ M	10 – 10.3	8.5 – 8.8
50% Na_2HPO_4 50% Na_3PO_4 $2.5\ 10^{-3}$ M total	11 – 11.3	10.9 – 11.1

The effective action of sulfuric acid is due to the fact that its concentration is in excess compared to that of the continuously formed nitric acid. The use of sulfuric acid was preferred to that of nitric or hydrochloric acids based on the fact that nitric acid is an oxidizer and chloride can be oxidized by hydroxyl radical to atomic chlorine, which can react with the target compound ($Cl^- + {}^\bullet OH \rightarrow ClOH^-$; $ClOH^- + H^+ \rightarrow Cl^\bullet + H_2O$) [115].

In the case of Na_2CO_3 solutions, the pH decreased by two units in 4 hours. However, due to the ${}^\bullet OH$ scavenging effect of carbonate species [115], it was preferred not to increase the concentration of this buffer salt. In some experiments phosphate buffer was used instead of hydrocarbonate to eliminate CO_2 release due to the buffer and the consequent interference in the measurement of CO_2 released by oxidation of the organic compound.

The concentration of maleic and fumaric acids in the solutions subjected to plasma treatment was equal to $5 \cdot 10^{-4}$M or $2.5 \cdot 10^{-4}$M each if used in mixture.

Conductivity and pH of the initial and final solutions were monitored during the experiments.

3.1.4.2 Determination of the gas phase composition

The determination of the concentration of ozone produced in the corona discharge and CO_2 released from the solution during the treatment of the compound were performed by FT-IR. The ozone concentration was determined by FT-IR quantitative analysis integrating the band in the range 980-1080 cm^{-1}. Calibration of the instrument response was performed by carrying out simultaneous determinations of the treated gas by FT-IR and by the well-established iodometric titration method [152]. FT-IR spectrometer was also employed for the determination of the CO_2 produced from the oxidation of maleic and/or fumaric acid. In this case the integrated band is in the range 2390-2290 cm^{-1} and the calibration was performed by analyzing three standards of CO_2 in air at a known concentration (commercial cylinders of specified concentrations of 49.2, 249.8 and 498.5 ppm).

Thanks to an automatic procedure, the measurement was performed every 3 min, which is the time necessary for the gas to flow through the line connecting the reactor to the spectrometer and to renew the gas into the cell.

The concentration of ozone produced in humid air by the DBD discharge when no water is present into the reactor is equal to about 1050 ppm. Thus, to perform the experiments of ozonation the system was adjusted to obtain the same concentration in the absence of the solution. Only once the concentration of ozone was stable, that is after about 40 minutes from the switching on of the ozonizer, the solution containing the organic compound was added into the reactor: at this point the reaction starts immediately as CO_2 emission increases rapidly and ozone concentration goes down to another stable level corresponding. The area of the IR bands of ozone and CO_2 in an ozonation experiment are shown in Fig. 3.1.6a as an example. By integrating the area under the CO_2 curve, as for example under that in Fig 3.1.6a, it is possible to obtain the total amount of CO_2 produced during the process and so the carbon percentage released in the gas phase, Fig 3.1.6b.

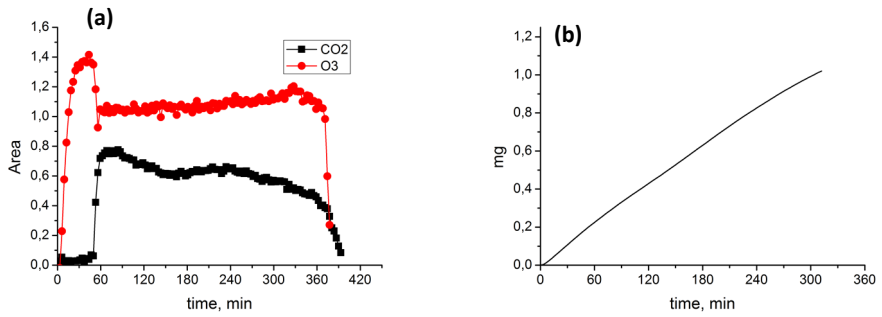

Fig. 3.1.6. (a) Area of the signals of CO_2 and ozone during an experiment of ozonation and (b) CO_2 release from the solution.

3.2 Results and discussion

3.2.1 Plasma treatment of phenol

3.2.1.1 Effect of phenol initial concentration

It is known from previous experiments performed in our group [106, 107] that phenol is efficiently decomposed by plasma treatment. The experiments were performed at an initial concentration of $5 \cdot 10^{-4}$ M in milliQ, in tap water and in solutions buffered at different pH, while the effect of the initial concentration was never investigated. In the literature it was observed that the efficiency of the decomposition of VOCs in air depends on the initial concentration of the organic pollutant [153, 154], for this reason the investigation of this effect was extended to the plasma treatments of pollutants in the liquid phase.

Solutions with six different values of phenol initial concentration, $[PhOH]_0$, namely 10^{-4}M, $1.4 \cdot 10^{-4}$M, $2 \cdot 10^{-4}$M, $5 \cdot 10^{-4}$M, $7.5 \cdot 10^{-4}$M and $5 \cdot 10^{-3}$M, were prepared in milliQ water. The decomposition process was monitored by measuring the organic pollutant conversion as a function of treatment time maintaining constant the applied voltage. To this end, at desired times the discharge was briefly interrupted and a 0.5 mL aliquot of the treated solution was withdrawn and analyzed by HPLC/UV-Vis. For aromatic compounds the absorption at the wavelength of 270 nm was used. The concentration $5 \cdot 10^{-3}$ M was too high and out of the dynamic range for HPLC analysis. Therefore, each sample was diluted by a factor of 10 before injection.

The data obtained and their exponential interpolations are shown in Fig. 3.2.1 for the experiments run at 10^{-4} M, $1.4 \cdot 10^{-4}$ M and $2 \cdot 10^{-4}$ M initial concentration of phenol.

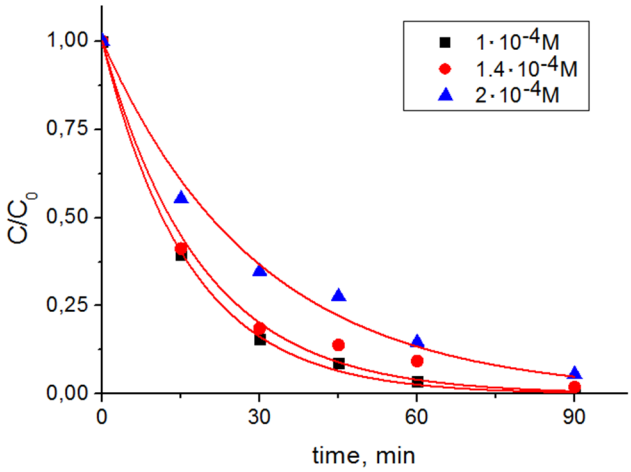

Fig. 3.2.1. Exponential interpolation of phenol conversion data for experiments run with initial concentrations of 10^{-4} M, $1.4 \cdot 10^{-4}$ M and $2 \cdot 10^{-4}$ M

It is evident that the rate of phenol decomposition depends on the pollutant initial concentration, C_0. The rate constants obtained in all the experiments run at different initial concentration of phenol are plotted as a function of the reciprocal of $[PhOH]_0$ (Fig. 3.2.2). It is evident that, within the range explored, the rate constant depends linearly on the reciprocal of $[PhOH]_0$.

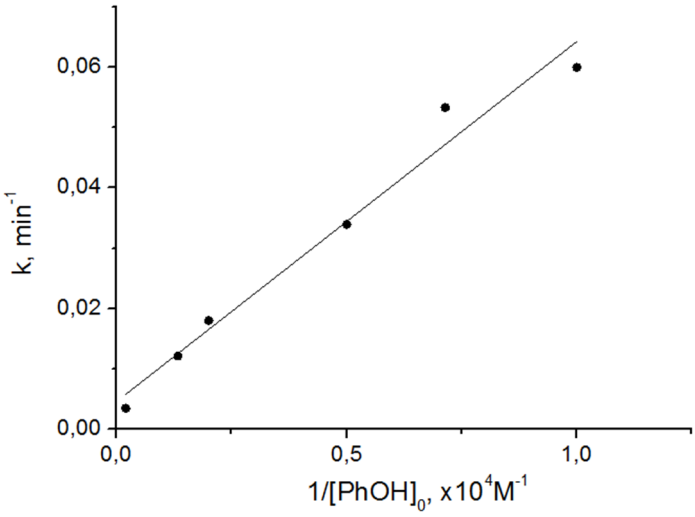

Fig. 3.2.2. Dependence of rate constant on phenol initial concentration

Thus, the lower the pollutant initial concentration the faster is its oxidation. This phenomenon is completely analogous to that observed previously for non-thermal plasma induced oxidation of volatile organic compounds in air, which is explained in terms of a mechanism of inhibition by products [153, 154]. This mechanism can be summarized by the following three reactions

$G \rightarrow X$	S
$PhOH + X \rightarrow I$ + other products	k_1
$I + X \rightarrow Z$ + other products	k_2

where X is the plasma oxidizing reactive species formed with a rate S, and I and Z are reaction intermediates. The following kinetic expressions are derived for such reaction scheme:

$$\frac{d[X]}{dt} = S - k_1[X][PhOH] - k_2[X][I] \qquad (3.2.1)$$

$$\frac{d[PhOH]}{dt} = -k_1[X][PhOH] \qquad (3.2.2)$$

By assuming that X is in the stationary state, i.e. $\frac{d[X]}{dt} = 0$, that k_1 is similar to k_2 $k_1 \approx k_2$, and that $[Z] << [I]$, as is the case in the process initial stages, so that $[PhOH]_0 = [PhOH] + [I]$, then the differential equations are integrated to provide the following kinetic expression:

$$[PhOH] = [PhOH]_0 e^{(-S/[PhOH]_0 \cdot t)} = [PhOH]_0 e^{(-k \cdot t)} \qquad (3.2.3)$$

which predicts that k depends inversely on $[PhOH]_0$ and directly on S, the rate of formation of the reactive species X. Further support for this mechanistic interpretation was obtained from the time profiles of the concentration of various reaction intermediates of phenol oxidation in our DBD reactor. Such findings are presented and discussed in the section dealing with product analysis.

3.2.1.2 Substituent effect

Despite the very strongly oxidizing properties of air non-thermal plasmas, some substrate selectivity was observed when comparing the reactivity of different mono-substituted phenols. Indeed using a set of phenols bearing different substituents on the benzene ring we found that the rate constant of oxidation under the same experimental conditions in the DBD reactor depends on the type substituent (X) and on its site of substitution. The experiments were performed with phenol, *meta*-nitrophenol (m-NO_2-), *para*-nitrophenol (p-NO_2-), *meta*-chlorophenol (m-Cl-), *meta*-dimethylamino-phenol (m-$(CH_3)_2N$-) in initial concentration of $5 \cdot 10^{-4}$ M in milliQ water. In Table 3.2.1 a summary of the obtained kinetic constants k_x is reported. The relative rates with respect to phenol were then correlated with the substituents characteristic constants in Hammett type analysis.

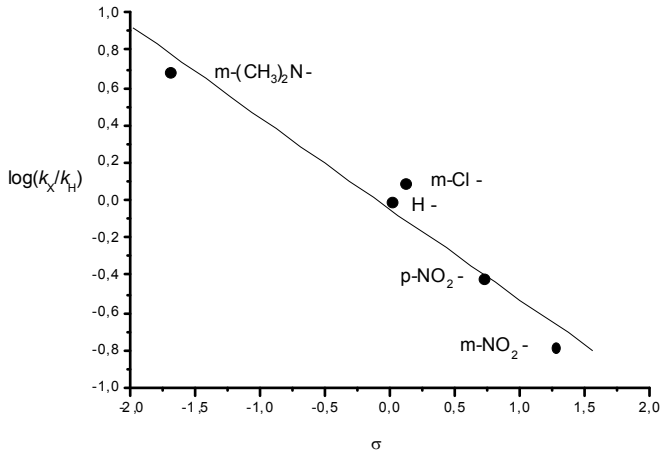

Fig. 3.2.3. Effect of substituent in phenol ring.

Table 3.2.1. The rate constants and σ–values for substituted phenols

Compound	k_X	k_X/k_H	$\log(k_X/k_H)$	σ
PhOH	0.018	1.000	0	0
m-ClPhOH	0.022	1.222	0.087	0.11
p-NO_2PhOH	0.007	0.389	-0.410	0.71
m-$(CH_3)_2$NPhOH	0.088	4.889	0.689	-1.7
m-NO_2PhOH	0.003	0.167	-0.778	1.27

As seen in Fig. 3.2.3, a reasonably good linear correlation ($r^2 > 0.97$) is found between $\log(k_X/k_H)$ and resonance sigma substituent constants (σ^+ and σ^-) [155] chosen by considering attack by an electrophilic reagent, such as the $^{\bullet}OH$ radical, at a ring position activated by the OH group. This is shown in Fig. 3.2.4 for attack at the ortho position: so for m-substitution (X) σ_p and for p-substitution (Y) σ_m were used.

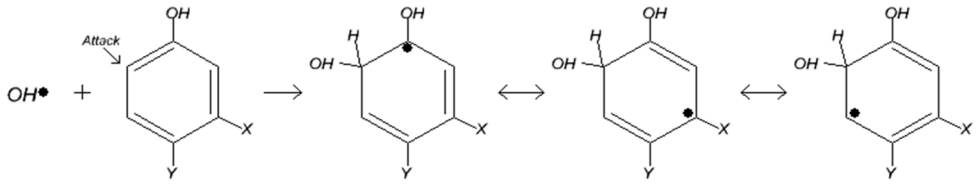

Fig. 3.2.4. Illustration of $^{\bullet}OH$ attack on substituted phenols.

The negative slope (ρ = -0,48) found for the Hammett correlation shown in Fig. 3.2.3 is consistent with such a mechanism. The very low value of such slope is typical of highly reactive/poorly selective oxidants, like the OH radical: thus a similar value (ρ = -0.41) was reported for reaction of OH radical with aromatic compounds [156]. In contrast, a ρ = -3 was reported for reaction of ozone with substituted benzenes [157]. This means that the reaction of ozone with the aromatic ring system is highly electrophilic and also highly selective [158].

3.2.1.3 Decomposition products analysis

The main byproducts of phenol decomposition detected by HPLC are substituted phenols (1,2-dihydroxyphenol, 1,4-dihydroxyphenol) and organic acids coming from the cleavage of the aromatic ring (maleic acid, fumaric acid, *cis,cis*-muconic acid and *trans,trans*-muconic acid) [106]. The typical chromatogram of the phenol decomposition products at the Fig 3.2.5 is presented. The concentration of most of them initially increases and then decreases during the treatment, while CO_2, the final oxidation product, continues to be released from the solution.

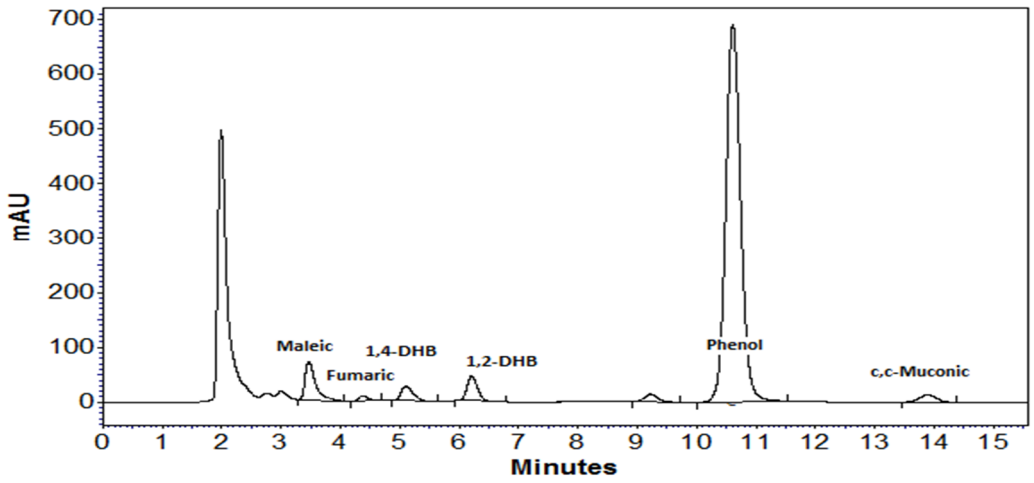

Fig. 3.2.5. Typical chromatogram of the phenol decomposition (270 nm).

For carbon balance calculation the absolute molar concentrations of the initial pollutant and of its oxidation intermediates are necessary. So, calibration of HPLC-UV response to the concentration of the intermediates was performed using solutions of authentic samples in known concentration ($1\cdot10^{-5}$ M, $5\cdot10^{-5}$ M, $1\cdot10^{-4}$ M, $5\cdot10^{-4}$ M, $1\cdot10^{-3}$ M) .

A summary of the determination of the concentration of phenol, of the intermediates detectable by HPLC and of CO_2 is presented in Table 3.2.2 for an experiment in which PhOH ($5\cdot10^{-4}$ M) was treated for 180 min in the corona-DBD reactor.

Table 3.2.2. The concentration of the products of phenol decomposition

t, min	[PhOH] , M	maleic acid, M	fumaric acid, M	1,4-DHB, M	1,2-DHB, M	c,c muconic acid, M	CO_2, M [a]	% C_{undet}
0	2.0E-04	0.0	0.0	0.0	0.0	0.0	0.0	0
30	1.1E-04	1.3E-06	2.1E-07	2.0E-06	1.1E-06	1.7E-06	3.4E-06	39
60	7E-05	1.7E-06	2.2E-07	1,9E-06	1.1E-06	2.0E-06	8.2E-06	57
90	4.1E-05	2.5E-06	1.3E-07	1,7E-06	8.4E-07	1.6E-06	1.3E-05	69
120	2.3E-05	2.5E-06	1.2E-07	9,8E-07	8.2E-07	1.1E-06	1.8E-05	76
180	4.3E-06	2.3E-06	0.0E+00	1,7E-07	3.2E-07	4.3E-07	2.8E-05	82

The percentage of undetected carbon was calculated using the following formula:

$$\%C_{un\,\det} = \left[\frac{C_{tot} - C_{\det}}{C_{tot}}\right] \cdot 100\% = \left[1 - \frac{moles_{CO_2} + \sum_i n_i \cdot moles_i}{6 \cdot \left(moles_{PhOH}\right)_0}\right] \cdot 100\% \qquad (3.2.4)$$

where m_i is the number of moles of species *i* (phenol and intermediates) and n_i is the number of carbon atoms in species *i* (i.e. 6 for phenol, 4 for maleic acid and so forth).

It can be seen that the detected intermediates are always present in very small amounts and are decomposed in subsequent oxidation steps. It is also seen that significant amounts of carbon remain undetected by our analyses. Moreover, the fraction of undetected carbon goes up in time and this means that some organic material accumulates in solution which is more stable than the precursor phenol.

The TOC analysis shows that the carbon unaccounted for is due to the formation of organic byproducts not detectable by HPLC-UV-Vis. Effectively, it was demonstrated before that, even if the HPLC column and the analysis conditions used are specific for the determination of organic acids, the peak due to nitric acid coelutes with those due to short chain organic acids as formic, acetic and oxalic, making their detection and quantification not viable under these conditions. It has to be underlined that the toxicity of such short-chain organic acids is much lower compared to that of phenol.

3.2.1.4 Intermediates decomposition kinetics

Besides evaluating the carbon balance, quantitative chromatographic analysis allows to follow the concentration of the intermediates during the treatment. This gives some indication of their degradation reactivity relative to that of the phenol precursor. The main products of phenol decomposition in plasma-liquid system detected by HPLC are maleic and fumaric acids, catechol, hydroquinone and, in very small amounts, muconic acid isomers (mainly *cis,cis*-muconic acid). It can be supposed that at first phenol reacts with an oxidizing agent with rate constant k_1 and then each intermediate (*I*) reacts with another oxidizing species with the rate constant k_2:

$$PhOH + X \rightarrow^{k_1} I$$
$$I + X \rightarrow^{k_2} products$$

Assuming that the decomposition of the intermediates has a pseudo-first order kinetic as the initial compound, the concentration of each intermediate can be described by eq. (3.2.5) [159]:

$$C_{\text{int}}(t) = A[e^{-x(t)} - e^{-Bx(t)}] \qquad (3.2.5)$$

Where:

$$A = \alpha[PhOH]_0 \frac{k_1}{k_2 - k_1}$$

$$B = \frac{k_2}{k_1},$$

$$x = \ln([PhOH]_0 / [PhOH]_t)$$

α is the yield of the reaction of phenol with X. Thus, interpolating the ratio between the concentration of each intermediate and the initial phenol concentration with respect to *x*, it is possible to obtain k_2. In Table 3.2.3 and in Fig. 3.2.6 the results of this analysis carried out for a phenol solution with initial concentration $5 \cdot 10^{-4}$ M are presented.

Table 3.2.3. Calculated rate constants determined phenol products decomposition

Constant	**Maleic acid**	**Fumaric acid**	**1,4-DHB**	**1,2-DHB**	**c,c-muconic acid**
$A/[PhOH]_0$	-0.027	0.0076	0.06	0.088	0.171
B	0.096	1.87	1.64	1.188	1.168
k_2, min^{-1}	0.0017	0.034	0.03	0.021	0.018

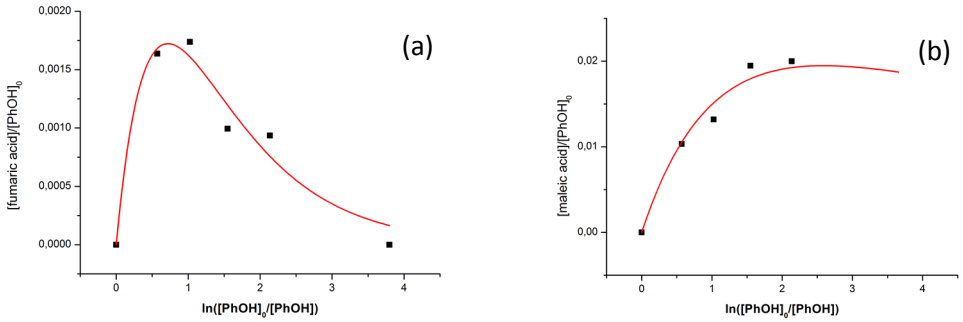

Fig. 3.2.6. Fumaric acid (a) and maleic acid (b) interpolation according to the procedure indicated in the text.

These results show a big difference in the reactivity of fumaric and maleic acids. Furthermore, $B < 1$, found for maleic acid, could indicate that it is less reactive than phenol and needs a longer treatment time to be decomposed. However, due to the dependence of the reactivity on the initial concentration of the organic compounds in plasma systems, no trustful conclusions can be drawn. For this reason fumaric and maleic acids were subjected to independent decomposition experiments to investigate on their behavior in this system when they are treated separately and in mixture. A thorough and detailed investigation aimed at understanding the mechanism of decomposition of these compounds was moreover undertaken and is presented in the next paragraphs.

3.2.2 Plasma treatment and ozonation of maleic acid

Due to the influence of pH on the reactive species present into the system and on the dissociation states of maleic and fumaric acids, the experiments with these compounds were performed by buffering the solution at different pH. Moreover, to investigate on the mechanism of decomposition of these compounds and on its dependence on the pH of the solution, the results obtained in plasma treatment were compared to those achieved in ozonation experiments.

DBD produces a high amount of ozone which is considered an important agent in the plasma oxidation processes. In water ozone can react directly with the target compound, generally by addition to a double bond, or can be decomposed giving rise to the production

of OH radical [160], which has a higher oxidation potential than ozone and reacts with every organic compound.

The comparison of the oxidation process of maleic and fumaric acids induced by plasma with the process induced by ozone can clarify the role of ozone and of OH radical in the plasma oxidation process.

To achieve an interaction of ozone with the organic compounds as similar as possible to that which takes place in the plasma-induced process, the same reactor used in the experiments with plasma was also employed in the ozonation experiments, the concentration of ozone was adjusted to be equal to that produced by the DBD discharge and ozone was not bubbled into the solution but simply flowed above the water surface at the same flow rate employed in the experiments with plasma. In the case of plasma treatment the discharge generates the so called 'ion wind' which is a stream of ionized gas which moves the water surface. In the case of ozonation, the first experiments were performed under static conditions, but, as reported in paragraph 3.2.4.5, the decay of the organic compounds proceeded irregularly. For this reason the following experiments, reported in this paragraph, were carried out by magnetically stirring the solution.

In Fig. 3.2.8 the decomposition of maleic acid ($5 \cdot 10^{-4}$ M) induced by plasma treatment and by ozonation is shown as a function of treatment time for the different pH investigated. The curves have been fitted by an exponential function (eq. 3.1.1) and the kinetic constants obtained are reported in Table 3.2.4.

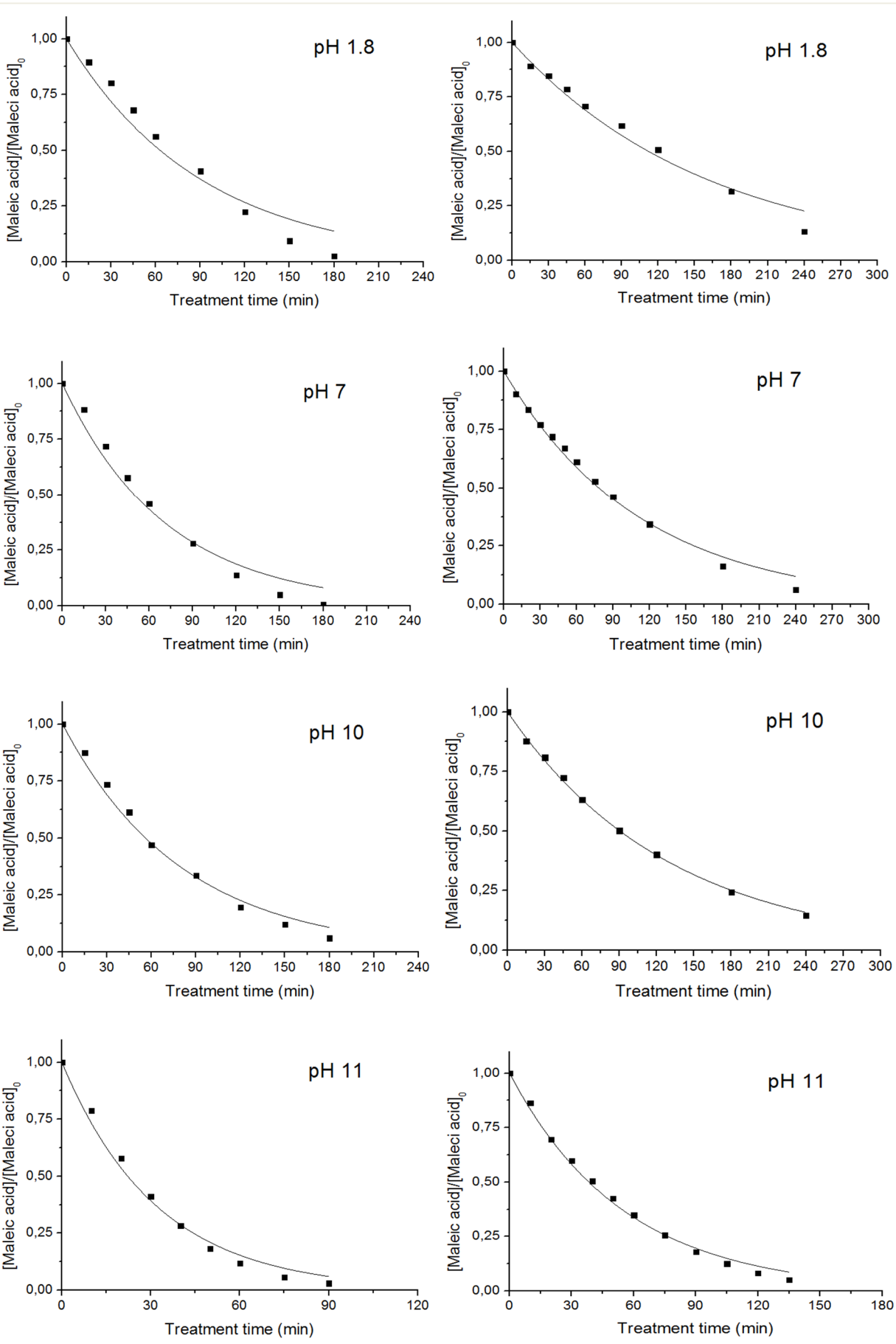

Fig. 3.2.7. Decomposition of maleic acid ($5 \cdot 10^{-4}$ M) in aqueous solution at pH: 1.8, 7, 10 and 11 by (left) plasma treatment and (right) ozonation.

Table 3.2.4. Observed rate constants determined for maleic acid decomposition

Experimental conditions	Plasma: k, min^{-1}	Ozonation: k, min^{-1}
pH 1.8 (H_2SO_4 $1.7\cdot10^{-2}$ M)	0.011	0.0062
pH 7 ($NaHCO_3$ $4.4\cdot10^{-3}$ M)	0.014	0.0089
pH 10 (Na_2CO_3 $4.4\cdot10^{-3}$ M)	0.013	0.0077
pH 11.3 (Na_2HPO_4/Na_3PO_4 $2.5\cdot10^{-2}$ M)	0.031	0.018

It is seen from the plots in Fig. 3.2.7 that a significant deviation from the exponential decay ($R^2 \leq 0.98$) was observed for the data obtained in the plasma treatment at pH 1.8 and 7 and in ozonation at pH 1.8. These data appear to be following more a linear than an exponential decay. The shape of the obtained curves is important to have an idea of the ratio between the rate of formation of the reactive species and their rate of reaction with the organic compounds present in solution. In our experiments the discharge is applied after the solution has been introduced into the reactor; thus, if the reactive species do not reach a stationary concentration in a time negligible with respect to that for their reaction with the organic molecules, they are consumed as fast as they are formed and this gives rise to a decay of the organic molecule which is initially linear. This behavior is shown in the simulation in Fig. 3.2.8 (blue line), performed considering reactions (3.2.6)-(3.2.8).

S, generically indicated as the rate of formation of the oxidant *Ox*, is assumed to be constant and is intended as the rate with which *Ox* is available in solution. Based on its identity, this oxidant can be formed in the gas phase and transferred into the solution (as for example O_3) or require an additional conversion step (as for example $^{\bullet}OH$ formed from O_3). k_m is the rate of the reaction of *Ox* with the organic molecule M and k_{Ox} is the rate of decomposition of the oxidant (by self-decomposition or by scavenging by a different species which is in excess compared to the oxidant itself).

$$G \rightarrow Ox \qquad S \qquad (3.2.6)$$

$$M + Ox \rightarrow I \qquad k_m \qquad (3.2.7)$$

$$Ox \rightarrow ... \qquad k_{Ox} \qquad (3.2.8)$$

The simulation results come from the resolution of the following equations:

$$\frac{d[M]}{dt} = -k_m[Ox][M] \qquad (3.2.9)$$

$$\frac{d[Ox]}{dt} = S - k_m[Ox][M] - k_{Ox}[Ox] \qquad (3.2.10)$$

When treated with plasma, the rate of reaction of maleic acid increases in the order pH 1.8 < pH 7 ≈ pH 10 << pH 11 (Table 3.2.4). The same trend is observed in the case of ozonation. Comparing the observed rates of plasma treatment and ozonation, it is evident that plasma is more efficient than ozonation under all pH conditions. The rate constants of the plasma process are always higher than those of ozonation by a factor of about 1.6-1.7. Thus, it seems that in plasma there is an additional contribution which is constant under all pH conditions. Based on what was found in previous experiments [106], this can be ascribed to the fact that plasma induces the formation of additional reactive species besides ozone, notably OH radicals, whose rate constant with maleic acid is independent on pH (Table 3.2.5).

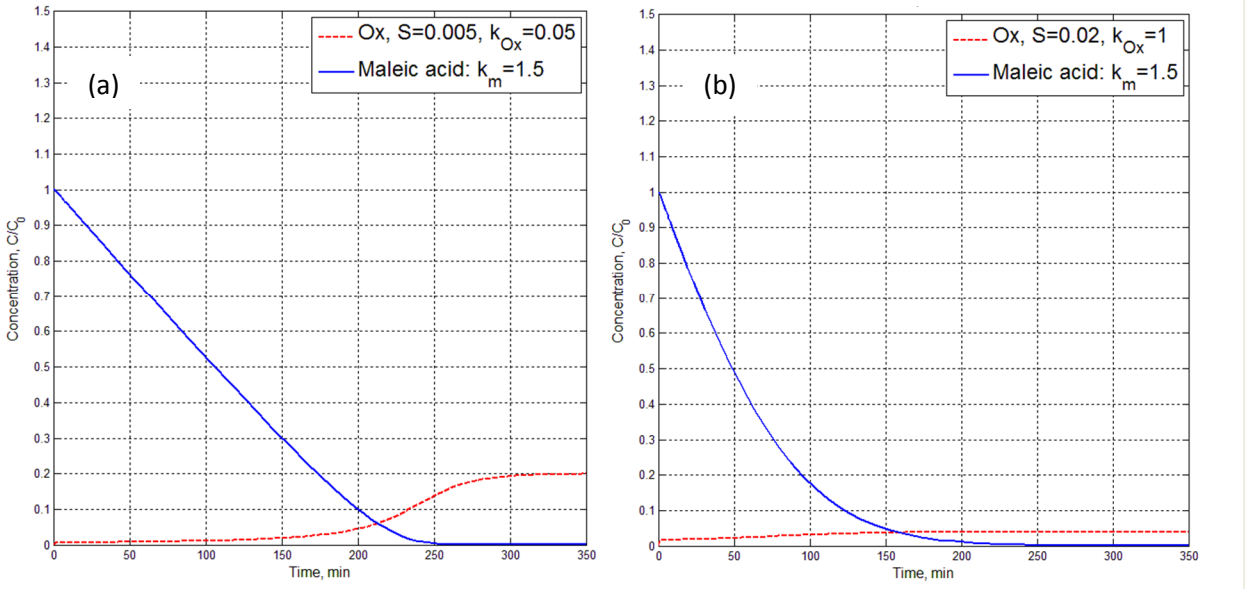

Fig. 3.2.9. Simulations of the decay of an organic compound, maleic acid, (blue line) reacting with an oxidant (dot red line) present in defect (a) or in quasi-stationary concentration (b).

Table 3.2.5 Kinetic constants for reaction of maleic and fumaric acids with ozone and with OH radical

Acid	pK_a	k_{O3}			k_{OH}[d]
		Free acid	Monoanion	Dianion	(pH 4-10.5)
Maleic acid	1.6, 6.1	$1.4 \cdot 10^3$ [a]	$4.2 \cdot 10^3$ [a]	$\sim 7 \cdot 10^3$ [a]	$6 \cdot 10^9$
			$1 \cdot 10^3$ [b]	$5 \cdot 10^3$ (pH 6)[b]	
				$2.4 \cdot 10^4$ [c]	
Fumaric acid	3.0, 4.4	$8.5 \cdot 10^3$ [a]	$2.65 \cdot 10^4$ (pH 3.1)[a]	$\sim 6.5 \cdot 10^4$ [a]	$6 \cdot 10^9$
			$6 \cdot 10^3$ (pH 2)[b]	$1 \cdot 10^5$ (pH 5)[b]	

[a] A. Leitzke, C. von Sonntag. *Ozone Sci. Eng.* **2009**, *31*, 301.

[b] Hoigné, H. Bader. *Water Res.* **1983**, *17*, 185.

[c] W.A. Pryor, D.H.Giamalva, D.F. Church. *J. Am. Chem. Soc.* **1984**, *106*, 7094.

[d] Buxton, G.V., Greenstock, C.L., Helman, W.P., Ross, A.B. J. Ph. Chem. Ref. Dat. **1988**, 17, 513-886.

In particular, experiments performed recently in our group, demonstrate that if t-BuOH, a known quencher of $^{\bullet}OH$ which does not react with ozone, is added in large excess ($5 \cdot 10^{-2}$ M) to a phenol solution ($5 \cdot 10^{-4}$ M) and this mixture is subjected to plasma treatment, the decomposition of phenol is significantly slowed down by the competition of t-BuOH for OH radicals. Moreover, if t-BuOH is treated alone ($5 \cdot 10^{-4}$ M) by plasma at pH 7, it is decomposed; on the contrary, if it is subjected to ozonation under the same conditions it does not react. An important thing which must be taken into account and that the above described experiments aimed to clarify is that in the air plasma experiments there can be two sources of OH radicals: one is plasma itself, in which $^{\bullet}OH$ can be formed by dissociation of water (reaction 3.2.11) or by reaction of atomic oxygen with water (reaction 3.2.12) [1], the other is the decomposition of ozone in water. As mentioned in the introduction, this second process [83, 93, 114, 161, 162] is favored at basic pH values.

$$H_2O + e^- \rightarrow {}^{\bullet}OH + H \qquad (3.2.11)$$

$$O(^1D) + H_2O \rightarrow 2\,{}^{\bullet}OH \qquad (3.2.12)$$

$$O_3 + {}^{-}OH \rightarrow O_2^{-\bullet} + HO_2^{\bullet} \qquad (3.2.13)$$

$$O_3 + HO_2^{\bullet} \rightarrow 2O_2 + {}^{\bullet}OH \qquad (3.2.14)$$

$$O_3 + {}^{\bullet}OH \rightarrow O_2 + HO_2^{\bullet} \qquad (3.2.15)$$

$$O_3 + O_2^{-\bullet} \rightarrow O_3^{-\bullet} + O_2 \qquad (3.2.16)$$

$$O_3^{-\bullet} + H^+ \rightarrow HO_3^{\bullet} \qquad (3.2.17)$$

$$HO_3^{\bullet} \rightarrow O_2 + {}^{\bullet}OH \qquad (3.2.18)$$

Experiments of ozonation of t-BuOH alone ($5 \cdot 10^{-4}$ M) were carried out in our group at different pH values to verify in which conditions of pH ozone is efficiently converted into OH radical. The results (unpublished) showed that in ozonation experiments t-BuOH reacts only at pH 11, suggesting that at pH 1.8 and 7 no significant amounts of $^{\bullet}OH$ are produced from ozone. Thus, we can conclude that the conversion of t-BuOH observed in plasma treatment experiments at pH 1.8 and 7 is due to OH radicals produced directly by the discharge.

Taking into account these findings in the evaluation of the results obtained in the experiments described here, it is possible to conclude that the decomposition of maleic acid induced by ozonation at pH 1.8 and 7 is due only to reaction of the acid with ozone, while at pH 11 there is also a contribution by the reaction with OH radicals formed from the decomposition of ozone. Considering that the rate constant of the reaction of $^{\bullet}OH$ with maleic acid is six orders of magnitude higher than that with ozone (Table 3.2.5), this conclusion explains why at pH 11 the decomposition of maleic acid proceeds with a rate constant which is about twice that obtained at pH 1.8 and 7 (Table 3.2.4). On the contrary, the slight increase in the rate constants observed at pH 7 with respect to pH 1.8 (Table 3.2.4)

can be related to the different dissociation state of maleic acid at these two different pH values (pK_{a1}=1.6, pK_{a2} = 6.1) and to the different rate constants for reaction with ozone of the undissociated acid, the monoanion and the dianion (Table 3.2.5): at pH 1.8 maleic acid is about half undissociated and half monodissociated, while at pH 7 it is almost completely doubly dissociated (Table 3.2.5).

In the case of plasma treatment the dependence of the process efficiency on pH is analogous to that observed in the case of ozonation. Considering that the reaction of $^{\bullet}OH$ with maleic acid is independent on pH, this leads to conclude that the main contribution to the decomposition of maleic acid induced by plasma at pH values of 1.8 and 7 is due to ozone; OH radicals participate to the oxidation process determining an increase in efficiency with respect to simple ozonation but are not responsible for the main process.

A separate comment deserves the case of pH 10: while previous experiments allowed us to conclude that bicarbonate used in $4.4 \cdot 10^{-3}$ M concentration to obtain pH 7 is not able to compete for OH radical [107], recent experiments with t-BuOH show that carbonate $4.4 \cdot 10^{-3}$ M used to obtain pH 10 does indeed act as a competitor for OH radicals. Indeed, the rate constant for the reaction of carbonate with OH radicals, equal to $3.9 \cdot 10^{8}$ $M^{-1}s^{-1}$ [115], is about 50 times higher than that of bicarbonate. Thus, this competition explains why the results obtained at pH 10, both in ozonation and plasma treatment, differ significantly from those obtained at pH 11 also if the dissociation state of maleic acid is the same at these two pH values.

3.2.3 Plasma treatment and ozonation of fumaric acid

The oxidative removal of fumaric acid induced by plasma treatment and by ozonation at different pH values is shown in Fig. 3.2.9. As in the case of maleic acid, plasma treatment is more efficient than ozonation. The order of reactivity as a function of pH is pH 1.8 < pH 7 ≈ pH 10 ≈ pH 11. This order is in agreement with the reaction rates of fumaric acid with ozone because at pH 1.8 fumaric acid is undissociated and has a lower kinetic constant with respect to that of the completely dissociated form, which is the one present at pH 7, 10 and 11 (pKa1 = 3.0, pKa2 = 4.4). As in the case of maleic acid, the higher rates obtained in

the oxidation induced by plasma are ascribed to the additional contribution of OH radicals produced by the electrical discharge. On the contrary, if at pH 11 the conversion of ozone to $^{\bullet}OH$ does not induce any significant increase in the decomposition rate of fumaric acid either in ozonation or in plasma treatment, as is instead observed in the case of maleic acid, this can be ascribed to the relative reactivity of fumaric acid with ozone and with $^{\bullet}OH$ and to the higher reactivity of fumaric acid with ozone with respect to that of maleic acid (Table 3.2.6).

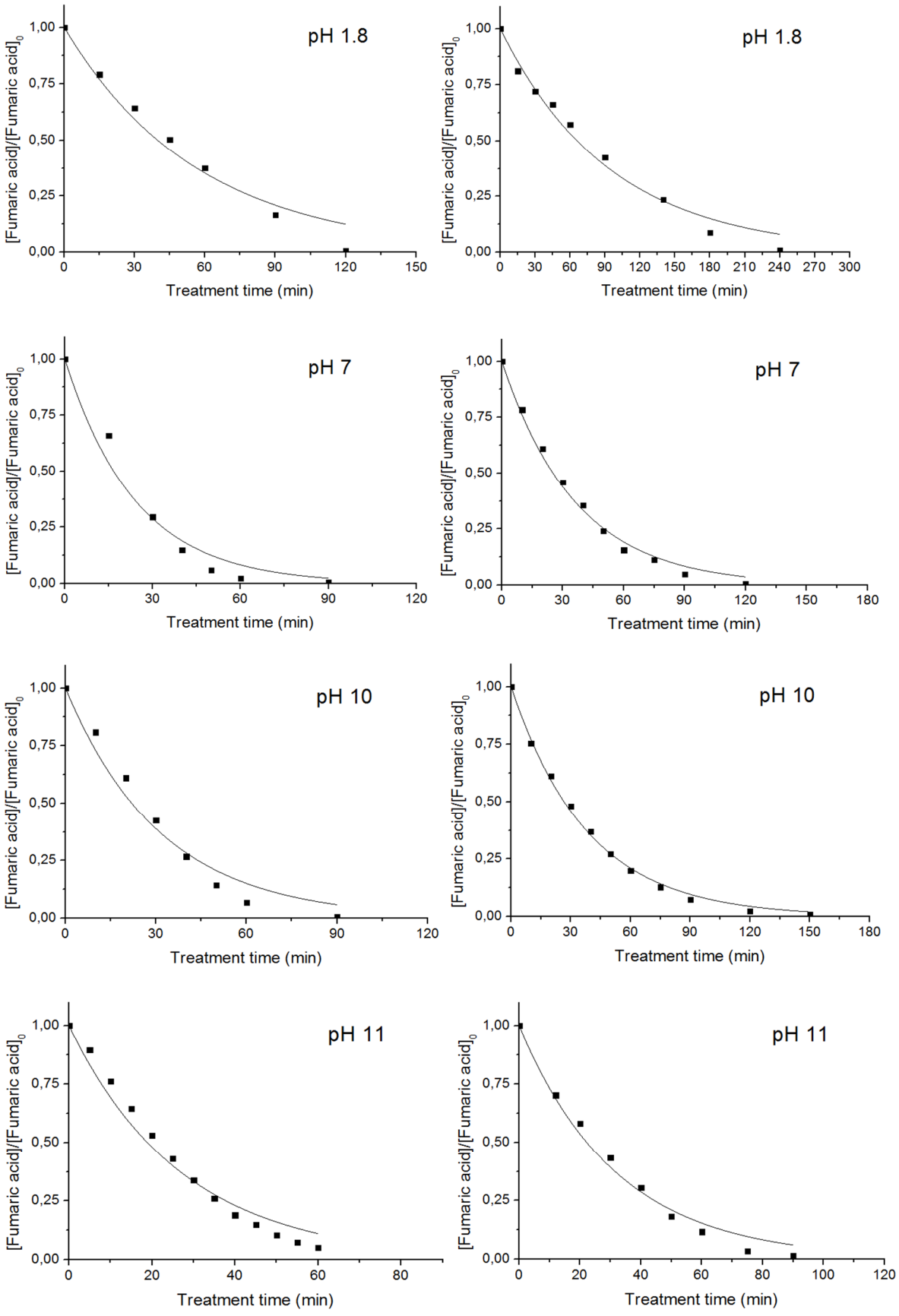

Fig. 3.2.9. Decomposition of fumaric acid ($5 \cdot 10^{-4}$ M) in aqueous solution at pH: 1.8, 7, 10 and 11 by (left) plasma treatment and (right) ozonation.

Table 3.2.6 Observed rate constants determined for fumaric acid decomposition

Experimental conditions	Plasma: k, min^{-1}	Ozonation: k, min^{-1}
pH 1.8 (H_2SO_4 $1.7\cdot10^{-2}$ M)	0.018	0.011
pH 7 ($NaHCO_3$ $4.4\cdot10^{-3}$ M)	0.042	0.028
pH 10 (Na_2CO_3 $4.4\cdot10^{-3}$ M)	0.032	0.026
pH 11.3 (Na_2HPO_4/Na_3PO_4 $2.5\cdot10^{-2}$ M)	0.037	0.031

The competition between reaction with ozone and reaction with OH radical depends on the products of their kinetic constant and concentration. While the kinetic constants of the reaction of maleic and fumaric acid with $^{\bullet}OH$ are the same, the kinetic constant of the reaction of fumaric acid with ozone is one order of magnitude higher than that of maleic acid (Table 3.2.5). Assuming that the decomposition of maleic acid induced by plasma at pH 11 is solely due to the reaction with $^{\bullet}OH$, as discussed in the previous section, and considering that $^{\bullet}OH$ is present at a stationary concentration, this can be estimated as follows from the k_{obs} value reported in Table 2.1: $[^{\bullet}OH] = k_{obs}/k_{OH} = 8.6\cdot10^{-14}$ M. If the higher decomposition rate of fumaric with respect to maleic acid is due to the contribution of ozone, one can estimate from equation (3.2.19) (M = fumaric acid) that the stationary concentration of ozone which reacts with fumaric acid is $1.53\cdot10^{-9}$ M and that it induces an increase of the reaction rate of fumaric acid from 0.031 min^{-1} to 0.037 min^{-1}. Using this estimated stationary concentration of ozone ($1.53\cdot10^{-9}$ M), one can now evaluate the contribution of the reaction with ozone in the decomposition of maleic acid induced by plasma at pH 11 (eq. 3.2.19, M = maleic acid): it is evident that this contribution is negligible as it would not change significantly the observed rate constant (0.032 min^{-1} vs 0.031 min^{-1}).

$$-\frac{d[M]}{dt} = [M](k_{OH}[^{\bullet}OH] + k_{O_3}[O_3]) \qquad (3.2.19)$$

The above reasoning and calculations were useful to clarify that indeed the reaction with ozone can be really significant only for one of the two isomeric acids, fumaric, whereas they do not allow to conclude that the decomposition of maleic acid depends uniquely on the reaction with $^{\bullet}OH$. However, considering the little difference between the rate of decomposition of maleic and fumaric acids induced by plasma at pH 11, it can be reasonably concluded that, since $^{\bullet}OH$ reacts with the same kinetic constant with both acids (Table 3.2.5), under these conditions this is the species which plays the major role in the oxidation of both acids.

3.2.4 Plasma treatment and ozonation of binary mixtures

Most of the studies on the application of plasma to the treatment of organic pollutants published in the literature deal with the oxidation of a single organic compound. This is due to the need of simplifying an extremely complex system, so this is still under study and development. To approach more realistic conditions, we have undertaken the study of binary mixtures and chosen to start with a mixture of two intermediates of phenol oxidation, maleic and fumaric acids. Since both are formed from phenol, they constitute a mixture of practical interest.

When two compounds are treated together they can compete for the same reactive species. On the other hand, as discussed in previous paragraphs, the decomposition efficiency of a single compound depends on its initial concentration due to the competition for the reactive species by its own reaction products/intermediates. For this reason to compare the reactivity of a compound when treated alone and in mixture, the initial concentration of the compounds must be carefully considered. In the experiments described here, the initial concentration of the compounds was halved with respect to the experiments in which they were treated as single compounds. It has to be considered that when two compounds are treated in mixture three different scenarios are possible:

- the two organic compounds react with different oxidizing species, thus they do not influence each other. The kinetic constants obtained in the experiments in mixture

are equal to those obtained when the compounds are treated individually at the same initial concentration;

- the two organic compounds react with the same oxidizing species, thus their competition for it (or them) can be evaluated by comparing the k obtained in the experiments in mixture with those obtained in experiments of treatment of a single compound at a double initial concentration. Therefore, the competition between the two compounds (Compound **1** $2.5 \cdot 10^{-4}$ M + Compound **2** $2.5 \cdot 10^{-4}$ M) was compared with the "autocompetition" of the single compound (Compound **1** $2.5 \cdot 10^{-4}$ M + Compound **1** $2.5 \cdot 10^{-4}$ M);
- the decomposition efficiency of the organic compounds increases or decreases when they are treated in mixture because one of them or a species originating from one of them reacts with the other.

The first experiments of plasma treatment and ozonation of the mixture of maleic and fumaric acids were performed at pH 7. The decomposition curves obtained are reported in Fig. 3.2.10.

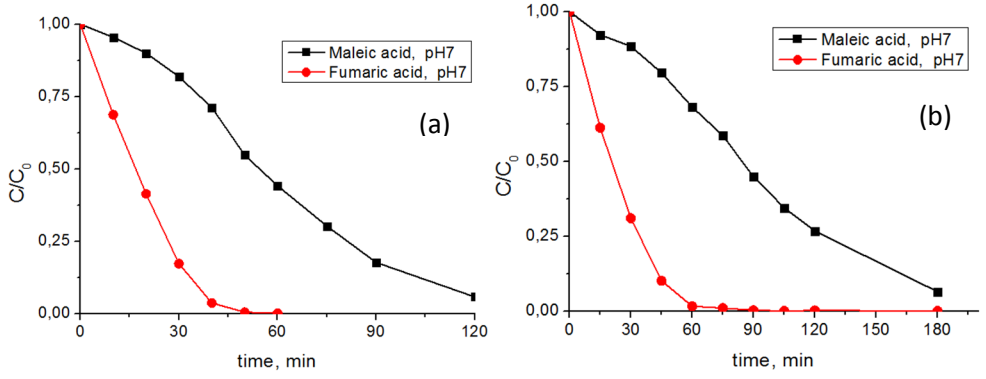

Fig. 3.2.10. Decomposition of a 1:1 mixture of maleic and fumaric acids ($2.5 \cdot 10^{-4}$ M each) in aqueous solution at pH 7 by (a) plasma treatment and (b) ozonation.

It can be seen that the concentration vs reaction time profiles of these acids change dramatically when they are treated in mixture: in particular the decomposition of maleic acid shows an induction period in which its reaction is slowed down by the presence of fumaric acid and an acceleration when fumaric acid is significantly decomposed. The results

show that in all cases the trend which is observed is not typical of a simple competition of the two acids for the reactive species, as this would affect the pseudo-first order kinetic constant but entail an independent decomposition process for each acid. On the contrary, only fumaric acid is removed with a pseudo-first order kinetics, while the concentration of maleic acid remains the same or decreases only slightly during the oxidation of fumaric acid, and decreases exponentially only when fumaric acid is totally decomposed.

Different hypotheses were considered to explain this particular behavior. One is the possibility of an isomerization reaction between the two compounds. However, this hypothesis was ruled out since no significant amount of the other isomer was detected in the experiments performed with only one of the acids. Moreover, in the literature it is reported that ozonation does not induce the isomerization of maleic and/or fumaric acid in water [163]. Before investigating in more detail the decomposition of these two acids, other model mixtures were considered to understand if the behavior of maleic and fumaric acids in mixture is typical of their specific combination or of the experimental system under study.

3.2.4.1 Plasma treatment of a mixture of phenol and m-chlorophenol

The first mixture chosen to be compared with that of maleic and fumaric acids was composed by phenol and m-chlorophenol, two similar compounds, which, when treated separately in milliQ water, gave similar decay constants (see Table 3.2.1 in paragraph 3.2.1.2). If, when treated in mixture at a halved concentration, these are decomposed independently each from the other, it will be expected that both decay exponentially with about the same rate constant observed when they are treated alone at a double concentration. The separate treatment of the two compounds was performed at pH 7 in hydrocarbonate buffer $4.4 \cdot 10^{-3}$ M at the same initial concentration ($C_{Phenol} = C_{mClPhenol} = 5 \cdot 10^{-4}$M) used in the experiments in pure milliQ water. The results are reported in Fig. 3.2.11a and in Table 3.2.7. The kinetic constants of the two compounds at pH 7 differ by 15%, which is similar to the 18% previously found in milliQ water (Table 3.2.1).

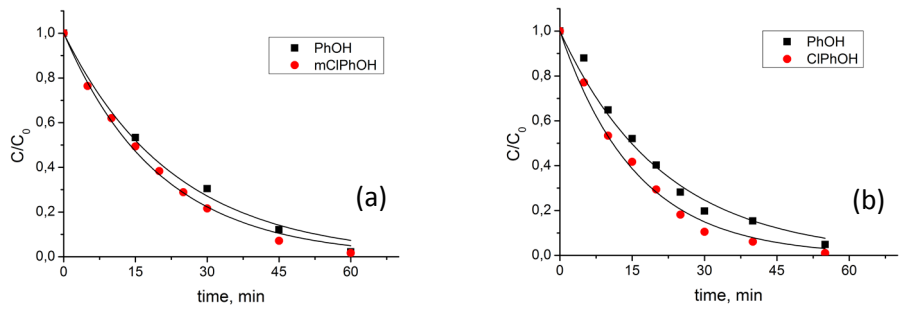

Fig. 3.2.11. Decomposition of phenol and m-chlorophenol treated separately (a) and in mixture (b) at pH 7.

Table 3.2.7. Rate constants for phenol and m-chlorophenol decay in plasma treatment at pH 7 ($4.4 \cdot 10^{-3}$M $NaHCO_3$).

Experiment	k_{phenol}, min^{-1}	$k_{m\text{-}chlorophenol}$, min^{-1}
Phenol alone ($C_0 = 5 \cdot 10^{-4}$M)	0.043	–
m-Chlorophenol alone ($C_0 = 5 \cdot 10^{-4}$M)	–	0.050
Phenol and m-chlorophenol in mixture ($C_0 = 2.5 \cdot 10^{-4}$M for each)	0.046	0.062

In Fig. 3.2.11b and in Table 3.2.7 the results are reported of an experiment in which phenol and m-chlorophenol were treated in mixture, each being present at an initial concentration ($C_{Phenol} = C_{mClPhenol} = 2.5 \cdot 10^{-4}$M) which is half of that used in the experiments in which they were treated separately. The rate constant obtained for m-chlorophenol is slightly higher than that obtained when it is treated separately. Nevertheless, the good exponential fitting obtained for both compounds induces to conclude that phenol and m-chlorophenol do not interact with each other but only compete for the oxidating species, so their decomposition channels are independent.

3.2.4.2 Plasma treatment of a mixture of phenol and maleic or fumaric acid

The next step for better understanding the anomalous competition process between maleic and fumaric acids consisted in performing an experiment with each acid in mixture with phenol. The initial concentration of each compound was equal to $2.5 \cdot 10^{-4}$ M

and the pH was equal to 7. The decay curves obtained are shown in Fig. 3.2.12 and the rate constants are reported in Table 3.2.8.

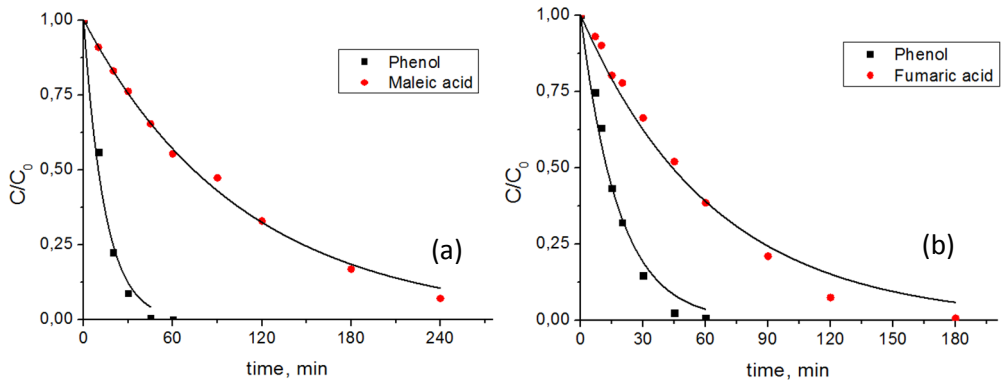

Fig. 3.2.12. Phenol and maleic acid (a) or fumaric acid (b) decomposition in mixture at pH 7.

Table 3.2.8. Comparison of the rate constants of maleic acid, fumaric acid and phenol treated separately and in mixtures at pH 7 ($4.4 \cdot 10^{-3}$M $NaHCO_3$).

Experiment	k_{Phenol}, min^{-1}	$k_{maleic\ acid}$, min^{-1}	$k_{fumaric\ acid}$, min^{-1}
Phenol and fumaric acid in mixture ($C_0 = 2.5 \cdot 10^{-4}$M for each)	0.055	–	0.016
Phenol and maleic acid in mixture ($C_0 = 2.5 \cdot 10^{-4}$M for each)	0.070	0.0093	–
Phenol alone ($C_0 = 2.5 \cdot 10^{-4}$M)	0.10	–	–
Phenol alone ($C_0 = 5 \cdot 10^{-4}$M)	0.045	–	–

The addition of maleic or fumaric acid decreases the decomposition rate of phenol. However, due to the difference in reactivity between phenol and the two acids and to the fact that maleic and fumaric acids are intermediate products of the phenol decomposition, it is difficult to make any prediction. The significant result obtained in these experiments is that the shape of the decomposition curve of any compound in the mixtures is not modified by the presence of the other component.

3.2.4.3 Plasma treatment and ozonation of a 1:1 mixture of maleic and fumaric acids at different pH

Once verified that the oxidation behavior of fumaric and maleic acids induced by plasma and by ozonation observed when the two compounds are treated in mixture at pH 7 is typical of them, the investigation was extended to the other pH values studied in the case of the decomposition of the single compounds, i.e. pH 1.8, 10 and 11. The ratio of the two compounds in the mixtures was maintained equal to 1:1 and the concentration of each acid was half of that used when studied alone, i.e. $2.5 \cdot 10^{-4}$ M each. In Fig. 3.2.13 the results obtained in the experiments are shown, while in Table 3.2.9 the observed rate constants of the curves which follow an exponential decay are reported.

Table 3.2.9. Observed rate constants determined for maleic and fumaric acids decomposition treated in mixture

Experimental conditions	Maleic acid $2.5 \cdot 10^{-4}$ M k, min^{-1}		Fumaric acid $2.5 \cdot 10^{-4}$ M k, min^{-1}	
	Plasma	Ozonation	Plasma	Ozonation
pH 1.8	-	-	0.025	0.014
pH 7	-	-	0.052	0.041
pH 10	0.014	-	0.042	0.030
pH 11	0.025	0.016	0.039	0.031

The shapes of the decomposition curves obtained in the case of plasma treatment and ozonation at the same pH are very similar, while the decomposition rates obtained for each acid for plasma treatment are always higher than the corresponding ones for ozonation. At pH 1.8, as it was observed at pH 7, maleic acid decays with an S-shape curve: its decomposition is initially very slow and increases after fumaric acid is consumed. Considering that in the ozonation at pH 1.8 and 7 the reactive species is ozone, from the observed behavior of maleic and fumaric acids it can be deduced that the rate determining step is the ozone transfer to the liquid phase and that the ozone concentration in water is

not able to reach a stationary state in a time negligible with respect to the rate of the reaction of ozone with the organic acids. Thus, as soon as ozone is becoming available in solution, it reacts preferentially with the competitor which has the higher reaction rate, fumaric acid. Simulations confirm that indeed an S-shape concentration profile can be due to this effect: in Fig. 3.2.14a the simulation relative to the reactions system (3.2.20)-(3.2.23) reported in equations (3.2.24)-(3.2.26) is shown.

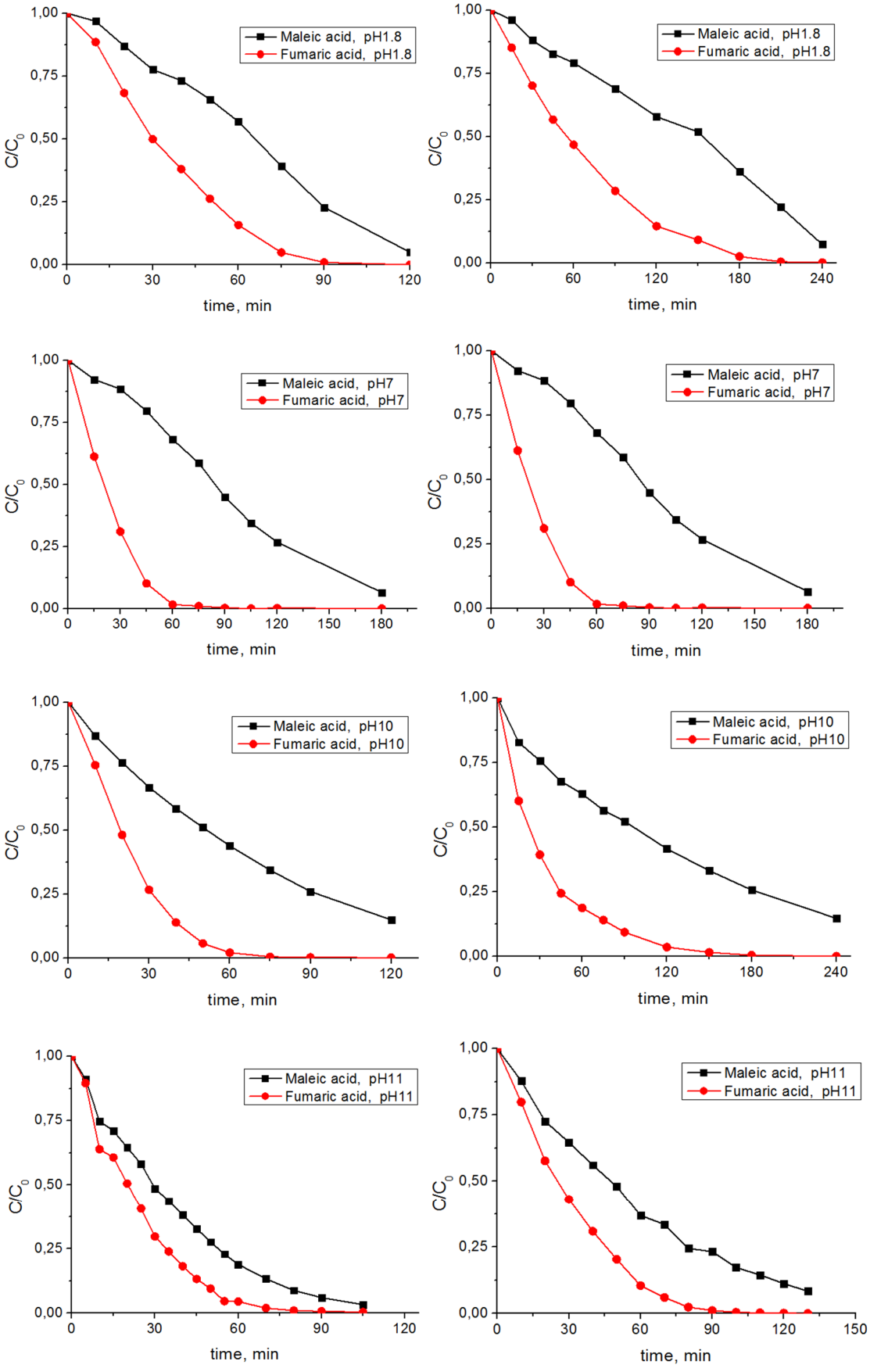

Fig. 3.2.13. Decomposition of a 1:1 mixture of maleic and fumaric acids ($2.5 \cdot 10^{-4}$ M each) in aqueous solution at pH: 1.8, 7, 10 and 11 by (left) plasma treatment and (right) ozonation.

$G \rightarrow Ox_1$	S_1	(3.2.20)
$MA + Ox_1 \rightarrow I$	k_m	(3.2.21)
$FA + Ox_1 \rightarrow I$	k_f	(3.2.22)
$Ox_1 \rightarrow ...$	k_{Ox1}	(3.2.23)

The model considers that the 'rate of formation' of the oxidant Ox_1 is constant (S_1)

Maleic (MA) and fumaric acids (FA) react with Ox_1, producing the same intermediate I. This assumption is justified by the fact that they are isomers; if we consider the ozonation process, this compound could be one of the known products described in the literature [113], such as glyoxylic or oxalic acid.

The simulation results, shown in Fig. 3.2.14a, come from the resolution of the following equations:

$$\frac{d[MA]}{dt} = -k_{m1}[Ox_1][MA] \quad (3.2.24)$$

$$\frac{d[FA]}{dt} = -k_{f1}[Ox_1][FA] \quad (3.2.25)$$

$$\frac{d[Ox_1]}{dt} = S_1 - k_{m1}[Ox_1][MA] - k_{f1}[Ox_1][FA] - k_{Ox1}[Ox_1] \quad (3.2.26)$$

The trend of the oxidant is represented in red. It is possible to see that its concentration is strongly reduced by the reactions with the target compounds and only when almost all of them are decomposed, its concentration increases and reaches a stationary state. For this reason the decomposition curve of the less reactive compound (maleic acid in this case) is not exponential and has an induction period.

The hypothesis to explain the higher efficiency obtained in the plasma treatment with respect to ozonation, analogously to the processes studied with the single compounds, considers the participation of OH radicals to the oxidation activated by plasma. To confirm that the involvement of a second reactive species, with a lower observed rate constant and which reacts at the same rate with both compounds present into the system, does not change the shapes of the curves, a simulation was performed. This is shown in Fig. 3.2.14b, it is referred to the system described by reactions (3.2.20)-(3.2.23) and (3.2.27)-(3.2.30).

$G \rightarrow Ox_2$ S_2 (3.2.27)

$MA + Ox_2 \rightarrow I$ k_m (3.2.28)

$FA + Ox_2 \rightarrow I$ k_f (3.2.29)

$Ox_2 \rightarrow ...$ k_{Ox2} (3.2.30)

In this case the equations are:

$$\frac{d[MA]}{dt} = -k_{m1}[Ox_1][MA] - k_{m2}[Ox_2][MA] \quad (3.2.31)$$

$$\frac{d[FA]}{dt} = -k_{f1}[Ox_1][FA] - k_{f2}[Ox_2][FA] \quad (3.2.32)$$

$$\frac{d[Ox_1]}{dt} = S_1 - k_{m1}[Ox_1][MA] - k_{f1}[Ox_1][FA] - k_{Ox1}[Ox_1] \quad (3.2.33)$$

$$\frac{d[Ox_2]}{dt} = S_2 - k_{m2}[Ox_2][MA] - k_{f2}[Ox_2][FA] - k_{Ox2}[Ox_2] \quad (3.2.34)$$

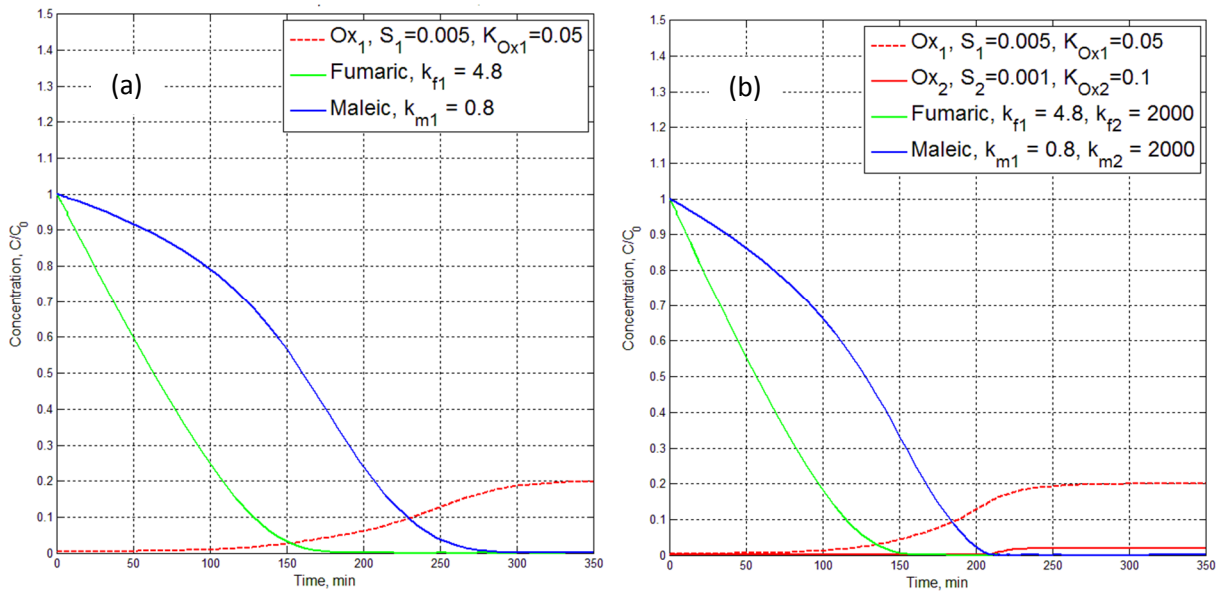

Fig. 3.2.14. Simulations of the decay of two organic compounds (blue and green lines) reacting (a) with one oxidant (dotted red line) or (b) with two oxidants of different reactivity.

The simulation demonstrates that if the observed rate constants of the reactions of the organic compounds with the second oxidizing species are much lower than those with the main oxidant, the shape of the curve is not affected by the additional reaction channel due to this second reactive species but its presence simply increases the decomposition rates of both the compounds.

At pH 11 the decomposition of ozone into OH radicals and the availability of these more reactive species, presumably in concentration higher than that produced by plasma, induces also a change in the ratio of the rate of formation of the reactive species and the rate of their reactions with the organic compounds. This is the reason why the decomposition of maleic acid does not show an S-shape but fits sufficiently well an exponential decay. Moreover, at this pH the difference of reactivity between fumaric and maleic acids is reduced with respect to the other pH values and this confirm the conclusion that at pH 11 the OH radical assumes an important role in the oxidation process.

At pH 10, the competition of carbonate for the OH radical complicates further the system. The rather high difference in reactivity between maleic and fumaric acids indicates a strong contribution of ozone, while the higher reactivity of both acids in plasma treatment

with respect to ozonation indicates that carbonate was not added in concentration sufficient to quench all •OH present into the system.

3.2.4.4 Argon plasma treatment of a 1:1 mixture of maleic and fumaric acids

To gain support for the interpretation of the experimental results described in the previous paragraphs, two experiments of plasma treatment of a 1:1 mixture of maleic and fumaric acid ($2.5 \cdot 10^{-4}$ M each) were performed, one at pH 1.8, the other at pH 7, using argon instead of air as discharge gas. Due to the absence of oxygen, no ozone is formed in plasma of argon and the main reactive species is •OH [164]. The decomposition curves obtained for maleic and fumaric acids in these experiments are shown in Fig. 3.2.15.

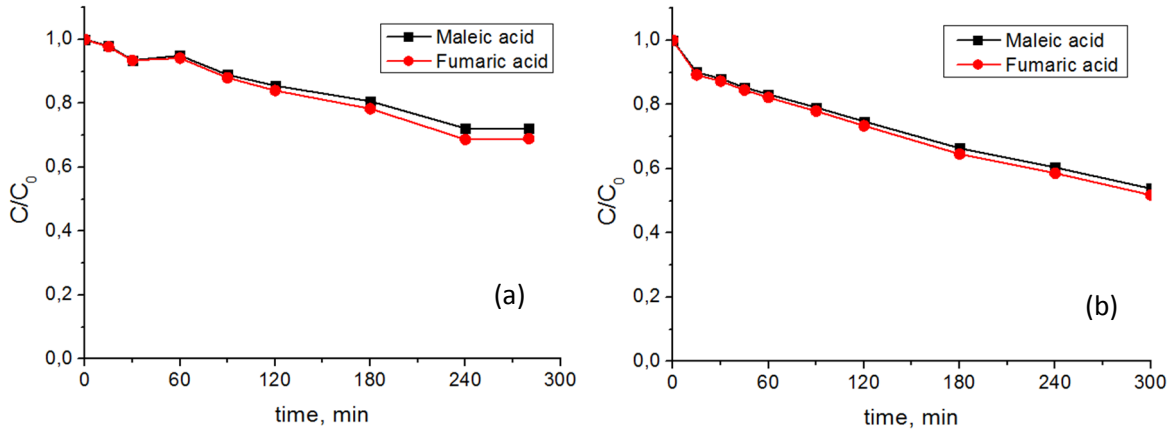

Fig. 3.2.15. Decomposition of a 1:1 mixture of maleic and fumaric acids ($2.5 \cdot 10^{-4}$ M each) in aqueous solution at pH 1.8 (a) and pH 7 (b) by argon plasma.

Due to the low stability of the discharge in argon, it is not possible to compare the rates obtained at the two different pH nor to compare them with those obtained in the air plasma treatment. The only comparison which can be safely done is that of the reaction rates of maleic and fumaric acids obtained in the same experiment. From this comparison it is possible to conclude that maleic and fumaric acids react with the same rate when subjected to reaction with •OH both at pH 1.8 and 7. Thus, considering the difference in reactivity observed between maleic and fumaric acids treated by air plasma, this result

constitutes another piece of evidence that at pH 1.8 and 7 ozone is the main reactive species responsible for the decomposition of the acids induced by air plasma.

3.2.4.5 Ozonation of maleic and fumaric acids without stirring the solution

The final part of this chapter addresses the issue of mass transfer, which can greatly affect kinetic behavior in heterogeneous systems. While all experiments described in the previous paragraphs were done under stirring, the very first experiments of ozonation had been performed without stirring the solution. These early experiments, dealing with one organic compound as well as with two organic compounds treated in mixture, will be briefly reviewed here since they provide further insight into the reactivity within these complex heterogeneous systems. In experiments with only one compound the following conditions were used: the compound concentration was $5 \cdot 10^{-4}$M is solutions at pH 1.8, stabilized by sulfuric acid, or in MilliQ water without any buffering system. The experiments with the two compounds in mixture were performed using a concentration of $2.5 \cdot 10^{-4}$ M for each compound and a pH equal to 1.8 or 7.1 with NaH_2PO_4/Na_2HPO_4 $4.4 \cdot 10^{-3}$ M (Table 3.1.1).

In Fig. 3.2.16 the decomposition curves obtained in the case of ozonation of maleic and fumaric acids at pH 1.8 are shown. The decay of the residual fraction of each acid does not fit either an exponential or a linear behavior and this can be ascribed to the absence of stirring during the process.

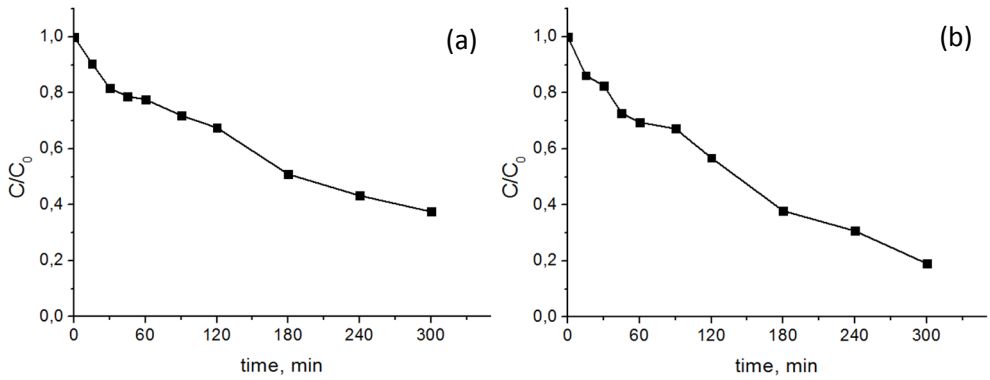

Fig. 3.2.16. Maleic acid (a) and fumaric acid (b) decomposition in ozonation at pH 1.8.

A very interesting behavior can indeed be observed in the case of ozonation experiments of the mixture of maleic and fumaric acids without stirring. As shown in

Fig. 3.2.17, contrary to what is observed when the solution is magnetically stirred (see Fig. 3.2.13), the decay of each acid is not influenced by the presence of the other and no induction period for the decomposition of maleic acid occurs (at pH 1.8 and pH 7). Indeed, if the decomposition curves obtained when the acids are treated separately and in mixture are compared, these appear to be very similar.

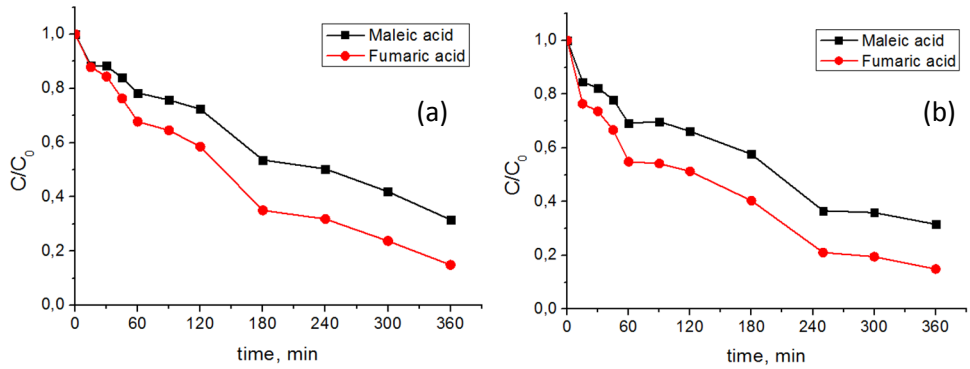

Fig. 3.2.17. Decomposition of a mixture of maleic and fumaric acids during ozonation at pH 1.8 (a) and at pH 7 (b) without stirring.

Such dramatic difference in behavior depending on whether the ozonation is conducted under stirring or under static conditions is due to ozone mass transfer between the gas and liquid phases and to diffusion processes.

Mass transfer and its interdependence with chemical reactions in ozonation has been reviewed recently [165]. When material is transferred from one phase to another across a separating interface, resistance to mass transfer causes a concentration gradient to develop in each phase (Fig.3.2.18):

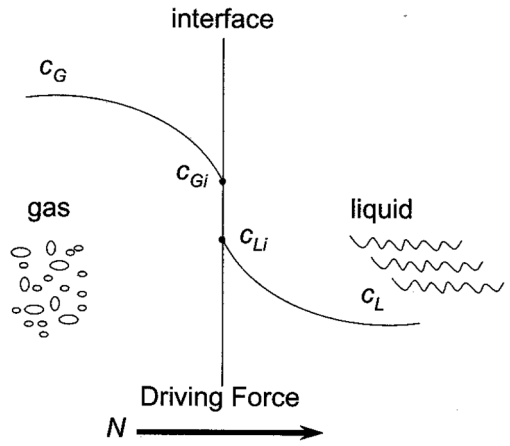

Fig. 3.2.18. Concentration gradients at the interface between gas and liquid phases [165].

This concentration difference is the driving force for mass transfer. In the absence of chemical reaction, the mass transfer flux *N* out of one phase is equal to the flux into the second phase (eq. 3.2.35)

$$N = k_G (c_G - c_{Gi}) = k_L (c_{Li} - c_L) \qquad (3.2.35)$$

where k_G and k_L are the film mass transfer coefficients, which are proportional to the molecular diffusion *D* elevated to some power *n* (*n* = 0.5 – 1.0 depending on the system turbulence) and inversely proportional to δ, the film width.

$$k \propto \frac{D^n}{\delta} \qquad (3.2.36)$$

The concentrations of the diffusing material in the two phases immediately adjacent to the interface, c_{Gi} and c_{Li}, are generally not equal but are usually assumed to be related to each other by the laws of thermodynamic equilibrium. When the controlling resistance is in the liquid phase, the overall mass-transfer coefficient K_L is generally used and eq. 3.2.35 is rewritten as 3.2.36

$$N = K_L (c_L^* - c_{Li}) \qquad (3.2.36)$$

where K_L is the overall mass-transfer coefficient and c_L^* is the liquid concentration in equilibrium with the bulk gas concentration. For dilute nonreacting solutions, Henry's law is used to describe the linear equilibrium distribution of a compound between the gas and liquid phases.

If a reactive compound is present in the solution its presence changes the ozone concentration gradient in the liquid film. The size (characteristic width) of this effect depends on the relative rates of mass transfer and of chemical reaction. These processes are interdependent: the concentration of ozone affects the reaction rate and in turn the reaction rate influences the ozone consumption, thus enhancing the ozone mass transfer from the gas phase.

In Fig. 3.2.19 [165] four different kinetic regimes are presented with characteristic concentration profiles of ozone (c_L) and of the reacting compound M, *c(M)*, in the liquid film. Typical ozonation conditions were considered, in which the transfer interface is in the form of bubbles (conditions approached in our experiments conducted under stirring).

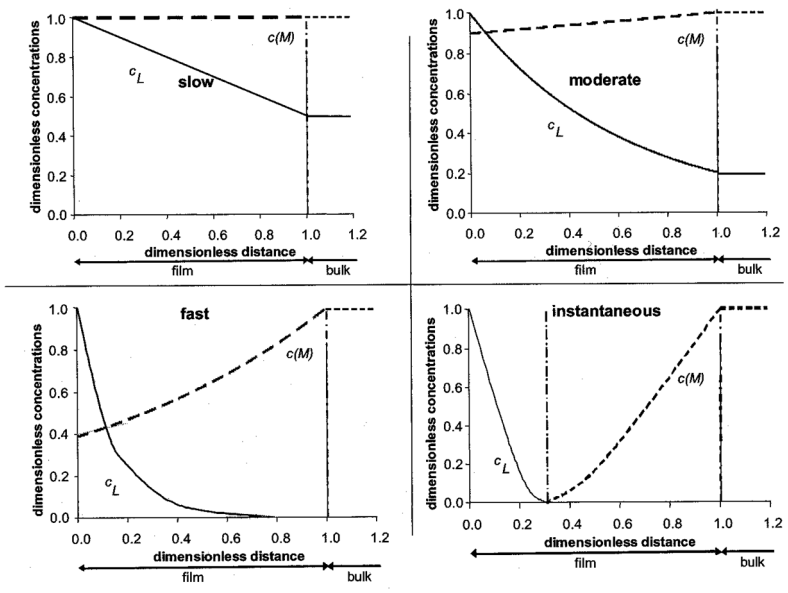

Fig. 3.2.19. The concentration profiles of the compound c(M) and ozone in the liquid film c_L in case of the stirred reactor [165].

The concentration of the reacting compound M and of ozone in the film depends on the relative rates of chemical reaction and of ozone mass transfer. If M reacts slowly with ozone, a comparatively high concentration of ozone will be present in the solution, where the reaction takes place. If the compound reacts with ozone more effectively, the ozone concentration profile in the film becomes steeper and steeper as the kinetic regime goes from moderate to fast to instantaneous reactions (Fig. 3.2.19). The ozone bulk concentration becomes lower and lower as the reaction moves further into the film. Finally it is possible to achieve the situation where in some film depth the concentrations of both ozone and M approach zero: this is the so called instantaneous reaction regime. The steeper gradient enhances ozone mass transfer while the reaction rate becomes dependent on the rate of ozone transferred into solution. In this case ozone mass transfer becomes rate controlling so that the reaction occurs entirely in the film.

In our experiments in which the solution was not stirred the decomposition kinetics are also controlled by the compound diffusion into the liquid film which remains saturated by ozone. A qualitative description is shown in Fig. 3.2.20: the concentration of the compound approaches zero near the gas phase where the concentration of ozone could be relatively high.

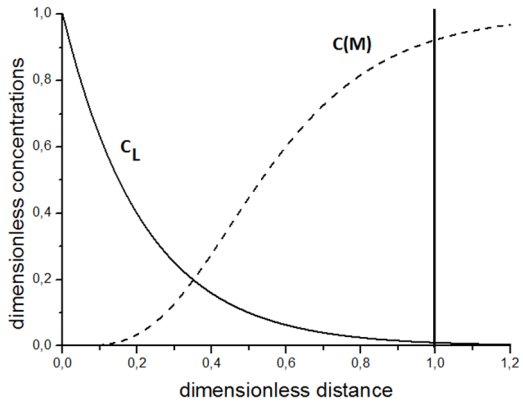

Fig. 3.2.20. The concentration profiles of the compound c(M) and ozone in the liquid film c_L in case of the not stirred reactor.

It is reasonable to expect that in this case the ozone mass transfer could be controlled by the diffusion of the compound from the bulk (compare to the reaction rate controlled transfer when instantaneous regime occurs in the stirred reactor).

Under this regime of kinetics controlled also by diffusion of the compound, if two compounds (maleic and fumaric acids) are present in the same solution at equal initial concentrations, both will react in the film due to the high concentration of ozone present in the film, nevertheless their kinetic constants for reaction with ozone are different. In other words, the decomposition occurs in time which is less than the time for renewal of the solution in this film (due to diffusion, convection or turbulence): competition for ozone is not observed and the reaction is not chemically selective.

In contrast, if the solution is stirred and made homogeneous, reaction in the bulk will be controlled not only by ozone mass transfer (which also becomes more efficient) but also by reaction rates. The gaseous oxidant (ozone) transfer process in the bulk for a batch set-up (with respect to the liquid) as used in our experiments, can be described as follows:

$$\frac{d[Ox]}{dt} = k_L a([Ox]^* - [Ox]) - r_L \qquad (3.2.37)$$

where $k_L a$ is a volumetric mass transfer coefficient and r_L represents the total rate at which the oxidant is chemically decomposed (including self-decomposition, scavenging by the media, reaction with different compounds). *[Ox]** is a saturation concentration of Ox which is reached in the case of pure mass transfer in the absence of any oxidant consuming reaction ($r_L = 0$).

It is possible to see that eq. (3.2.37) with

$$r_L = k_m[Ox][M] + k_f[Ox][F] + k'_{Ox}[Ox] \qquad (3.2.38)$$

is another representation of eq. (3.2.26):

$$\frac{d[Ox]}{dt} = S - k_m[Ox][MA] - k_f[Ox][FA] - k_{Ox}[Ox]$$

in which $S = k_L a[Ox]^*$ and $k'_{Ox} = k_{Ox} - k_L a$ which represents the scavenging, decomposition of the oxidant and its transfer limiting due to decreasing of the concentration

gradient between the real concentration in the solution and the saturated concentration achievable in the absence of chemical reaction. So the reaction between the oxidant and the compounds can be described by the kinetic model presented in paragraph 3.2.4.3 and characterized by competition occurring in the bulk solution between the two compounds for a limited source of oxidant (Fig. 3.2.14).

3.2.5 Comparison of ozonation and plasma treatment with and without magnetic stirring

To compare the efficiency of the different oxidizing means, ozonation vs plasma, maleic acid was selected as model compound, while pH was maintained equal to 1.8. Maleic acid was chosen considering the low dependence of its decomposition rate on pH. Both the experiments, ozonation and plasma treatment, were performed with and without stirring the solution. The results are shown in the decomposition graphs of Fig. 3.2.21.

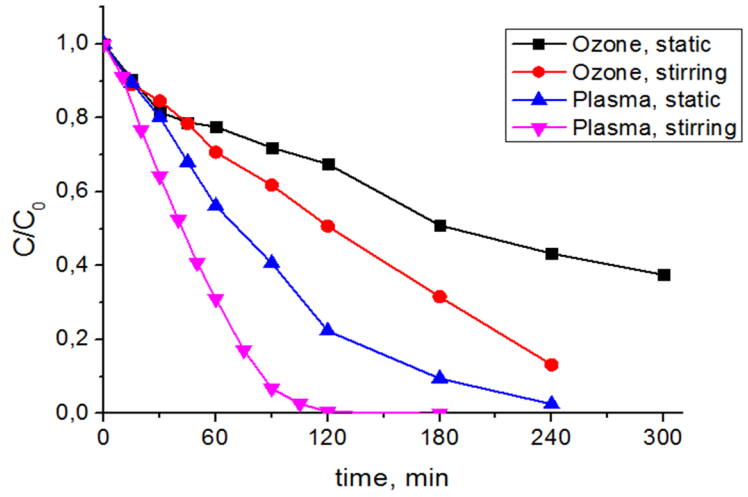

Fig. 3.2.21. Comparison of different oxidation regimes for maleic acid at pH 1.8

It is possible to see that in both cases, with and without stirring, plasma treatment performs a more efficient oxidation of the compound with respect to ozonation. Furthermore, plasma treatment can also be enhanced by stirring or using the closed-loop circulating water flow system. The shape of the decomposition curves becomes more regular and more exponential-like as the decomposition rate increases. According to the numerical model described in paragraph 3.2.2, this can be ascribed to the increase of the concentration of the oxidant in the solution.

3.3 Conclusions

In this chapter plasma induced oxidation of various organic pollutants, alone and in mixture, was studied in a prototype DBD reactor. In this device the discharge is applied in the air above the solution and the reactive species are transferred into the aqueous phase, where they can react directly with the organic pollutants, or be converted to different oxidizing species. However, the reaction between the oxidants and the organic compounds can also take place on the surface of water. From previous studies [106, 107] it is known that the two main oxidizing species in the DBD reactor under investigation are OH radical and ozone. OH radical can be formed in air by the discharge but can also be formed in water from ozone decomposition. As it was clarified in the present Thesis, the relative role of these two species depends mainly on the organic compound under investigation and on the pH of the solution. The investigations performed in this chapter provide some important insight into the mechanism of plasma induced oxidation of phenol, substituted phenols, maleic and fumaric acids.

It is shown that the observed rate constant of phenol decomposition depends linearly on the reciprocal of its initial concentration and this finding is consistent with a simple mechanistic model of inhibition by products. Support for this model also comes from the concentration changes of the major reaction intermediates of phenol decomposition as a function of treatment time.

Despite its high reactivity air plasma displays some selectivity. The rate of oxidation of monosubstituted phenols (m-$(CH_3)_2$N-, m-Cl-, p-NO2- and m-NO_2-) depends linearly on the Hammett substituents constant yielding a □ value of -0.48 which is characteristic of electrophilic attack by the OH radical.

Some products and intermediates of phenol decomposition were detected and quantified by HPLC/UV analysis. Also determined was the total organic carbon which allows to conclude that the contribution of the non-detectable species, such as short-chain organic acids, is significant.

The behavior of two intermediates of phenol oxidation, maleic acid and fumaric acid, was investigated in detail since they are very common water secondary pollutants formed in the oxidative degradation of most aromatic compounds but also because it was found that when present in mixture these show a very particular trend as a function of the

treatment time, not observed with any other studied mixture (phenol and chlorophenol, phenol and maleic acid, phenol and fumaric acid). To clarify the origin of their particular behavior maleic and fumaric acids were investigated in experiments in which were treated separately and also in mixture under different pH conditions. Besides plasma treatment, they were subjected to experiments of ozonation conducted under the same experimental conditions except for the fact that ozone was produced ex situ. All these experiments allowed to investigate on the contribution of the major oxidizing species, hydroxyl radical and ozone, to the decomposition of the organic acids. The study allowed to conclude that in the presence of compounds highly reactive with ozone, as in the case of organic compounds with -C=C- double bonds, the decomposition process is mainly due to this species. Depending on the pH of the solution, ozone reacts directly with the organic molecules or is converted to OH radicals. However, the OH radical directly produced by the electrical discharge also contributes to the oxidation of maleic and fumaric acids in the air-liquid plasma system, independently on the pH used. Its contribution to the overall process depends on the relative ratio of the rate constants of the particular organic compound with ozone and with OH radical. However, the direct formation of •OH constitutes a big advantage in the production of reactive species applying the discharge above the water surface with respect to the production of ozone ex-situ. In particular, while ozonation is not effective in oxidizing some classes of organic compounds at acidic pH values because the reactive species is ozone itself, which is a very selective species, the plasma treatment is effective also when ozone is unreactive. This is due to the direct production of OH radicals which react with all the classes of organic molecules.

The obtained results were also very useful to disclose the importance of the transfer of the reactive species from the gas phase to the solution. In fact, contrary to phenol, which decays with an exponential trend under all experiment conditions, maleic and fumaric acids sometimes showed a linear behavior due to the consumption of the reactive species as these are formed. However, comparing the behavior of maleic and fumaric acids in plasma treatment and in ozonation, it was demonstrated that the ion wind present in the DBD reactor due to the transfer of the charged species formed by the discharge plays a great role in mixing the solution. In fact, the ozone produced ex-situ needs the magnetic stirring of the solution to allow the reaction to take place also in the bulk and not only on the surface of water, while in the case of plasma treatment magnetic stirring increases the rate of the reaction but does not change significantly the shape of the oxidation curves.

4. PLASMA DRIVEN DRY REFORMING OF METHANE

4.1 Experimental methods and procedures

This paragraph describes the experimental set-up, the materials and the methods used for the research activity dealing with plasma driven dry reforming of methane.

4.1.1 Chemicals

Pure CH_4, CO_2, CO and Ar in high pressure cylinders were purchased from Air Liquide and placed in a special safety storage cabinet (Exacta supplier). All the pressure regulators were supplied from the Air Liquide. Pure air used in the experiments was a synthetic mixture of 80% nitrogen and 20% oxygen purchased from Air Liquide with specified impurities of H_2O (< $3ppm_v$) and C_nH_m (< $0.5ppm_v$).

Hydrogen was generated by a hydrogen generator (DBS Analytical Instruments, NMH2-250), which is based on water electrolysis and separates hydrogen by a diffusion membrane.

4.1.2 Instrumentation

The diagnostics employed for characterizing the plasma driven process of dry reforming of methane includes a gas chromatography system with thermal conductivity (TCD) and flame ionization (FID) detectors and a gas chromatography system with TCD, FID and mass spectrometry (MS) detector, described in paragraph 4.1.4.1**,** a gas mass flow meter (M-200SCCM-D-G/5M, Alicat Scientific) and a spectrometer for emission spectroscopy analysis, described in paragraph 4.2.7.

4.1.3 The experimental set-up

The development of plasma driven methane dry reforming process was a project completely new in the Plasma Group of the Department of Chemical Sciences of the University of Padova. It required the design and the construction or, more easily, the acquisition of the overall experimental apparatus, which includes the reactor, the high voltage power supply, the gas feeding system equipped with mass flow controllers for the preparation of gaseous mixtures of desired and stable composition, the furnace and the systems for chemical and electrical diagnostics. The overall system was designed to have the possibility to study the process of dry reforming of methane not only when driven by plasma, but also when activated by heterogeneous catalysis or by the combination of plasma with a catalyst placed into the discharge zone. The most challenging requirement for the reactor to reach this objective were the thermal resistance up to 800°C, necessary for the studies of purely catalytic processes, and the transparency to UV-Vis light to perform emission spectroscopy measurements. In the description of the apparatus reported in the following paragraphs these aspects will be underlined.

4.1.3.1 The gas reforming reactor

The reactor casing (Fig. 4.1.1) consists of a quartz tube of 4 mm of thickness, 45 mm of external diameter and 570 mm of length (Technical Glass, GB), to which two quartz flanges of 100 mm of diameter are welded on the extremities and a quartz ring is placed in the middle of the tube (H.T.S. srl, Cavenago Brianza, MB).

Quartz was chosen as transparent to UV-Vis radiation, thus allows the monitoring of the excited active species within the plasma by emission spectroscopy. Moreover, it makes the reactor resistant to temperatures up to 800°C.

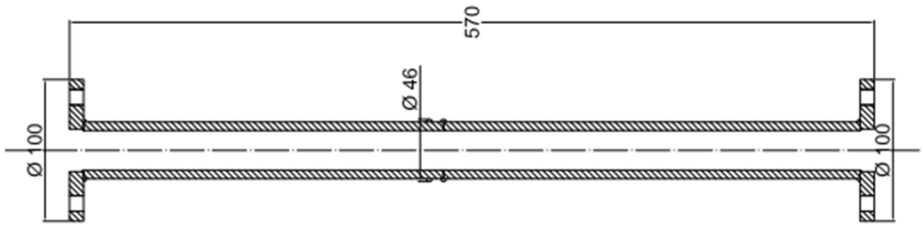

Fig. 4.1.1. Reactor casing

Two inox flanges are sealed to the quartz ones with Viton fluorocarbon or silicon rings and are fixed by screws which rely on soft gaskets to prevent cracking of the fragile quartz material. The working position of the reactor is vertical, but it could work in any position. The reactor is placed inside a furnace (Carbolite, VST12/200 series) which is used also like a stand.

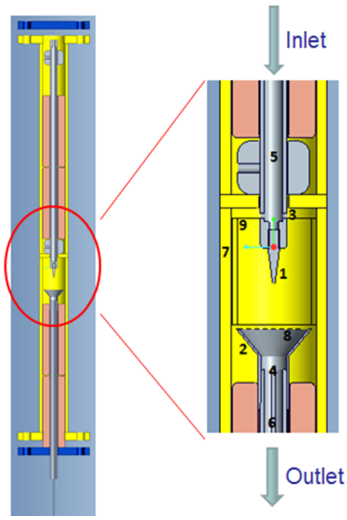

Fig. 4.1.2. Schematics of the reactor and enlargement of the plasma region

The electrodes which constitute the plasma source are situated in the middle of the tube (Fig. 4.1.2). These are a tip (1), to which the high voltage is applied, and a conic grounded counter electrode (2) covered by an Inox mesh (8). The electrodes geometry is thus of “tip-to-plate” type and the distance between the electrodes is 15 mm. The tip is screwed into an Inox tube (5) coaxial to the quartz tube, from which the gas is supplied to

the plasma zone exiting from two lateral holes (3). The counter electrode is connected to the grounded tube (6) which serves for the gas exhaust.

The mesh (8) could also be used to support the pellets of a catalyst in the case of combination of the plasma with catalysis. A piece of Pyrex tube (9) is introduced into the reactor to collect possible deposits in the discharge region. This allows to protect the quartz walls from the possible depositions and to easily clean the reactor by removing and washing this tube.

The up and down parts of the quartz casing (7) of the reactor are filled with ceramic discs to decrease as much as possible the dead volume inside the reactor. These ceramics were supplied by RS components and machinery treated in the workshop of the Department.

A N-type thermocouple (Delta-Ohm) is introduced into the reactor through the grounded exhaust tube (6) to monitor the temperature of the discharge zone. It is connected to a universal thermometer equipped with a digital display and RS-232 interface. The communication interface of the thermometer is galvanically isolated to avoid the parasitic currents in signal ground lines. Thus the temperature log during the experiment could be recorded.

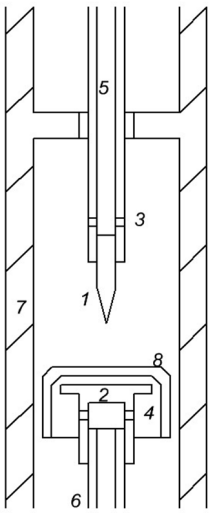

Fig. 4.1.3.

The reactor configuration described above was used to perform the trials with glow and corona discharge and to perform the main set of experiments with spark discharge. However, as it will be described in paragraph 4.2.1, some preliminary experiments were performed also with a dielectric barrier discharge and this required the modification of the device.

In particular, the electrode system of the reactor (Fig. 4.1.2) was changed to situate a dielectric material between the electrodes. Thus, the funnel-shaped counter electrode (2 in Fig. 4.1.2) was substituted with a stainless steel plate (2 in Fig. 4.1.3) and was covered by a glass cup (8 in Fig. 4.1.3) to form a solid dielectric layer on it. In this system the gas flows

between the glass cup and the internal walls of the reactor and enters into the tube (6) through four lateral holes (4 in Fig. 4.1.3) on the electrode (2). As in the previously described configuration the exhaust tube (6) is used also as a ground connection.

4.1.3.2 The feeding line

The gas feeding system is shown in Fig. 4.1.4. The gases (Ar, CH_4 and CO_2) are supplied from high pressure gas tanks, flow through mass-flow controllers (MFC, Alicat Scientific, 16 series), which allow independent setting of an accurate flow for each gas, and are mixed in the desired composition in a mixing chamber (Swagelok sample cylinder, 40 mL). Check valves were added to protect the MFC from the back-flow.

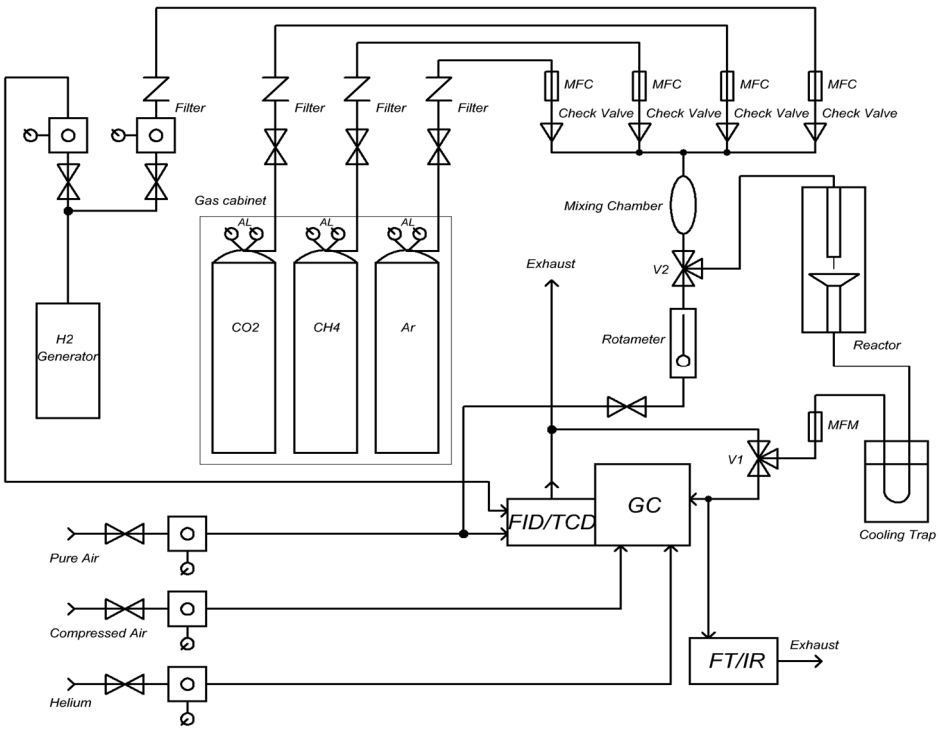

Fig. 4.1.4. Schematics of the gas feeding line

Then, the reactant mixture reaches the reactor, where it is processed by the application of a discharge. The gas exiting from the reactor passes through a cooling trap, generally filled with dry ice in acetone, to allow possible liquid products to condense. The output of the cooling trap is connected to a mass flow meter (MFM, Alicat Scientific, 16

series) to measure the flow rate of the resulting gaseous mixture. Through a three-way valve the output gas can be then addressed to the exhaust or to a gas line connected with the sampling loop of the GC. This valve is also used to equilibrate the pressure in the sampling loop before the injection into the GC system, as described in detail in paragraph 4.1.4.1.

A gas line for hydrogen controlled by a MFC is also available for GC calibration and reduction of the catalysts placed inside the reactor in case catalytic or plasma-catalytic processes are performed

4.1.3.3 Power supply and electrical monitoring

The type of discharge which was tested and found efficient in promoting the conversion of methane and carbon dioxide into syngas is a spark discharge.

The schematic of the power supply developed for the production of this type of discharge is shown in Fig 4.1.5. The high voltage power supplies (Spellman, PTV30 series), one for positive and the other for negative polarity are able to supply a DC voltage up to 30 kV and a current until 11 mA. The modules have an external control and a monitoring system and can work in current stabilization mode.

The current is supplied through a high voltage current limiting resistor, R1 in Fig. 4.1.5, (3 MOhm nominal resistance), which charges a high voltage ceramic capacitor C2 (400 pF). When the voltage on this capacitor reaches a particular threshold value the electrical breakdown occurs. The phenomenon is further explained in paragraph 1.3.3. After the breakdown and formation of the spark, the capacitor C2 discharges to the voltage at which the discharge cannot be sustained, which is much lower than the voltage at which the discharge initiates.

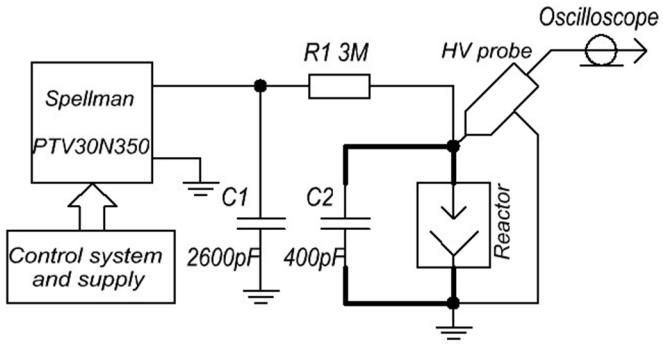

Fig. 4.1.5. Schematics of the power supply system

During the breakdown, the current through the capacitor C2 and the reactor is extremely high, much higher than the charging current. To sustain it, the connections between the reactor and the capacitor have been reinforced (thick lines in Fig 4.1.5) with respect to the initial circuit configuration. Moreover, precautions have been taken in the ground organization to minimize EMI and parasitic currents inside the ground lines: high current discharging line was topologically separated and a ferrite bead was added in the charging network.

The high voltage power supply works as a current source. Changing the supply current is possible to control the frequency of the pulses and thus the power applied to the system.

The power applied to the system was estimated by measuring the voltage on the reactor by a Rigol DS1052E digital phosphor oscilloscope using the Tektronix HV probe (Fig 4.1.5). In Fig. 4.1.6 a picture of the discharge and a typical oscillogram acquired in an experiment in negative polarity are shown (CO_2:CH_4 = 1:1, total flow 50 mL/min).

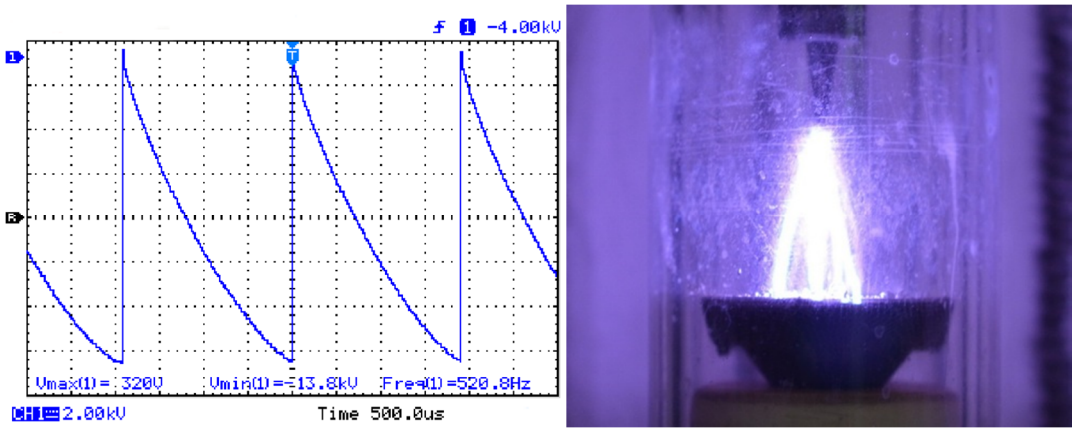

Fig. 4.1.6. A typical oscillogram of the voltage on the reactor and picture of the discharge.

From such oscillogram it is possible to know the minimum voltage (V_{min}) remaining after the discharge, the voltage at which the discharge starts (the threshold or breakdown voltage, V_{thres}) and the frequency f of the voltage pulses. These three parameters allow to estimate the consumed power by eq. (4.1.1), where C is the capacitance value of the capacitor C2 in Fig 4.1.5.

$$< P >= \frac{1}{2} C (V_{thres}^2 - V_{min}^2) f \qquad (4.1.1)$$

As it was mentioned above and as is possible to see in the oscillogram reported in Fig.4.1.6, $V_{thres} >> V_{min}$, so we can assume that in each cycle the capacitor discharges completely. Eq. (4.1.1) can thus be simplified into eq. (4.1.2):

$$< P >= \frac{1}{2} C V_{thres}^2 f \qquad (4.1.2)$$

V_{thres} and f strongly depend on the process characteristics, as for example on the temperature, on the gas composition and on the current supplied. Electrode distance remained the same in all experiments with a good reproducibility of V_{thres}. To obtain the

same power input in different experiments, first V_{thres} was measured and then the current supplied was adjusted to obtain the *f* which gives the desired power (for example, 20 W).

To perform the glow discharge the electrical circuit was the same described above except the absence of the capacitor C2, thus a constant current flows through the discharge. The resistor R1 acts like a current limiter preventing the transition to the spark discharge.

On the contrary, to supply the DBD reactor shown in Fig. 4.1.3 the AC power supply at 50 Hz and up to 20 kV, generally used in the research dealing with water purification by plasma, was used (Fig. 3.1.4 in chapter 3).

4.1.4 Experimental procedures and calculation of the parameters to evaluate the results

4.1.4.1 Experimental procedures

The experiments were performed by using a mixture of the pure CH_4 and CO_2, in some cases diluted with argon. The CH_4:CO_2 ratio was varied from 4:1 to 1:4, however, the usual ratio used was 1:1. Some experiments in pure CH_4 and CO_2 were also made. The input flow rate of the gas was varied between 25 to 100 mL/min.

The analysis of the gas was carried out with a GC (7890 A, Agilent Technologies) equipped with two PLOT columns, connected in series as shown in Fig. 4.1.7, and two detectors, TCD and FID, in series. The two columns were respectively a PLOT Q (30 m length, 0.53 mm ID, film thickness 40 µm), able to separate CO_2 and hydrocarbons up to C_{12}, and a PLOT Molesieve (15 m length, 0.53 mm ID, film thickness 30 µm), suitable for the separation of permanent gases and thus used to separate Ar, H_2, CH_4 and CO. A switching valve (Valve 1) allows to exclude the Molesieve column, which is highly retentive.

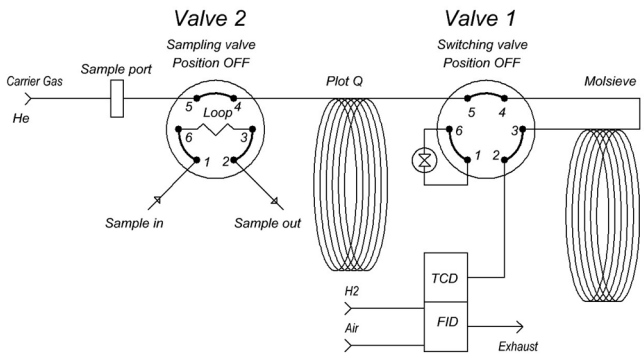

Fig. 4.1.7 Schematics of the GC used for the analyses

The development of the analysis method required the optimization of the oven temperature and of the switching times of Valve 1 to separate Ar, H_2, CO, CH_4 and CO_2. Initially the Molesieve column is connected in line. The first peak eluted from PLOT Q contains unresolved Ar, H_2, CO and CH_4. Once these components are introduced into the Molesieve, this column is bypassed to allow CO_2 to elute from PLOT Q. Then, Molesieve is

connected in line again and the trapped components are eluted and separated. In Table 4.1.1 the analysis procedure is outlined in detail. This includes the timing of the automatic sampling valve (Valve 2), which collects the sample into a loop and then injects it into the two column system (Fig. 4.1.7).

Table 4.1.1 The GC analysis procedure.

Time, min	Temperature, °C	Valves events	State
0	35	Valve 1 OFF Valve 2 OFF	Initial conditions: PLOT Q and Molsieve columns are connected in series, the sample loop is disconnected
0.1	35	Valve 2 ON	Start sampling: the gas flows through the sampling loop
0.6	35	Valve 2 OFF	Stop sampling and injection
0.6 - 2.2	35		Elution of an unresolved peak containing H_2, Ar, CH_4 and CO from PLOT Q to Molsieve
2.2	35	Valve 1 ON	Disconnection of Molsieve, where the unresolved peak of H_2, Ar, CH_4 and CO has been introduced
2.2 – 2.8	35		Elution of CO_2 from PLOT Q directly to the detectors
2.8	35	Valve 1 OFF	Reconnection of Molsieve
2.8 – 4.7	35		Elution and separation of H_2, Ar, CH_4 and CO from Molsieve
4.7	35	Valve 1 ON	Disconnection of Molsieve
4.7-15.25	35 - 220		Elution of other possible volatile gaseous byproducts
15.25-18.25	220		Elution of other possible volatile gaseous byproducts

Before the application of the discharge, the reagent mixture is analyzed to verify its composition and stability. For this purpose the thermal gradient included in the method is not activated and the analysis is stopped after 4.7 min.

Before to start the measurement a time of 20 min is necessary to stabilize the gas composition into the system. The volume of the reactor (discharge zone) is near 30 mL so at a flow rate equal or higher than 50 mL/min the gas inside the line and the reactor is

completely renewed in 20 min. When a flow of 25 mL/min is used, a stabilization time of 30 min is preferable to remove the undesirable traces of air from the system.

After the discharge is turned on the reaction starts immediately as is evident from the immediate increase of the output gas flow rate. However, at least other 20 min are necessary to stabilize the system before the measurement. In this time not only the gas composition is stabilized but also the power input and the temperature in the reactor. When the gas composition and the electrode temperature are stabilized the frequency and threshold voltage remains unchanged for hours. The threshold voltage when the conditions are stabilized is lower than the initial one (14-15 kV vs 23-25 kV) when the discharge has just started in the cold reactor with the initial gas composition (CH_4 and CO_2 only). For maintaining the same power (eq. 4.1.2) under stabilized conditions the frequency is higher than the initial one.

The calibration curves for H_2, CO, CH_4 and CO_2 were performed by introducing the gases in mixture with Ar in different ratio at a constant flow rate of 50 and 100 mL/min. Ar, H_2, CO and CO_2 were detected by TCD, while CH_4 was detected by both, TCD and FID.

The calibration curves for H_2, CO, CH_4 and CO_2 are shown in Fig. 4.1.8. The linearity of the instrument response to CH_4 and CO_2 was proved up to 100% when the pure gases were used, while for H_2 and CO such concentration was never used. As already mentioned, the concentration of hydrogen was measured by the TCD. Due to the fact that the carrier gas is helium, the hydrogen peak is negative and the system has a low sensitivity compared to other components of the gas mixtures. However, the chromatographic separation of the peak of the hydrogen is good and a good linearity of the calibration curve is achieved (Fig. 4.1.8).

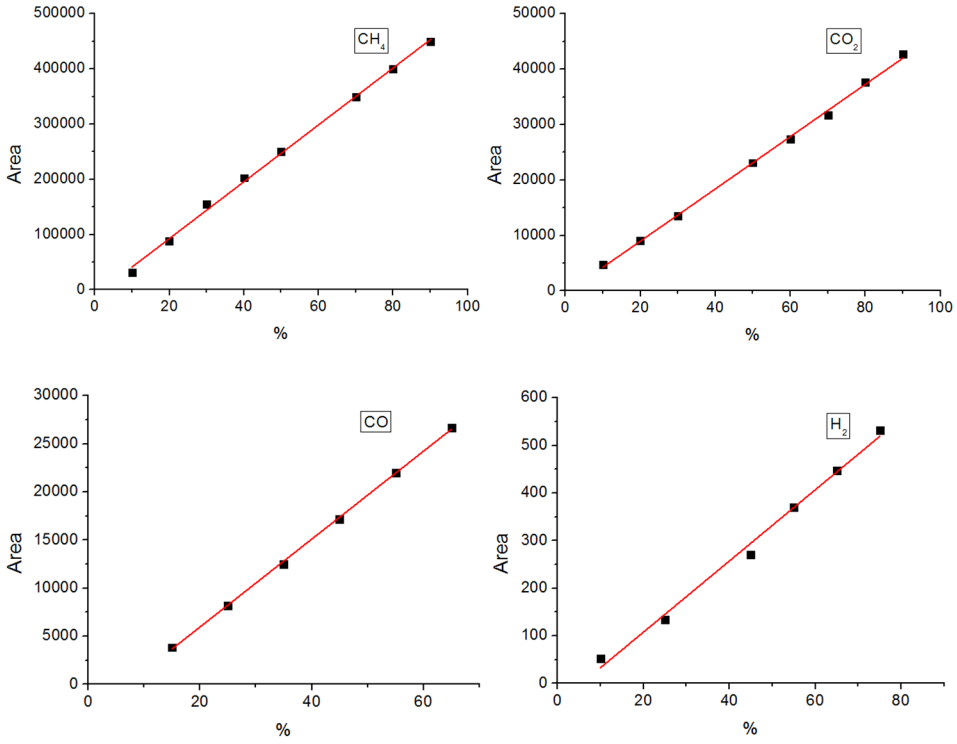

Fig. 4.1.8 GC calibration curves for CH_4, CO_2, CO and H_2.

During the calibration it was noticed that the areas of the peaks are strongly dependent on the working gas flow: higher flow rate caused an additional compression of the gas inside the sampling loop, increasing the area of the peak. Effectively, some commercial GC systems contain an additional valve for pressure equilibration in the sampling loop: this allows to eliminate the dependence of the GC response on the flow of the gas. Another problem, detected carrying out the experiments was that the pressure dropout at the sampling valve of the GC even at 50 mL/min was near 0.3-0.4 bar which influenced the pressure inside the reactor. This caused a dependence of the reactor pressure on the flow, influencing consequently the discharge process. The solution for all these problems was obtained by adding the valve V1 (Fig 4.1.4) which allows the connection of the reactor exhaust to the atmosphere bypassing the sampling loop. In this way the pressure dropout is almost absent and the reactor works at normal atmospheric pressure. When the GC injection is needed the valve V1 is switched to the GC for a time necessary to completely refresh the gas in the sampling loop with the gas coming from the reactor. It was estimated experimentally that 90 seconds at 50 mL/min is a time sufficient to completely refresh the gas inside the loop. During this time the pressure on the reactor starts to increase, but due

to the shortness of this time period and to the volume of the reactor this pressure increase is not significant. After the refreshing of the loop the valve V1 is again switched to the atmosphere. Thus, the reactor pressure returns quickly back to atmospheric and the flow inside the sampling loop completely stops, equilibrating the pressure inside it. After that, the analytical procedure described in Table 4.1.1 starts.

To identify some peaks due to unknown compounds a qualitative analysis was performed by mass spectrometry using a GC/FID/TCD/MSD (Agilent Technologies 7890). The GC/FID/TCD part of this instrument is identical to the GC used routinely except for the diameter of the PLOT Q column, which is 0.32 instead of 0.53 mm. The MSD is equipped with an electron ionization source and a quadrupole analyzer.

To perform the analysis the output gas was sampled and injected into the GC with a syringe. Only the PLOT Q column was used, while all the available chromatograms, FID, TCD and total ion current (TIC), were recorded. The mass spectra of the unknown peaks were compared with those present in the NIST mass spectra database [170].

4.1.4.2 Calculation of conversion, yield, selectivity and energy efficiency

The GC analyses give only the percentage of the different gases in the mixture analyzed. For the calculation of the real molar flow of each gas the knowledge of the total flow is necessary.

Due to the stoichiometry of the dry reforming reaction ($CH_4 + CO_2 \rightarrow 2\ CO + 2\ H_2$), during the process the flow of the gas at the output of the reactor increases. Theoretically, in case of an efficiency of 100% and at constant pressure before and after the reactor the output flow has to be double comparing to the input one. In the real situation this flow is less than double, thus it has to be measured to calculate the conversion efficiency and the reaction yield. The measurement is performed by the digital flow meter placed after the cooling trap of the reactor.

The percentage of the conversion $\eta(X)$ of the species X (X = CH_4 or CO_2) is the ratio between the amount of moles/min of X consumed in the reaction and the total moles/min of X introduced:

$$Conversion\ (X) = \eta(X) = \frac{\nu_{in}(X) - \nu_{out}(X)}{\nu_{in}(X)} \qquad (4.1.3)$$

In case of constant pressure and temperature eq. (4.1.3) can be presented as the ratio between the flows:

$$Conversion\ (X) = \eta(X) = 1 - \frac{\omega_{out}(X) F_{out}}{\omega_{in}(X) F_{in}} \qquad (4.1.4)$$

where $\omega_{out}(X)$ and $\omega_{in}(X)$ are the percentage of gas X in the input and output gas flows, F_{in} and F_{out} are the flows obtained from the mass flow controllers and the mass flow meter which measure the input and the total output flows, respectively.

The yield of the products is given by the ratio between the moles of the species produced in the process and the total molar input flow of the molecules from which the product can be formed. For CO eq. (4.1.5) is used:

$$Yield\ (CO) = \frac{\nu_{out}(CO)}{\nu_{in}(CO_2) + \nu_{in}(CH_4)} = \frac{\omega_{out}(CO) F_{out}}{F_{in}} \qquad (4.1.5)$$

For H_2 eq. (4.1.6) is used:

$$Yield\ (H_2) = \frac{\nu_{out}(H_2)}{2\nu_{in}(CH_4)} = \frac{\omega_{out}(H_2) F_{out}}{2F_{in}(CH_4)} \qquad (4.1.6)$$

In the case of formation of some higher hydrocarbons C_mH_n as byproducts the selectivity is calculated using the equation 4.1.7:

$$Yield\ (C_mH_n) = \frac{m\,\nu_{out}(C_mH_n)}{\nu_{in}(CH_4)+\nu_{in}(CO_2)} = \frac{m\,\omega_{out}(C_mH_n)F_{out}}{F_{in}(CH_4)+F_{in}(CO_2)} \qquad (4.1.7)$$

The selectivity for CO is the ratio between the number of moles/min of CO produced and the total carbon consumed in the reaction (the sum of the number of moles/min of CH_4 and CO_2).

$$Selectivity\ (CO) = \frac{\nu_{out}(CO)}{\nu_{conv}(CH_4)+\nu_{conv}(CO_2)} = \frac{\omega_{out}(CO)F_{out}}{\eta(CH_4)F_{in}(CH_4)+\eta(CO_2)F_{in}(CO_2)} \qquad (4.1.8)$$

As for hydrogen, its source is only CH_4 and each mole of CH_4 produces two moles of hydrogen, thus selectivity for H_2 was calculated by eq. (4.1.9):

$$Selectivity\ (H_2) = \frac{\nu_{out}(H_2)}{2\nu_{conv}(CH_4)} = \frac{\omega_{out}(H_2)F_{out}}{2\eta(CH_4)F_{in}(CH_4)} \qquad (4.1.9)$$

In case $F_{in}(CH_4) = F_{in}(CO_2) = F_{in}/2$ the equations (4.1.8) and (4.1.9) could be simplified:

$$Selectivity\ (CO) = \frac{2\omega_{out}(CO)F_{out}}{(\eta(CH_4)+\eta(CO_2))F_{in}} \qquad (4.1.10)$$

$$Selectivity\ (H_2) = \frac{\omega_{out}(H_2)F_{out}}{\eta(CH_4)F_{in}} \quad (4.1.11)$$

The selectivity for the higher hydrocarbons C_mH_n obtained as byproducts is calculated using the equation (4.1.12):

$$Selectivity\ (C_mH_n) = \frac{m\,\nu_{out}(C_mH_n)}{\nu_{conv}(CH_4)+\nu_{conv}(CO_2)} = \frac{m\,\omega_{out}(C_mH_n)F_{out}}{\eta(CH_4)F_{in}(CH_4)+\eta(CO_2)F_{in}(CO_2)} \quad (4.1.12)$$

The calculation of the molar energy efficiency is made in units of mmol/kJ. This parameter is given by the ratio between the number of millimoles of CH_4 and CO_2 converted per second and the power applied to the reactor, as indicated in eq. (4.1.13).

$$ME = \frac{F_{in}(CH_4)\eta(CH_4)+F_{in}(CO_2)\eta(CO_2)}{V_m\,P} \quad (4.1.13)$$

where P is power and V_m is the molar volume. When CH_4 and CO_2 are introduced in 1:1 ratio, equation (4.1.13) can be simplified as indicated in eq. (4.1.14):

$$ME = \frac{(\eta(CH_4)+\eta(CO_2))F_{in}}{2V_m\,P} \quad (4.1.14)$$

4.2 Results and discussion

4.2.1 Preliminary experiments

The first type of discharge tested to activate the process of dry reforming of methane was a DC corona discharge. First CH_4 and CO_2 were used diluted in Ar (CH_4:CO_2:Ar = 1:1:2) and flowed at 50 mL/min. Under these conditions the maximum voltage which was possible to apply for obtaining a corona discharge was near 16 kV for both polarities. When the reagents were flowed without dilution the maximum applicable voltage increased to about 24 kV. However, it was very difficult to obtain a stable corona and to reach currents of the order of milliamperes with this gas composition and reactor geometry as breakdown occurred.

The analysis of the exiting gas showed no noticeable conversion either with positive or with negative DC corona. Time by time extremely small traces of CO were detected. However, from this and subsequent experiments it was deduced that the activation of the reagents to give CO was due to the occasional spark discharges, while the DC corona discharge does not provide enough energy.

Another type of discharge which was experimented to obtain methane dry reforming is the so called atmospheric pressure glow discharge (APGD). Its main characteristic is that the electric field of the space charge of the electron avalanches generated in the discharge is comparable with the external field, thus, the resulting discharge is pulseless and uniform.

The discharge bridges the electrodes covering a high volume but the reagents conversion was less than 5%. Moreover, the formation of dark filaments on the high voltage electrode was observed. These filaments grow in time and are conductive, as it can be deduced from the fact that the discharge starts form their ends. Due to their growing, the filaments are gradually approaching to the counter electrode until their distance from it becomes too short for the development of the discharge. These filaments were not

analyzed, however it can be likely assumed that they are made of carbon according to the known collateral reactions [171]:

$2CO \rightarrow CO_2 + C \qquad \Delta H = -171$ kJ/mol

$CH_4 \rightarrow 2H_2 + C \qquad \Delta H = 75$ kJ/mol

The conclusion is that this discharge regime favors these reactions while is not suitable for carrying out the process of dry reforming.

In the case of DBD supplied to the reactor modified as shown in Fig. 4.1.3 the voltage applied was 16 kV. One experiment with gases diluted with argon and one with pure methane and carbon dioxide 1:1 were performed. Due to the low frequency (50 Hz) of the power supply the corona discharge was extremely weak. GC analyses showed not significant conversion of the reagent gases. One of the reasons was attributed to the fact that the gas flows near the walls of the reactor bypassing the discharge zone. For this reason this reactor configuration was no more used.

The most efficient type of discharge was found to be the spark. It gives a high reagents conversion with a reasonable power input, so the following experiments described in this chapter were performed under this discharge regime.

4.2.2 Preliminary experiments with spark discharges

The first experiments with the spark discharge were performed with the gas diluted in argon, CH_4:CO_2:Ar = 1:1:2, using a total flow of 50 mL/min. In the presence of argon the optimum working voltage and frequency were 12 kV and 700 Hz, respectively. The chromatograms relative to an experiment in negative polarity are shown in Fig 4.2.1: in Fig. 4.2.1a the analysis of the initial mixture is reported, while in Fig 4.2.1b that of the gas subjected to the spark discharge. It is possible to see the strong decrease of the area of CO_2 and CH_4 and the appearance of a broad peak due to CO.

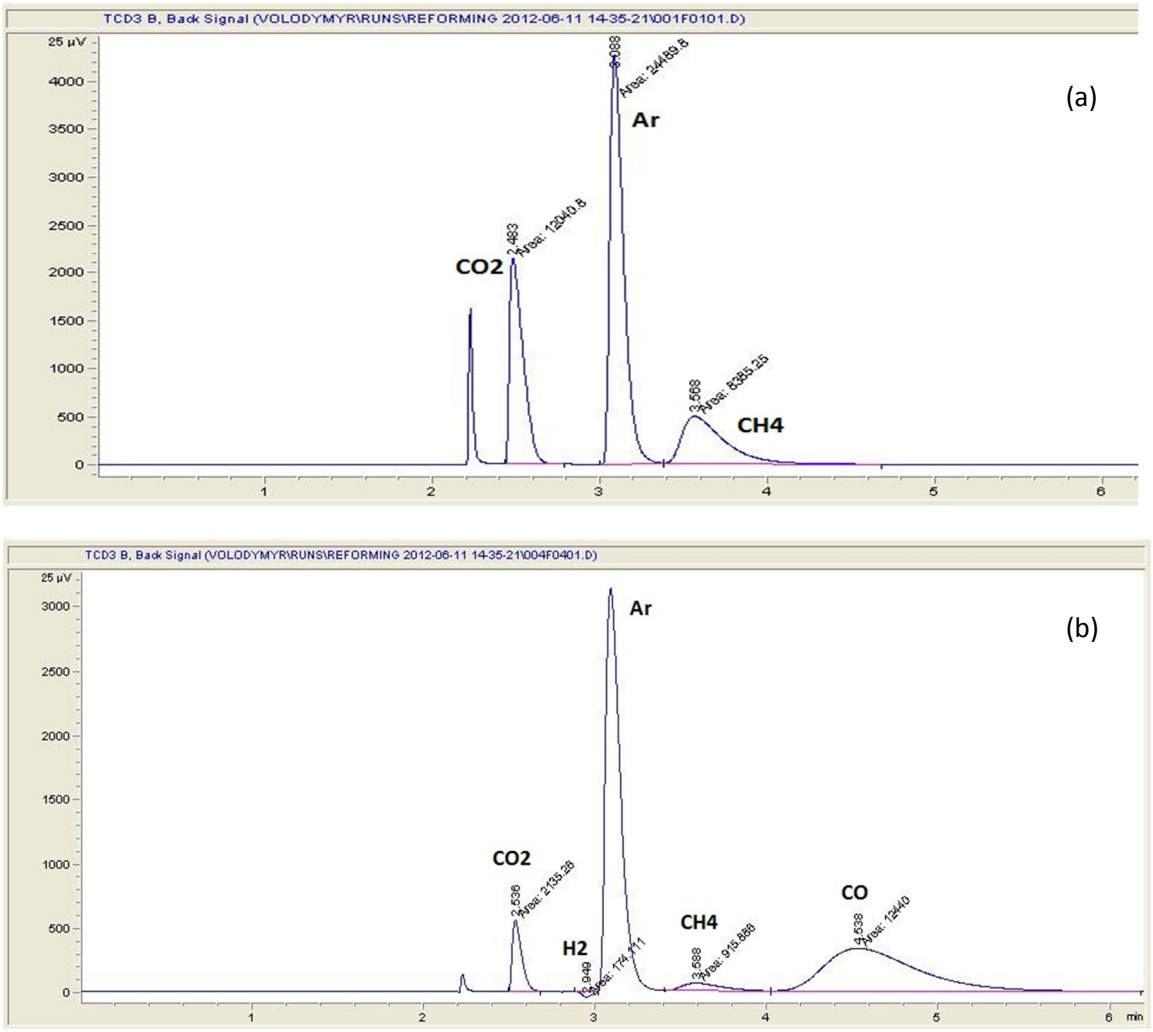

Fig. 4.2.1. GC/FID and TCD chromatograms of (a) the initial gas mixture and (b) the products obtained in an experiment of dry reforming in the presence of argon as dilution gas

The main set of the experiments were carried out in the pure gas mixture of CH_4:CO_2 = 1:1 at different flow rates and power inputs. Under these conditions the optimum working voltage was higher (14 kV) with respect to the discharge applied in the presence of argon, while the frequency of pulses was lower (500 Hz). Moreover, the stability of the discharge decreased. However, the presence of argon is not desirable in industrial processes due to its cost and to the lowering of the overall energy yield of the system. In Fig 4.2.2 the resulting chromatogram acquired at 50 mL/min and 20 W in negative polarity in an experiment performed with the pure mixture CH_4:CO_2 1:1 is shown.

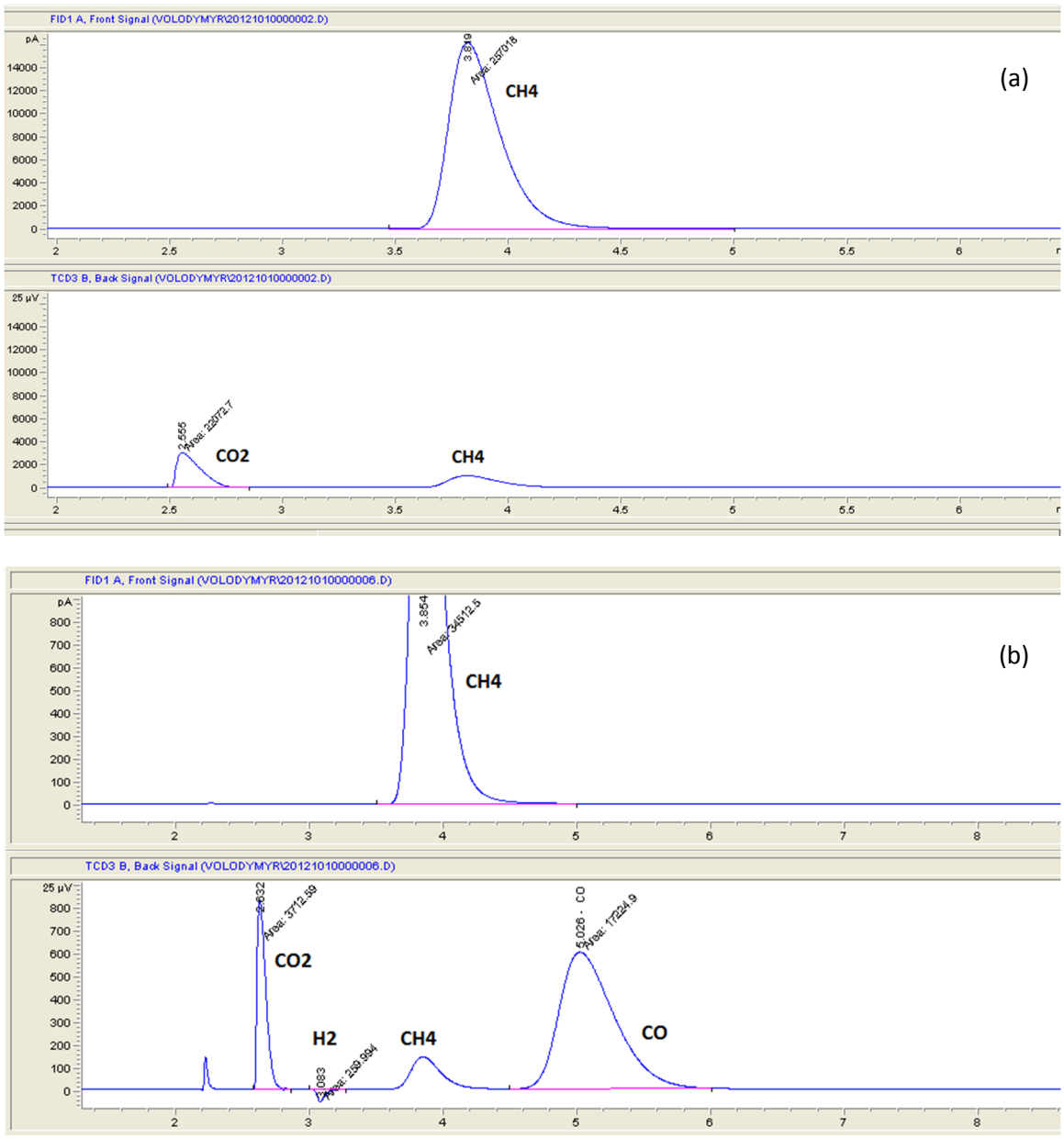

Fig. 4.2.2. GC/FID and TCD chromatograms of (a) the initial gas mixture and (b) the products obtained in an experiment of dry reforming without dilution

Additional experiments were performed in both polarities and it was noticed that when the average input power applied is the same the conversion, selectivity and energy efficiency of the process do not depend significantly on the polarity. This could be explained considering that the reaction between CH_4 and CO_2 takes place mainly in the hot spark channels whose lifetime is much higher than the time necessary for ionization and for the transition from a streamer to a spark regime.

Once verified that the MDR process is activated by the application of spark discharges of both polarities, the effect of the input flow rate, input power and CH_4:CO_2 ratio were investigated to characterize the process. In most of the experiments the negative polarity was preferred because in this case the tip works as the cathode and is consequently heated by ion collisions making the formation of the breakdown easier and more stable.

4.2.3 Effect of the input flow rate

The effect of the input flow rate was investigated by performing a series of experiments in negative polarity, changing the flow rate of the input gas mixture while maintaining constant the power input at 20 W and the CH_4:CO_2 ratio at 1:1. The results obtained are presented In Table 4.2.1. The conversion of the reagents and the yield of the products decrease as the flow increases as shown in Fig 4.2.3. This can be attributed to the decrease of the resident time of the gas inside the reaction zone and so to the lower treatment time. As the volume of the reaction zone is equal to 40 mL the residence time of the gas varies from 0.4 to 1.6 min.

The energy efficiency calculated by eq. (4.1.14) has the opposite trend, as increases as the total flow increases. The best flow rate regime cannot be considered the one which gives the highest of one of these parameters but has to be chosen considering reasonably high conversion, yield and energy efficiency.

Table 4.2.1

Power, W	Flow, mL/min	H_2 out, %	CO out, %	CH_4 conv, %	CO_2 conv, %	H_2 yield, %	CO yield, %	ME, mmol/kJ
20	25	41.2	46.1	81.2	75.0	75.4	84.3	0.70
20	50	40.3	44.9	78.3	72.8	65.1	72.4	1.35
20	75	39.5	43.2	76.5	70.6	59.7	65.3	2.0
20	100	38.9	41.0	71.2	64.7	56.0	59.1	2.44

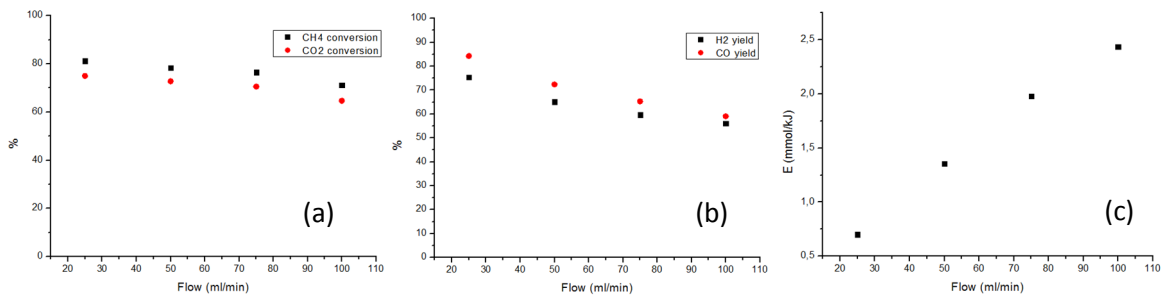

Fig. 4.2.3. Dependence of (a) conversion of the reagents, (b) yield of the products and (c) energy efficiency on the input flow rate.

4.2.4 Effect of the input electrical power

A series of experiments were performed changing the input power in negative polarity and maintaining constant the input flow rate at 100 mL/min. It is observed that increasing the power input the conversion of the reagents and the selectivity to syngas increase remarkably (Table 4.2.2). Moreover, due to the higher conversion, the percentage of H_2 and CO in the output gas goes closer to the ideal 50% ratio (Fig 4.2.4). As for the energy efficiency, this first decreases and then remains almost constant as the power input increases.

Table 4.2.2

Power, W	Flow, mL/min	H_2 out, %	CO out, %	CH_4 conv, %	CO_2 conv, %	H_2 yield, %	CO yield, %	ME, mmol/kJ
6	100	19.2	20.1	28.9	24.3	21.8	22.8	3.25
16	100	31.2	33.5	56.1	48.7	41.0	44.1	2.40
20	100	37.1	40.5	70.8	64.1	52.9	57.7	2.42
24	100	39.1	44.9	78.3	73.5	57.8	66.4	2.31

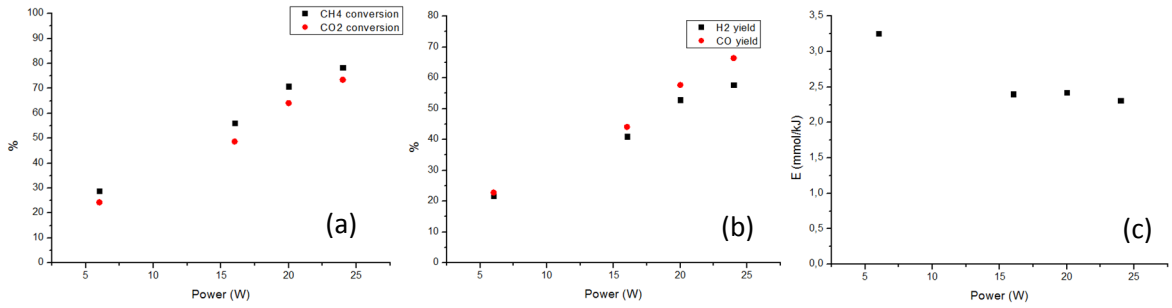

Fig. 4.2.4. Dependence of (a) reagents conversion, (b) yield of the products and (c) energy efficiency on the input electrical power.

The maximum power applied was 24 W because at higher values the frequency of the pulses increases up to 2 kHz. With this high repetition rate the time is not enough to renew the insulation of the gas: the sparks disappear and the discharge is transferred into a continuous glow regime. This change induces a drastic decrease of the conversion efficiency.

In all the experiments described in this and in the previous paragraphs the methane conversion is higher than that of a carbon dioxide, while the yield of hydrogen is lower than that of CO. This could be explained considering the formation of water which was trapped in the cooling trap as ice. Moreover, in all cases traces of gaseous carbon suboxide and its solid polymers are supposed to be formed [172]. This is deduced noticed by the deposition of a light brown material on the inner walls of the reactor and by the lachrymatory smell of the exhaust gas. However, the attempts to analyze these deposits were not successful.

The calculation of overall carbon balance shows that not more than 10% (worst case) of carbon is unaccounted for. However, this does not mean that this carbon is present in solid form as a deposit, but, as it will be shown in the next paragraph, some higher hydrocarbons are formed in the process.

The power of 20 W can be considered as optimal in terms of high conversion efficiency and low power input. The temperature profile of the reactor obtained when the power input of 20 W is applied was acquired using the N-type thermocouple and is shown in Fig 4.2.5.

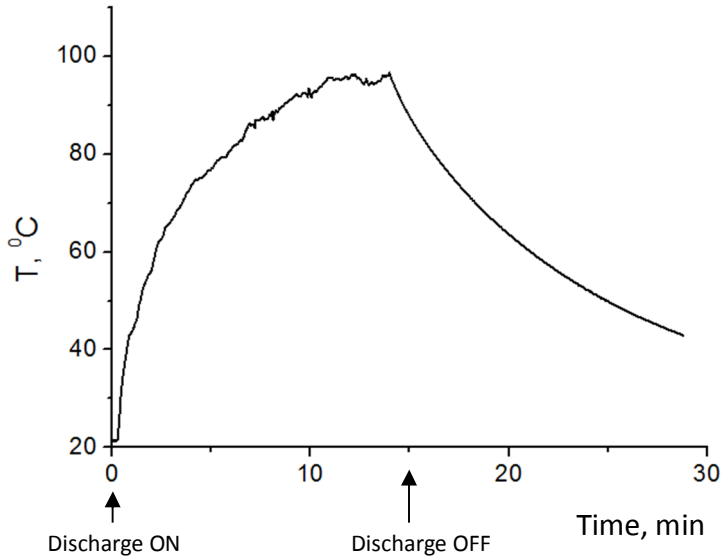

Fig. 4.2.5. Temperature profile of the reactor.

The heating is provided only by the discharge. The temperature increases after the application of the discharge and after about 10 minutes reaches a stable value near 95-100°C. When the discharge is switched off the temperature returns back to the room temperature.

4.2.5 Study of the process as a function of the CO_2:CH_4 ratio

Once determined the optimal conditions of polarity, electrical power input and flow rate, that is negative polarity, 20 W and 50 mL/min, respectively, these were established to study the process as a function of the ratio between CO_2 and CH_4. The CO_2:CH_4 ratios investigated are 4:1, 3:1, 7:3, 3:2, 1:1, 2:3, 3:7 and 1:4. The reagents conversion and products yield and selectivity obtained in the experiments are reported in the Fig. 4.2.6.

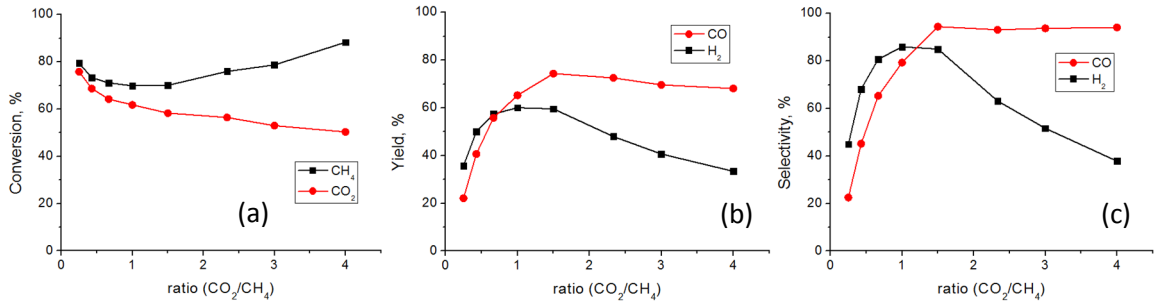

Fig. 4.2.6. Dependence of the (a) reagents conversion, (b) products yield and (c) products selectivity on the ratio between CO_2 and CH_4.

When the CO_2 content is increased the conversion of CO_2 goes down, while the conversion of methane decreases slightly until the CO_2 fraction becomes equal to that of CH_4, then, for a content of CO_2 higher than that of methane, goes up (Fig. 4.2.6a). The products yield and selectivity (Fig.s 4.2.6b and c) first increase with the increase of the percentage of CO_2, then decrease: for H_2 the highest yield and selectivity are obtained at the CO_2:CH_4 ratio equal to 1:1, while for CO at the ratio CO_2:CH_4 equal to 3:2, thus under a condition in which CO_2 amount is higher than that of CH_4.

A further significant experimental observation is the increase of the amount of water formed into the process and trapped into the cooling trap as the percentage of CO_2 increases with respect to that of methane. It was also observed that sometimes water condenses on the cold parts of the reactor.

These experimental results can be rationalized considering the occurrence of the reverse water gas shift (WGS) reaction, favored as the fraction of CO_2 increases.

$CO_2 + H_2 \rightarrow CO + H_2O + 41$ kJ/mol

This process contributes also to justify the increased formation of CO and the lower yield of hydrogen, formed and consumed by the WGS reaction, respectively, when the ratio CO_2:CH_4 is between 1:1 and 3:2.

For CO_2:CH_4 ratios higher than 3:2 the yield of CO goes slowly down as the CO_2 fraction increases and this is mainly due to the lower amount of CH_4, which also is a precursor of CO. However, the selectivity for CO remains very high as it is the main product formed from the CO_2, both in MDR and WGS reactions.

However, in addition to hydrogen and carbon monoxide, three other peaks were detected by FID, corresponding to byproducts formed in the process. Based on the mass spectrometric analysis, performed by the GC/FID/TCD/MS described in paragraph 4.1.4.1 using only the PLOT Q column, these peaks were attributed to, in order of elution, ethane, acetylene and ethylene. In Fig. 4.2.7 the total ion current obtained in the experiment with a CO_2:CH_4 ratio of 1:1 is shown. The signal of the peaks due to CH_4, CO and CO_2 is saturated due to the high sensitivity of the mass spectrometer detector; moreover these peaks are purely separated due to the absence of the PLOT MOLSIEVE column. The following three peaks, real object of this analysis, have a much lower area and were attributed to ethane, acetylene and ethylene, on the basis of the comparison between their corresponding mass spectra, reported in Fig. 4.2.8, with those in the NIST library [170].

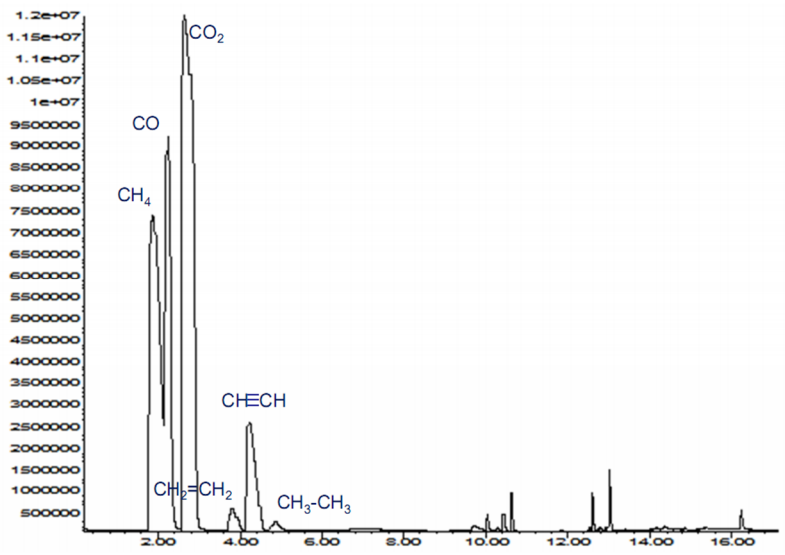

Fig. 4.2.7. TIC chromatogram of the products of plasma driven dry reforming.

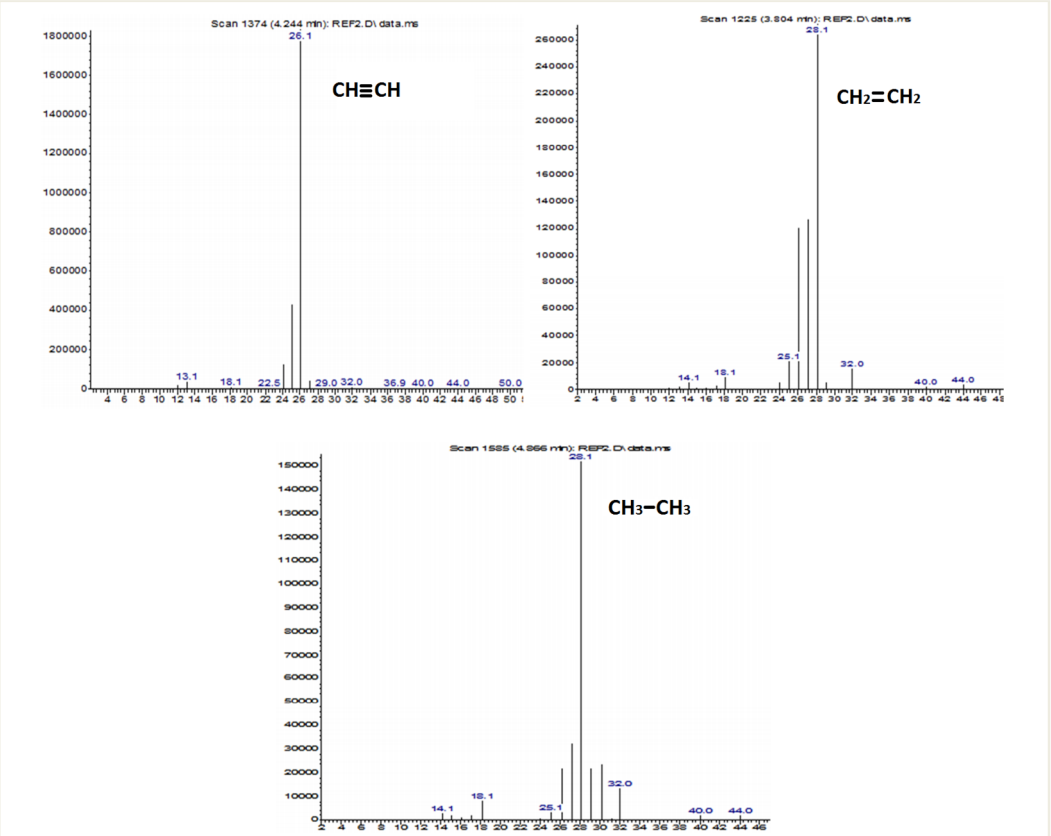

Fig. 4.2.8. Mass spectra of the byproducts of the plasma driven MDR, attributed to acetylene, ethylene and ethane.

Once identified, the area of these peaks were taken from the FID traces of the GC instrument routinely used. These are reported in Fig. 4.2.9 as a function of the ratio between CO_2 and CH_4. Assuming that the instrument response to the three compounds is similar, it can be noted that acetylene is the predominant one and that their relative concentrations follow the order acetylene > ethylene > ethane.

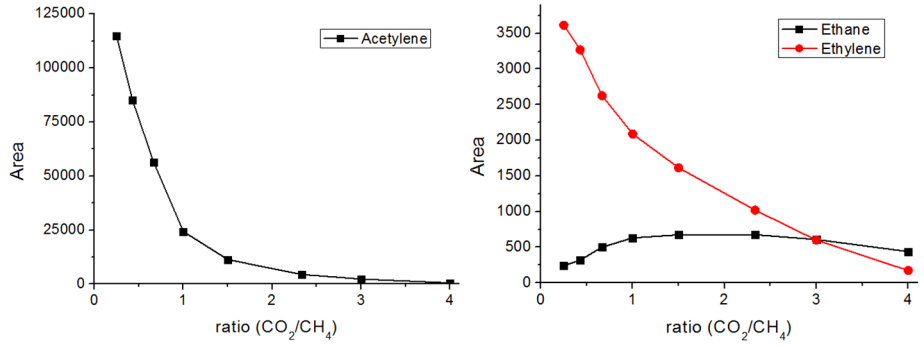

Fig. 4.2.9. GC area of the C_2 hydrocarbons obtained in MDR process as a function of the CO_2:CH_4 ratio.

The formation of ethane can be attributed to the recombination of CH_3 radicals (eq. 4.2.1), originating from the dissociation of methane (eq. 4.2.2) or from its reaction with atomic oxygen (eq. 4.2.3) [124, 125].

$$2\ CH_3 \rightarrow C_2H_6 \qquad (4.2.1)$$

$$CH_4 + e^- \rightarrow CH_3 + H + e^- \qquad (4.2.2)$$

$$CH_4 + O \rightarrow CH_3 + OH \qquad (4.2.3)$$

For the formation of ethylene and acetylene in the plasma driven MDR three main pathways are considered in the literature:

1. recombination of radicals (C, CH, CH_2) [124, 125, 131]:

$CH_2 + CH_2 \rightarrow C_2H_4$

$CH + CH \rightarrow C_2H_2$

$C + CH_2 \rightarrow C_2H_2$

$H + C_2H \rightarrow C_2H_2$

2. inelastic collisions of CH_4 with radicals [131]:

$C + CH_4 \rightarrow C_2H_4$

$C + CH_4 \rightarrow C_2H_2 + 2\ H$

3. ethane or ethylene dehydrogenation due to inelastic collisions with electrons [124, 125]:

$C_2H_6 + e^- \rightarrow C_2H_4 + H_2 + e^-$

$C_2H_4 + e^- \rightarrow C_2H_2 + H_2 + e^-$

The formation of ethylene and acetylene, as originates mainly from methane, increases significantly as the percentage of CH_4 in the initial mixture increases (Fig. 4.2.9). On the contrary, the concentration of ethane, also if this molecule has the same origin as ethylene and acetylene, is not much affected by the CO_2:CH_4 ratio. This can be ascribed to the subsequent processes of dehydrogenation which leads to the formation of ethylene and then acetylene. Acetylene proved to be the most stable compound under the applied discharge conditions and for this reason it is accumulated and reaches the highest concentration with respect to the other C2 hydrocarbons. This result differs from what is found in DBD and pulsed glow plasma, in which ethane is reported as an abundant product due to the high concentration of CH_3 radicals [131].

Thanks to the availability of a tank of acetylene, it was possible to build the calibration curve for this compound. Selectivity and yield of this byproduct were thus calculated and are reported in Table 4.2.3 and in Fig 4.2.10. It is possible to see that the selectivity and yield of acetylene decrease when the concentration of CO_2 increases; on the contrary, in the CH_4 rich gas the yield of acetylene is quite high in agreement with the high methane conversion and low H_2 yield and selectivity observed (Fig.s 4.2.6b and c).

Table 4.2.3

CO_2 flow, ml/min	**CH_4 flow, ml/min**	**CO_2/CH_4 ratio**	**Selectivity of acetylene, %**	**Yield of acetylene, %**
40	10	4:1	0.20	0.12
37.5	12.5	3:1	0.93	0.55
35	15	7:3	1.86	1.16
30	20	3:2	5.45	3.43
25	25	1:1	11.41	7.51
20	30	2:3	25.66	17.53
15	35	3:7	32.78	23.57
10	40	1:4	29.42	23.15

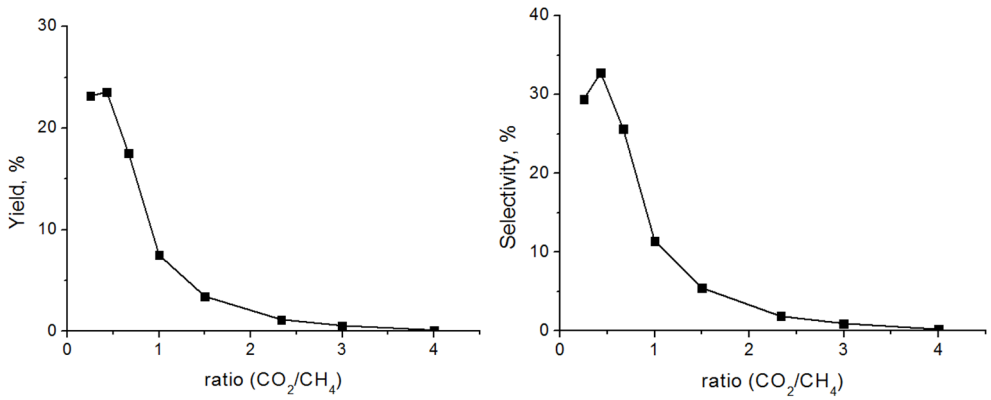

Fig. 4.2.10. Yield and selectivity of acetylene as a function of the input gas composition.

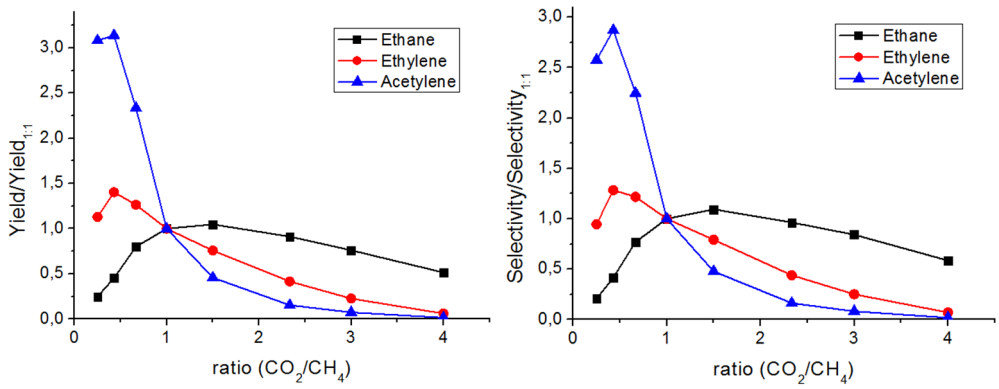

Fig. 4.2.11. Normalized yield and selectivity of C_2 hydrocarbons with respect yield and selectivity of acetylene obtained at CO_2/CH_4 stoichiometric ratio 1:1 as a function of the input gas composition.

To evaluate the yield and selectivity of the other two C_2 hydrocarbons, for which no standards were available, these parameters were normalized with respect to the yield and selectivity of acetylene obtained in the experiment with CO_2:CH_4 ratio equal to 1:1 (Fig. 4.2.11). As in the case of acetylene, the relative yields and selectivities of ethane and ethylene present a maximum. This is attributed to the relative contribution of reactions (4.2.2) and (4.2.3) in the formation of CH_3 radicals, as the first does not require the presence of CO_2, while the second does, as atomic oxygen originates from CO_2. This relative contribution is obviously dependent on the CO_2:CH_4 ratio.

Considering the formation of the C2 hydrocarbons as byproducts in the evaluation of the results reported in Fig. 4.2.6a it is possible to note that the monotonous decreasing of the conversion of CO_2 as its fraction in the initial mixture increases supports that fact that this is limited by the absence of reductants (CH_4 or H_2). Similarly, the conversion of CH_4 is favored by the presence of CO_2 for a CO_2:CH_4 ratio equal and higher than 1. For lower CO_2:CH_4 ratio the high conversion of CH_4 and the low yield and selectivity for syngas corresponds to an increased selectivity for hydrocarbons formation.

Moreover, it was observed that increasing the fraction of methane induces the appearance and increase of carbon deposition. However, this is usually not significant if the overall carbon balance is considered. Moreover, it does not influence the discharge, which remains substantially stable. Actually, what is worse for the stability of the spark discharge is the presence of humidity observed as the fraction of CO_2 increases.

4.2.6 Sparks discharges in pure CH_4, CO_2 and CO

To gain more insight about the process of MDR, experiments in which the spark discharge was applied in pure CH_4, CO_2 and CO were performed maintaining constant the conditions of flow rate (50 mL/min) and the power of 20W. In pure CO_2 the discharge is stable and does not cause any kind of deposition. During the processing, CO_2 is converted to form CO and O_2 by reactions (4.2.4) and (4.2.5)[173]:

$$CO_2 + e^- \rightarrow CO + O + e^- + 5.57\ eV \qquad (4.2.4)$$

$$O + O \rightarrow O_2 \qquad (4.2.5)$$

The TCD chromatogram obtained in the analysis of the output gas is shown in Fig. 4.2.12.

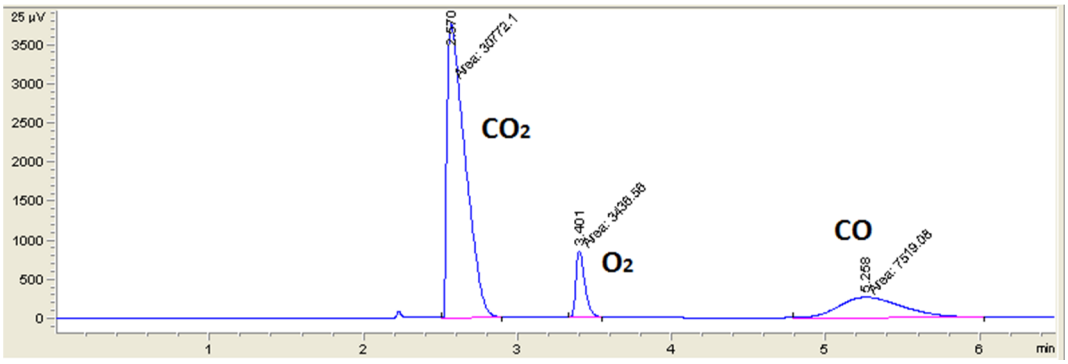

Fig. 4.2.12. Chromatogram of the output gas in the treatment of pure CO_2 with spark discharges.

The conversion of CO_2 was near 20%, the yield of CO 26% and the selectivity for CO near 100%.

The limited conversion of CO_2 can be ascribed to the recombination of CO and O formed from CO_2, due to the exothermicity of the reverse reaction:

$$CO + O \rightarrow CO_2$$

$$CO + O^- \rightarrow CO_2 + e^-$$

However, in the short plasma pulses these reactions are quenched thus favoring the CO_2 conversion.

In the case of the application of the spark discharges to pure CH_4 the main products detected are higher hydrocarbons and hydrogen. The chromatogram detected by FID is shown in Fig.4.2.13.

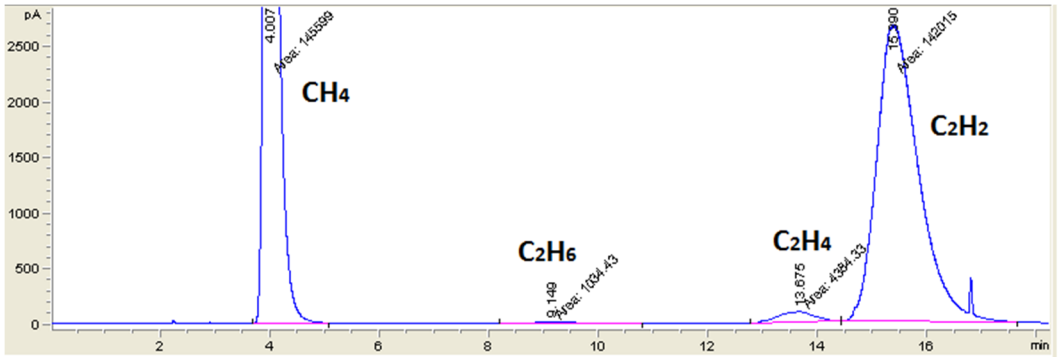

Fig. 4.2.13. FID chromatogram of the output gas in the treatment of pure CH_4 with spark discharges.

The yield of H_2 is only of about 25%, while the conversion of CH_4 is high, it reaches 75%. The concentration of the main product, acetylene, is near 14% (yield and selectivity 24% and 32%, respectively), while the concentrations of ethylene and ethane are much lower, leading to think that hydrocarbons higher than C_2 are formed under these conditions. In the literature there are some examples in which C3 and C4 hydrocarbons are formed by consecutive reactions of radical recombination [124]:

$$CH_4 + e^- \rightarrow CH_3 + H + e^-$$

$$CH_4 + e^- \rightarrow CH_2 + H_2 + e^-$$

$$2\ CH_3 \rightarrow C_2H_6$$

$$C_2H_6 + H \rightarrow C_2H_5 + H_2$$

$$C_2H_5 + CH_3 \rightarrow C_3H_8$$

$$C_2H_5 + C_2H_5 \rightarrow C_4H_{10}$$

In the presence of only methane, thus without any oxygenated species into the system, carbon deposition in the reactor was strong. However, the discharge remained stable.

An experiment in which the spark discharge was applied to pure CO shows that under these conditions carbon monoxide does not react. This is surely a positive finding as demonstrates that, once formed, the CO molecule is stable under the reaction conditions applied.

4.2.7 Optical Emission Spectroscopy (OES) investigation of plasma driven dry reforming of methane

Experimental apparatus and procedures

Emission spectroscopy was applied for the monitoring of the excited species formed in the discharge zone. The instrument was a high resolution Spectrograph Acton SP 2558, Czerny-Turner mounting, with a focal length of 500 mm, equipped with a rotating turret hosting two different reflecting gratings: 2400 grooves/mm (blazed holographic grating, 500 nm blazed) and 1800 grooves/mm (blazed holographic grating, UV optimized). The detector is a CCD camera PIXIS 100B_eXcelon, back illuminated, full frame, Large CCD sensor 1340 x 100 pixels, 20 µm x 20 µm pixel size, eXelon sensor technology for lowest etaloning and enhanced sensitivity. A unichrome UV coating is also present on the detector back surface of the CCD sensor to enhance the UV sensitivity of the device. With the 2400 gr/mm grating the plate factor is around to 0.13 Å/pixel, while with the 1800 gr/mm the plate factor is of about 0.18 Å /pixel. The spectral range achievable is 200 – 850 nm. Depending on the grating position and the corresponding wavelength a spectral resolution between 2 Å up to 0.5 Å can be obtained.

A 6 m long optical fiber was used to collect the emitted light from the plasma to the spectrometer. One optical fiber termination was held by a support at 15 cm from the reactor perpendicularly, at the same height of the plasma region developed in the middle of the reactor between the electrodes, while the other termination is directly mounted on the entrance slit of the spectrometer.

Results and discussion

An overall view of the emission recorded when the discharge was applied in pure CO_2 and in a 1:1 mixture of CO_2 and CH_4 is presented in Fig. 4.2.14. The traces shown, which span a very wide wavelength range (200 – 500 nm), were constructed by gluing together several spectral acquisitions obtained at high resolution over much smaller spectral regions (about 15 - 20 nm for each spectrum). As for the emission intensity, it should be noted that a quantitative comparison between the two traces cannot be made because of the different discharge conditions used. Thus, the applied voltages sufficient to ignite the discharge were 20 kV in the experiment in pure CO_2 (Fig. 4.2.14, black trace) and 16 kV in the experiment with a 1:1 mixture of CO_2 and methane (Fig. 4.2.14, blue trace). Nevertheless, some useful inferences and conclusions can be drawn from comparing the results obtained with pure CO_2, used as a reference, and with the dry reforming mixture.

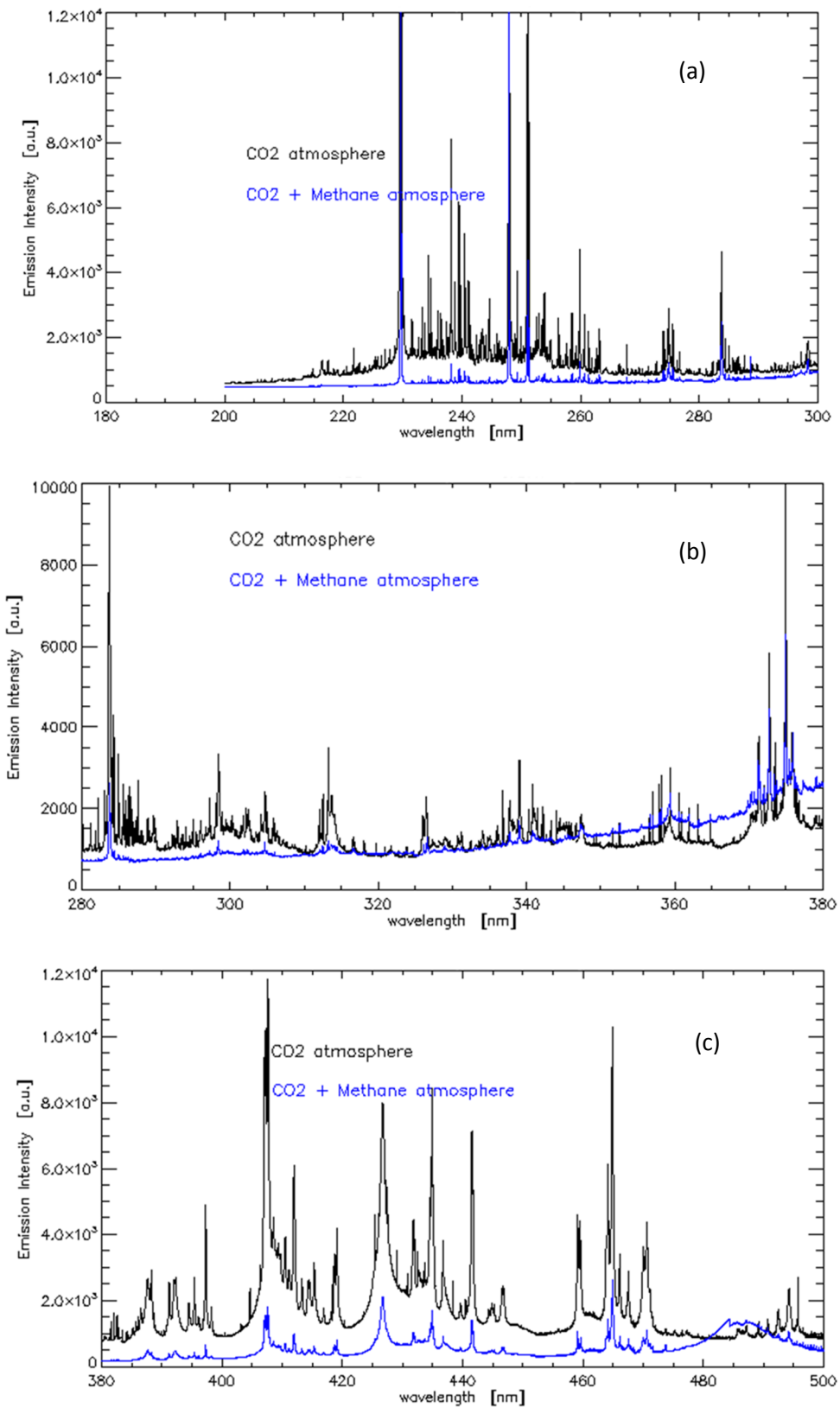

Fig. 4.2.14. Emission spectra acquired for discharge in pure CO_2 (black) and in 1:1 mixture of CO_2 and CH_4 (blue): (a) scan between 200 – 300 nm; (b) scan between 280 – 380 nm; (c) scan between 380 – 500 nm.

A first important observation concerns the fact that the two traces are very similar, showing mostly common bands and patterns. It therefore appears that the major emitting species are due to CO_2 and to its products also in the reforming gas mixture. Similar observations were reported in a recent paper describing the plasma-catalytic reforming of methane in an atmospheric dielectric barrier discharge reactor [174]. In this work, the comparison of the emission spectra in pure CO_2, in pure CH_4, in CO_2/CH_4 mixture and in presence of the mixture together with the catalyst are shown at a fixed discharge power of 50 W.

Numerous bands are attributed to CO_2, as shown in the expanded traces reported in Fig. 4.2.15:

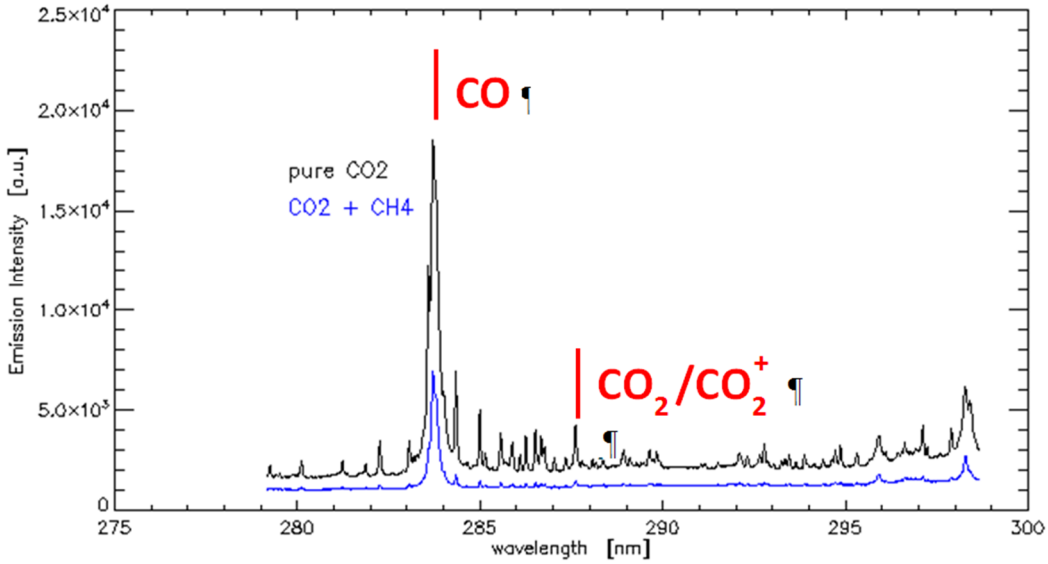

Fig. 4.2.15. Emission spectra acquired from 279 to 299 nm in pure CO_2 (black) and in 1:1 mixture of CO_2 and CH_4 (blue).

The difficult task of identification of the emission bands is substantially based on the data reported in the Pearse's book: actually there are possible limitation due to the fact, for example, that tabulated data do not discriminate between the neutral or ionized CO_2 species and the experimental conditions, although reported, might be quite different from ours [175].

Additional emission bands should be attributable to CO (Fig. 4.2.15) [174, 175] this attribution is consistent with the results of GC analysis of the gas at the reactor outlet which

shows the presence of CO as a product of the discharge treatment also of pure CO_2 (Fig. 4.2.12). CO emission appears to be more intense in the experiment with CO_2/CH_4, as is reasonable to expect due to the very high yield of CO obtained in this case. In addition to these common features, an additional important difference is found in the spectra recorded with the CO_2/CH_4 mixture in the 480 – 500 nm interval (Fig. 4.2.14c), due to the presence of a very intense and broad emission line presumably attributable to the H_β transition (486.132 nm), even if in that zone also a CO emission band should be visible (483.5 nm) [175].

Another important species detected in both experiments is atomic oxygen (OI) showing the characteristic triplet at 777 nm due to the $3p\ ^5P_0 – 3s\ ^5S_0$ transitions (Fig. 4.2.16) [176]. The triplet appears to be remarkably well resolved in both spectra. The relative intensities of the three emission lines belonging to the triplet are also consistent with the expected theoretical values.

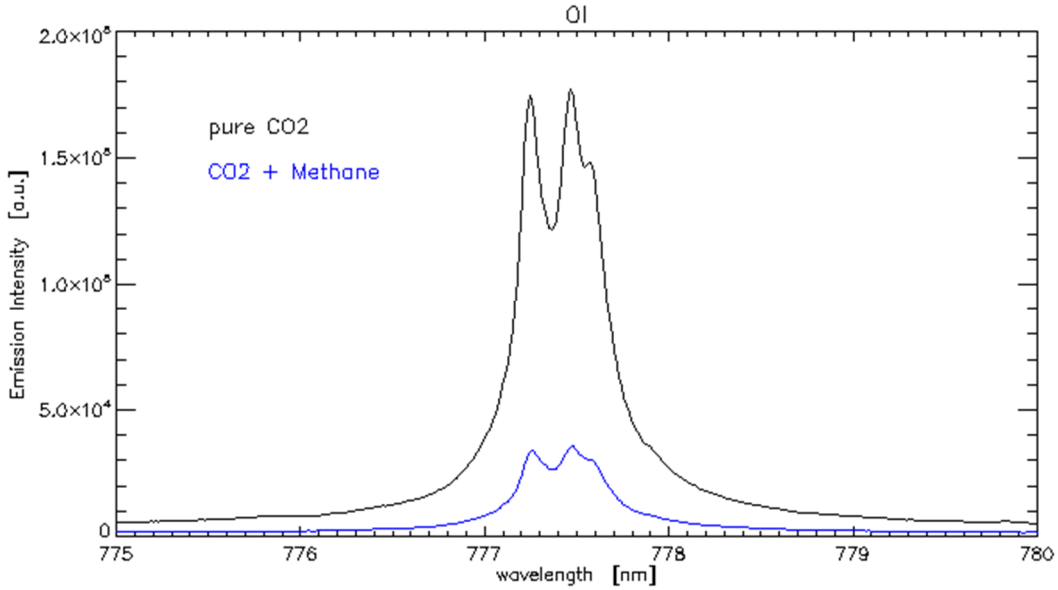

Fig. 4.2.16. The atomic oxygen triplet acquired in pure CO_2 (black) and in 1:1 mixture of CO_2 and CH_4 (blue).

Another remarkable difference between the two spectra with and without methane concerns the presence of the H_α (Fig. 4.2.17a) and H_β (Fig. 4.2.18b) emission lines found at 656.279 nm and 486.132 nm, respectively.

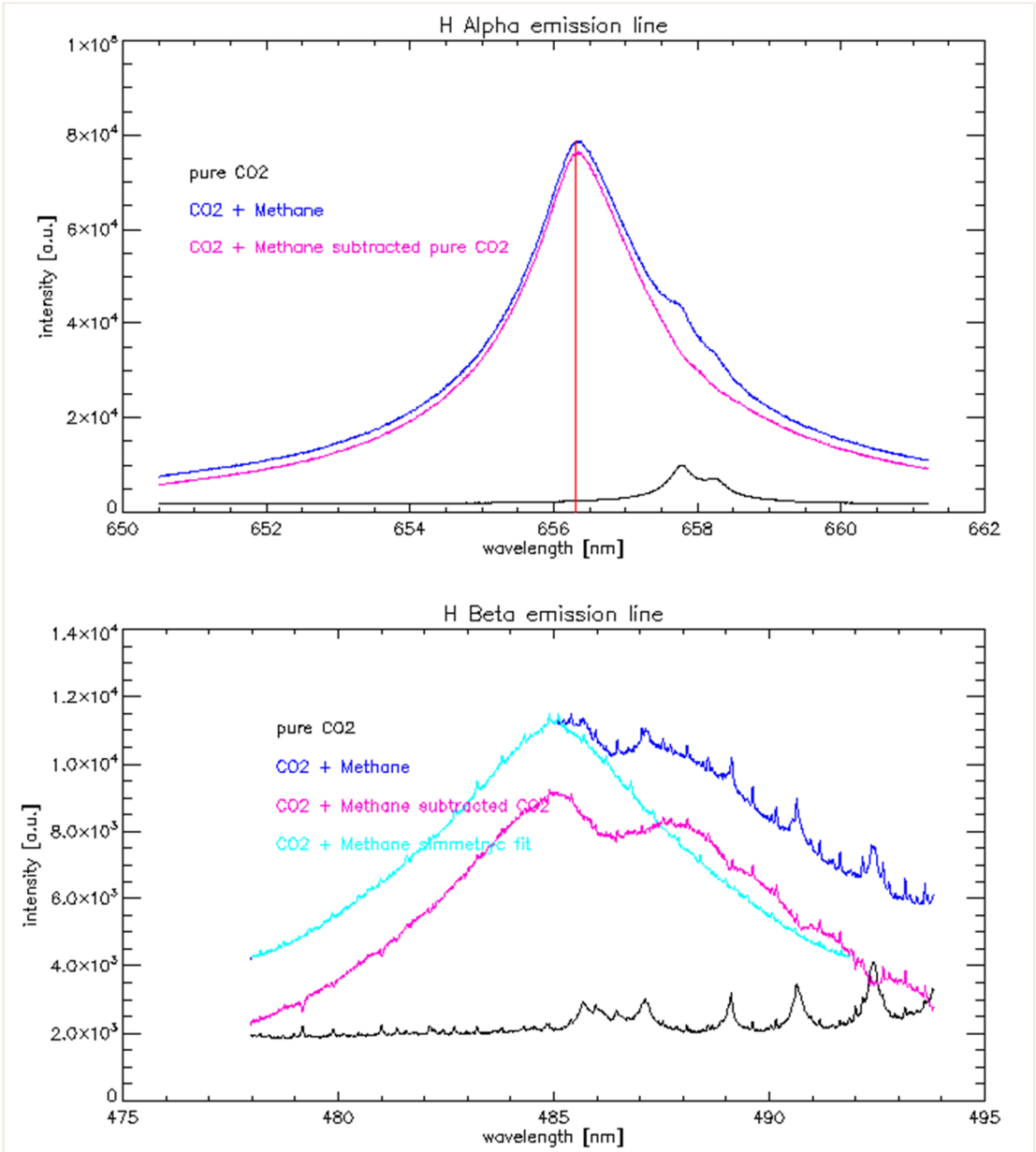

Fig. 4.2.16. H_α and H_β emission lines of oxygen triplet acquired in pure CO_2 (black) and in 1:1 mixture of CO_2 and CH_4 (blue).

The hydrogen emission lines of the Balmer series, which are obviously not detected in the experiment run with pure CO_2, provide a means to derive the average electron density, a most important data to characterize the plasma. The H_α emission line exhibits a Voigtian shape, given by the convolution of a Gaussian function due to the Doppler broadening and a Lorentzian function due to the natural broadening. A clear structure is visible on the right hand side of emissive curve and its presence persists also in the spectrum acquired with pure CO_2. Taking advantage of this, the spectrum in CO_2 has been scaled and

subtracted to the H_α emission line in order to eliminate this unknown contribution. With this expedient, it was possible to optimize the Voigtian fit simulation respect with to the experimental data.

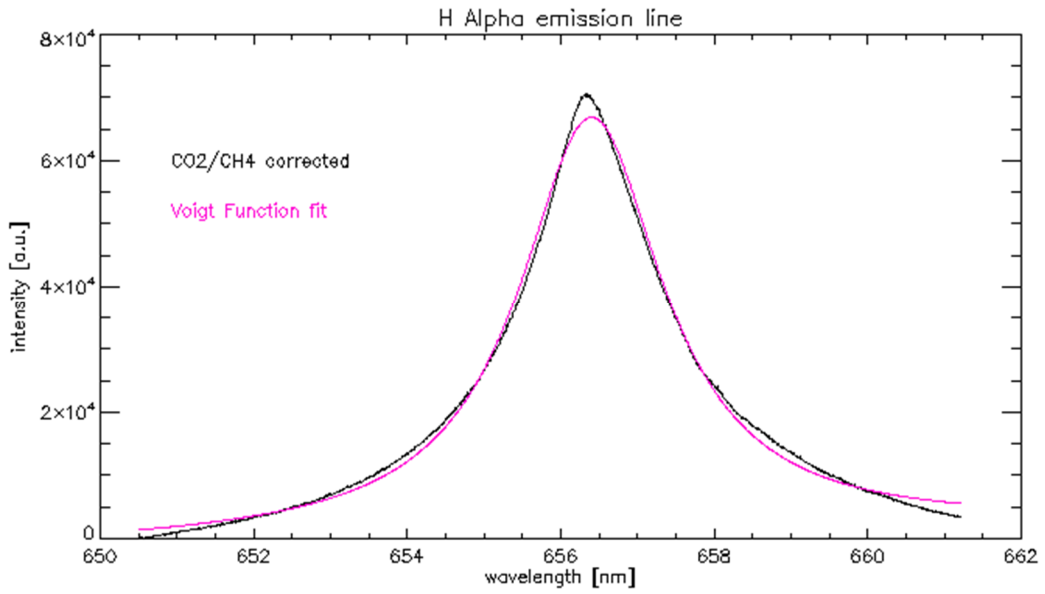

Fig. 4.2.16. Spectrum of the Hα emission line in CO_2/CH_4 mixture cleaned with the subtraction of the spectrum in CO_2 to eliminate the contribution of two unknown transitions (black); reconstruction of the Hα emission line by a Voigtian function fit (pink).

Applying the procedure described in the work of Konjevic [177], it was possible to fit the H_α emission light with a Voigtian function and to obtain an electron density of $5.7 \cdot 10^{14}$ cm^{-3}. The order of magnitude found is consistent with the expected value and, considering that the operational regime is below a critical density threshold, the procedure adopted is fully justified. Contrary to what observed by Whitehead et al., no bands due to CH stand out in the treatment of the mixture CO_2/CH_4. This can be related to the lower percentage of higher hydrocarbons formed in our process with respect to that reported in the literature.

4.3 Conclusions

The study of the process of dry reforming of methane driven by plasma required as first major task the design of the experimental apparatus to apply electrical high voltage discharges to produce atmospheric plasma. The requirements for this apparatus were very strict, in particular considering the choice to perform emission spectroscopy measurements and in view of future investigations on the combination of plasma with heterogeneous catalysis. Thus, the setup finally obtained is surely unique and very versatile.

The first experiments were aimed at finding the best type of electrical discharge, among a few which could be tested, to efficiently activate the process of dry reforming. The results clearly identified the spark discharge as the best candidate. When applied in our reactor, this discharge produces plasma with an average electron density of $5.7 \cdot 10^{14}$ cm^{-3}, as measured by emission spectroscopy techniques, and induces some heating of the gas, as shown by the measured bulk temperature approaching 100°C. However, the main characteristic of spark is the development of discharge filaments, in which the electron density and the temperature of the species, such as electrons, radicals, ions, but also atoms and molecules, are significantly higher than those of the bulk. In our reactor these filaments fill completely the plasma zone, thus, it can be estimated that the elementary processes of the reaction between methane and carbon dioxide take place inside these filaments.

Once the best discharge regime was established, the effect of different experimental conditions was investigated: discharge polarity, dilution with argon, flow rate, input electrical power, CH_4:CO_2 ratio. The best results, considering either conversion, yield and selectivity or energy efficiency and stability of the discharge, are obtained in negative polarity with a flow rate of 100 mL/min, a power input of 20 W and a CO_2/CH_4 ratio between 0.5 and 1.5. In particular, with a CO_2:CH_4 ratio equal to 1:1, the obtained conversion of CH_4 (74%) and CO_2 (69%) and selectivities for hydrogen (78%) and CO (86%) are quite high. The energy efficiency, equal to 2.3-2.4 mmol/kJ, is also very good if compared with the performance of other devices published in the literature [178]. Not many examples of spark discharges applied to dry reforming of methane were reported previously. However, our system proves to perform better than any of them. For example, a thyratron-triggered

kilohertz pulsed system, which produces spark discharges, described in the literature [133] gives a conversion of about 60% and 50% for CH_4 and CO_2, respectively, and an efficiency approaching 2.1 mmol/kJ.

In evaluating the results it has to be considered that our reactor is a pilot laboratory-scaled prototype. Scaling up is always a challenge. However, both the reactor and the process it sustains have the right characteristics to be easily scaled up. These are: the simplicity of the power supply schematic; the fact that the system is “self-triggering”, that is it is not controlled by high-voltage power switches like spark-gaps or thyratrons which cost and have a limited lifetime; the linear dependence of the reagents conversion and products yield on the input electrical power; the low dependence on the input flow rate.

Another important characteristic of our reactor is that it does not produce carbon deposition and is not much sensitive to any kind of deposits. Indeed, due to the strong but short pulse currents developing between the tip and the plate, the surfaces of the electrode are cleaned by the discharge itself and any possible deposition is avoided.

As for the dependence of reagents conversion and products selectivity on the gas composition, it was observed that these parameters are not significantly affected for a CO_2/CH_4 ratio between 0.5 and 1.5. This is another important result which gives flexibility to the process, necessary when natural feedstock and biomass are used.

Inferences on the mechanism of the process are derived from the observation of some byproducts, ethane, ethylene and acetylene, as confirms the formation of methyl radicals, which however can be due either to electron dissociation of methane or to reaction of methane with atomic oxygen. Additional important information concern the formation of many excited species, observed by emission spectroscopy measurements, and the observation of water formation at high CO_2 concentrations ($CO_2/CH_4 > 2$). It was deduced that this condition favors the reverse water gas shift reaction forming water and consuming carbon dioxide and hydrogen.

6. REFERENCES

[1] Van Veldhuizen EM. Electrical discharges for environmental purposes: fundamentals and applications. *Nova Science Publishers, Inc.,* Huntington, NY, 2000.

[2] IGBP, 2001 - Global Change and the Earth System: a Planet under stress – IGBP Science n.4

[3] UNEP, 2002 - Global Environment Outlook 3 – Earth scan

[4] Earth Policy Institute – website http://www.earth-policy.org

[5] World Watch Institute – website http://www.worldwtach.org

[6] World Resources Institute – website http://www.wri.org

[7] European Pollutant Emission Register – website http://eper.eea.europa.eu/

[8] Baird C, Cann M. Environmental Chemistry. 2nd Ed., 2006.

[9] Watson RT, Meira Filho LG, Sanhueza E, Janetos A. Greenhouse gases: sources and sinks. *IPCC Suppl Report* 1992; 29-46.

[10] Hester RE, Harrison RM. Volatile organic compounds in the atmosphere. *The Royal Society of Chemistry*, Letchworth, UK, 1995.

[11] ESRL Global Monitoring Division – web link http://www.esrl.noaa.gov/gmd/ccgg/globalview

[12] Pacala S, Socolow R. Stabilization Wedges: Solving the climate problem for the next 50 years with current technologies. *Science* 2004; 305: 968-972.

[13] Lehmann J. A handful of carbon. *Nature* 2007; 447: 143-144.

[14] Windle CD, Perutz RN. Advances in molecular photocatalytic and electrocatalytic CO_2 reduction. *Coordination Chem Rev* 2012; 256: 2562-2570.

[15] Varghese OK, Paulose M, LaTempa TJ, Grimes CA. High-rate solar photocatalytic conversion of CO_2 and water vapor to hydrocarbon fuels. *Nano Lett* 2009; 9(2): 731-737.

[16] GoNano Technologies, Inc. – web link http://gonano-technologies.com/pollution-control-products/carbon-capture-recycle/

[17] Pescarmona PP, Taherimehr M. Challenges in the catalytic synthesis of cyclic and polymeric carbonates from epoxides and CO_2. *Catal Sci Technol* 2012; 2: 2169-2187.

[18] Royal Society of Chemistry – web link http://www.rsc.org/chemistryworld/News/2009/October/09100901.asp

[19] Royal Society of Chemistry – web link http://www.rsc.org/chemistryworld/News/2010/July/28071001.asp

[20] Amato I. Catalytic conversion could be a gas. *Science* 1993; 259: 311.

[21] Satterfield CN. Heterogeneous catalysis in practice. 2nd Ed., McGraw-Hill, NY, 1991.

[22] Bhat SA, Sadhukhan J. Process intensification aspects for steam methane reforming: An overview. *AIChE Journal* 2009; 55(2): 408-422.

[23] Sridhar S, Smitha B, Aminabhavi TM. Separation of carbon dioxide from natural gas mixtures through polymeric membranes – A review. *Sep Purif Rev* 2007; 36(2): 113-174.

[24] Deutschmann O, Schmidt L. Two-dimensional modeling of partial oxidation of methane on rhodium in a short contact time reactor. *27th International Symposium on Combustion* 1998; 2283-2291.

[25] Abbas HF, WanDaud WMA. Hydrogen production by methane decomposition: A review. *Int J Hydrogen Energy* 2010; 35: 1160-1190.

[26] Wang S, Lu GQ. Carbon dioxide reforming of methane to produce synthesis gas over metal-supported catalysts: State of the art. *Energy Fuels* 1996; 10: 896-904.

[27] Fan MS, Abdullah AZ, Bhatia S. Catalytic technology for carbon dioxide reforming of methane to synthesis gas. *ChemCatChem* 2009; 1: 192-208.

[28] Gallucci F, Tosti S, Basile A, Pd–Ag tubular membrane reactors for methane dry reforming: A reactive method for CO_2 consumption and H_2 production. *A. J. Membr Sci* 2008; 317: 96-105.

[29] Chen HL, Lee HM, Chen SH, Chao Y, Chang MB. Review of plasma catalysis on hydrocarbon reforming for hydrogen production – Interaction, integration, and prospects. *Appl Catal B* 2008; 85: 1-9.

[30] Hu YH, Ruckenstein E. Catalytic conversion of methane to synthesis gas by partial oxidation and CO_2 reforming. *Adv Catal* 2004; 48: 297-345.

[31] Fidalgo B, Zubizarreta L, Bermúdez JM, Arenillas A, Menéndez JA. Synthesis of carbon-supported nickel catalysts for the dry reforming of CH_4. *Fuel Process Technol* 2010; 91: 765-769.

[32] Guczi L, Stefler G, Geszti O, Sajó I, Pászti Z, Tompos A, Schay Z. Methane dry reforming with CO_2: A study on surface carbon species. *Appl Catal A* 2010; 375: 236-246.

[33] García-Diéguez M, Pieta IS, Herrera MC, Larrubia MA, Alemany LJ. Improved Pt-Ni nanocatalysts for dry reforming of methane. *Appl Catal A: Gen* 2010; 377: 191-199.

[34] Castro Luna AE, Iriarte ME. Carbon dioxide reforming of methane over a metal modified Ni-Al_2O_3 catalyst. *Appl Catal A: Gen* 2008; 343: 10-15.

[35] Pawelec B, Damyanova S, Arishtirova K, Fierro JLG, Petrov L. Structural and surface features of PtNi catalysts for reforming of methane with CO_2. *Appl Catal A: Gen* 2007; 323: 188-201.

[36] Kohn MP, Castaldi MJ, Farrauto RJ. Auto-thermal and dry reforming of landfill gas over a Rh/γAl_2O_3 monolith catalyst. *Appl Catal B: Environ* 2010; 94: 125-133.

[37] Faroldi BM, Lombardo EA, Cornaglia LM. Surface properties and catalytic behavior of Ru supported on composite La_2O_3–SiO_2 oxides. *Appl Catal A: Gen* 2009; 369: 15-26.

[38] Carrara C, Múnera J, Lombardo EA, Cornaglia LM. Kinetic and stability studies of Ru/La_2O_3 used in the dry reforming of methane. *Top Catal* 2008; 51: 98-106.

[39] Langmuir I. Oscillations in ionized gases. *Proc. Natl. Acad. Sci.* U.S.A., 1928; 14: 627-637.

[40] Fridman A. Plasma chemistry. *Cambridge University Press*, New York, 2008.

[41] Bittencourt JA. Fundamentals of plasma physics. *Springer*, New York: Heidelberg, 2004.

[42] Chen FF. Introduction to plasma physics and controlled fusion: Plasma physics. 2nd Ed., *Plenum Press*, New York. 2000.

[43] Paschen F. *Wied. Ann.*, 1889; 37, 69.

[44] Raizer YP. Gas discharge physics. *Springer*, 1991.

[45] Goldman M, Goldman A. Corona Discharge, Gaseous Electronic. *Academic Press Inc.*, 1978; 1: 219-290.

[46] Siemens W. *Poggendorff Ann Phys Chem* 1857; 178: 66-122.

[47] Andrews T, Tait PG. *Phil Trans Roy Soc of London* 1860; 150: 113-131.

[48] Hautefeuille P, Chappuis J. *Compt Rend Acad Scé* 1881; 92: 80.

[49] Warburg E, Leithäuser G. *Ann Physik* 1909; 333: 313-325.

[50] Manley TC. *J. Electrochem. Soc.* 1943; 84: 83-96.

[51] Kogelschatz U. Dielectric-barrier discharges: their history, discharge physics, and industrial applications. *Plasma Chem Plasma Process* 2003; 23(1): 45p.

[52] Donohoe KG, Wydeven T. *J. Appl Polymer Sci.* 1979; 23: 2591-2601.

[53] Kanazawa S, Kogoma M, Moriwaki T, Okazaki SJ. *Phys D: Appl Phys* 1988, 21, 838-840.

[54] Massines F, Rabehi F, Decomps P, Gadri RB, Ségur P, Mayoux CJ. *Appl Phys* 1998; 83: 2950-2957.

[55] Boyers DG, Tiller WA. *Appl Phys Lett* 1982; 41: 28-30.

[56] Ammelt E, Schweng D, Purwins HG. Spatiotemporal pattern-formation in a lateral high-frequency glow discharge system. *Phys Lett A* 1993; 179: 348-354.

[57] Breazeal W, Flynn KM, Gwinn EG. Static and dynamic two patterns in self-extinguishing discharge avalanches. *Physical Review E* 1995; 52(2): 1503-1515.

[58] Kogelschatz U. Filamentary, patterned, and diffuse barrier discharges. *IEEE Trans Plasma Sci* 2002; 30(4): 1400-1408.

[59] Eliasson B, Kogelschatz U. Modeling and applications of silent discharge plasmas. *IEEE Trans Plasma Sci.* 1991; 19: 309-323.

[60] Steinle G, Neundorf D, Hiller W, Pietralla MJ. Two-dimensional simulation of filaments in barrier discharges. *Phys D: Appl Phys* 1999; 32: 1350-1356.

[61] Dřimal J, Gibalov VI, Samoilovich VG. Silent discharge in air, nitrogen andargon. *Czech J Phys: B* 1987; B37: 1248-1255.

[62] Gibalov VI, Dřimal J, Wronski M, Samoilovich VG. Barrier discharge. The transferred charge and ozone synthesis. *Contrib Plasma Phys* 1991; 31(1): 89-99.

[63] Lukas C, Spaan M, Schulz-von der Gathen V, Thomson M, Wegst R, Döbele HF, Neiger M. Dielectric barrier discharges with steep voltage rise: mapping of atomic nitrogen in single filaments measured by laser-induced fluorescence spectroscopy. *Plasma Sources Sci Technol* 2001; 10: 445-450.

[64] Kozlov KV, Wagner HE, Brandenburg R, Michel P. Spatio-temporally resolved spectroscopic diagnostics of the barrier discharge in air at atmospheric pressure. *J Phys D: Appl Phys* 2001; 34: 3164-3176.

[65] Kunze K, Miclea M, Musa G, Franzke J, Vadla C, Niemax K. Diode laser-aided diagnostics of a low-pressure dielectric barrier discharge applied in element-selective detection of molecular species. *Spectrochimica Acta B* 2002; 57: 137-146.

[66] Motret O, Hilbert C, Pellerin S, Pouvesle JM. Rotational temperature measurements in atmospheric pulsed dielectric barrier discharge - gas temperature and molecular fraction effects *J Phys D: Appl Phys* 2000; 33: 1493-1498.

[67] Spaan M, Leistikow J, Schulz-von der Gathen V, Döbele HF. Dielectric barrier discharges with steep voltage rise: laser absorption spectroscopy of NO concentrations and temperatures. *Plasma Sources Sci Technol* 2000; 9: 146-151.

[68] Bibinov NK, Fateev AA, Wiesemann K. Variations of the gas temperature in He/N_2 barrier discharges. *Plasma Sources Sci Technol* 2001; 10: 579-588.

[69] Loeb LB, *Science* 1965; 148: 1417.

[70] Meek JM, Craggs JD. Electrical breakdown of gases. *Oxford*, 1953.

[71] Raether H. Electron avalanches and breakdown in gases. *Butterworths*, 1964.

[72] Uman MA. Lightning. *McGraw*, 1969.

[73] Loizanskii ED, Firsov OB. Spark Theory [in Russian]. *Atomizdat*, 1975.

[74] Aleksandrov NL, Bazelyan EM. Ionization processes in spark discharge plasmas. *Plasma Sources Sci Technol* 1999; 8: 285–294.

[75] Sieck LW, Herron JT, Green DS. Chemical kinetics database and predictive schemes for humid air plasma chemistry. Part I: Positive ion-molecule reactions. *Plasma Chem Plasma Process* 2000; 20: 235-357.

[76] Ketkar SN, Dulak JG, Dheandhanoo S, Fite WL. Benzene charge-exchange at atmospheric-pressure for low-level detection of pollutants in ambient air. *Anal Chim Acta* 1991; 245: 267-270.

[78] Elvers B, Hawkins S, Schulz G. Ullmann's Encyclopedia of Industrial Chemistry, 5^{th} Ed., *Wiley-VCH* 1991; A18: 349-357.

[79] Boelter KJ, Davidson JH. Ozone generation by indoor, electrostatic air cleaners. *Aero Sci Technol* 1997; 27(6): 689-708.

[80] Mason NJ, Skalny JD, Hadj-Ziane S. Experimental investigations and modelling studies of ozone producing corona discharges. *Czech J Phys* 2002; 52: 85-94.

[81] Seinfeld JH, Pandis SN. Atmospheric Chemistry and Physics. From Air Pollution to Climate Change. *John Wiley & sons, Inc*. 1998.

[82] Kudryashov SV, Shchegoleva GS, Sirotkina EE, Ryabov AYu. Oxidation of hydrocarbons in a barrier discharge reactor. *High Energ Chem* 2000; 34: 112-115.

[83] Glaze WH. Drinking-water treatment with ozone. *Environ Sci Technol* 1987; 21: 224-230.

[84] Sano N, Kawashima T, Fujikawa J, Fujimoto T, Kitai T, Kanki T, Toyoda A. Decomposition of organic compounds in water by direct contact of gas corona discharge: influence of discharge conditions. *Ind Eng Chem Res* 2002; 41: 5906-5911.

[85] Sano N, Fujimoto T, Kawashima T, Yamamoto D, Kanki T, Toyoda A. Influence of dissolved inorganic additives on decomposition of phenol and acetic acid in water by direct contact of gas corona discharge. *Sep Purif Technol* 2004; 37: 169-175.

[86] Sharma AK, Josephson GB, Camaioni DM, Goheen SC. Destruction of pentachlorophenol using glow discharge plasma process. *Environ Sci Technol* 2000; 34: 2267-2272.

[87] Brisset JL. Air corona removal of phenols. *J Appl Electrochem* 1997; 27: 179-183.

[88] Hoeben WFLM, van Veldhuizen EM, Rutgers WR, Kroesen GMW. Gas phase corona discharges for oxidation of phenol in an aqueous solution. *J Phys D: Appl Phys* 1999; 32: L133-L137.

[89] Hoeben WFLM, van Veldhuizen EM, Rutgers WR, Cramers CAMG, Kroesen GMW. The degradation of aqueous phenol solutions by pulsed positive corona discharges. *Plasma Sources Sci Technol* 2000; 9: 361-369.

[90] Grabowski LR, van Veldhuizen EM, Rutgers WRJ. Removal of phenol from water: A comparison of energization methods. *Adv Oxid Technol* 2005; 8: 142-149.

[91] Grabowski LR, van Veldhuizen EM, Pemen AJM, Rutgers WR. Corona above water Reactor for systematic study of aqueous phenol degradation plasma. *Chem Plasma Process* 2006; 26: 3-17.

[92] Sato M, Tokutake T, Ohshima T, Sugiarto AT. Aqueous phenol decomposition by pulsed discharges on the water surface. *IEEE Trans Ind Appl* 2008; 44(5): 1397-1402.

[93] Forni L, Bahnemann D, Hart EJJ. Mechanism of the hydroxide ion initiated decomposition of ozone in aqueous solution. *Phys Chem* 1982; 86: 255-259.

[94] Flyunt R, Leitzke A, Mark G, Mvula E, Reisz EJ. Determination of $^{\bullet}OH$, $O_2^{\bullet-}$, and hydroperoxide yields in ozone reactions in aqueous solution. *Phys Chem B* 2003; 107: 7242-7253.

[95] Locke BR, Sato M, Sunka P, Hoffmann MR, Chang JS. Electrohydraulic discharge and nonthermal plasma for water treatment. *Ind Eng Chem Res* 2006; 45: 882-905.

[96] Sato M, Ohgiyama T, Clements JS. Formation of chemical species and their effects on microorganisms using a pulsed high-voltage discharge in water. *IEEE Trans Ind Appl* 1996; 32: 106-112.

[97] Sunka P, Babicky V, Clupek M, Lukes P, Simek M, Schmidt J, Cernak M. Generation of chemically active species by electrical discharges in water. *Plasma Sources Sci Technol* 1999; 8(2): 258-265.

[98] Sun B, Sato M, Clements JS. Use of a pulsed high-voltage discharge for removal of organic compounds in aqueous solution. *J Phys D: Appl Phys* 1999; 32(15): 1908-1915.

[99] Sun B, Sato M, Clements JS. Oxidative processes occurring when pulsed high voltage discharges degrade phenol in aqueous solution. *Environ Sci Technol* 2000; 34(3): 509-513.

[100] Malik MA, Ghaffar A, Malik SA. Water purification by electrical discharges. *Plasma Sources Sci Technol* 2001; 10(1): 82-91.

[101] Sunka P, Babicky V, Clupek M, Fuciman M, Lukes P, Simek M, Benes J, Locke B, Majcherova Z. Potential applications of pulse electrical discharges in water. *Acta Physica Slovaka*, 2004; 54: 135-145.

[102] Sahni M, Locke BR. The effects of reaction conditions on liquid-phase hydroxyl radical production in gas-liquid pulsed-electrical-discharge reactors. *Plasma Process Polym* 2006; 3: 668-681.

[103] Lukes P, Appleton AT, Locke BR. Hydrogen peroxide and ozone formation in hybrid gas-liquid electrical discharge reactors. *IEEE Trans Ind Appl* 2004; 40(1): 60-67.

[104] Grymonpré DR, Finney WC, Clark RJ, Locke BR. Hybrid gas-liquid electrical discharge reactors for organic compound degradation. *Ind Eng Chem Res* 2004; 43: 1975-1989.

[105] Lang PS, Ching WK, Willberg DM, Hoffmann MR. Oxidative degradation of 2,4,6-trinitrotoluene by ozone in an electrohydraulic discharge reactor. *Environ Sci Technol* 1998; 32(20): 3142-3148.

[106] Marotta E, Schiorlin M, Ren X, Rea M, Paradisi C. Advanced oxidation process for degradation of aqueous phenol in a dielectric barrier discharge reactor. *Plasma Process Polym* 2011; 8: 867–875.

[107] Marotta E, Ceriani E, Schiorlin M, Ceretta C, Paradisi C. Comparison of the rates of phenol advanced oxidation in deionized and tap water within a dielectric barrier discharge reactor. *Wat Res* 2012; 46: 6239–6246.

[108] Lukes P, Locke BR. Plasmachemical oxidation processes in a hybrid gas-liquid electrical discharge reactor. *J Phys D: Appl Phys* 2005; 38(22): 4074-4081.

[109] Lukes P, Clupek M, Sunka P, Peterka F, Sano T, Negishi N, Matsuzawa S, Takeuchi K. Degradation of phenol by underwater pulsed corona discharge in combination with TiO_2 photocatalysis. *Res Chem Intermed* 2005; 31: 285-294.

[110] Sahni M, Finney WC, Locke BR. J. Degradation of aqueous phase polychlorinated biphenyls (PCB) using pulsed corona discharges. *Adv Oxid Technol* 2005; 8(1): 105-111.

[111] Brisset, J.L. J. Removal of pentachlorophenol from water by AC corona discharge treatment in air. *Trace Microprobe Tech* 1998; 16(3): 363-370.

[112] Mvula E, von Sonntag C. Ozonolysis of phenols in aqueous solution. *Org Biomol Chem* 2003; 1: 1749-1756.

[113] Zazo JA, Casas JA, Mohedano AF, Gilarranz MA, Rodriaguez J. Chemical pathway and kinetics of phenol oxidation by Fenton's reagent. *Environ Sci Technol* 2005; 39: 9295-9302.

[114] Bader H, Hoigné J. Rate constants of reactions of ozone with organic and inorganic compounds in water—II: Dissociating organic compounds. *Water Res* 1983; 17(2): 185-194.

[115] Buxton GV, Greenstock CL, Helman WP, Ross AB. Critical-review of rate constants for reactions of hydrated electrons, hydrogen-atoms and hydroxyl radicals ($^{\bullet}$OH/$^{\bullet}$O-) in aqueous solution. *J Phys Chem Ref Data* 1988; 17: 513-886.

[116] Jorgensen P, Chapelle J, Czemichowski A, Meguemes K. *ISPC8*, Tokyo, p. 695 (1987).

[117] Lesueur H, Czernichowski A, Chapelle J. Production of synthetic ($CO+H_2$) gas from CH_4 oxidation by CO_2 in a gliding-discharge electroreactor. *Journal de Physique* 1990; 51: C549-C556.

[118] Lesueur H, Czernichowski A, Chapelle J. Electrically assisted partial oxidation of methane. *Int J Hydrogen Energy* 1994; 19(2): 139–144.

[119] Fridman A, Nester S, Kennedy LA, Saveliev A, Mutaf-Yardimci O. Gliding arc gas discharge. *Prog Energy Combust Sci* 1998; 25(2): 113-124.

[120] Li MW, Xu GH, Tian YL, Chen L, Fu HF. Carbon dioxide reforming of methane using DC corona discharge plasma reaction. *J Phys Chem* 2004, 108(10): 1687-1693.

[121] Li MW, Tian YL, Xu GH. Characteristics of carbon dioxide reforming of methane via alternating current (AC) corona plasma reactions. *Energy Fuels* 2007; 21(4): 2335-2339.

[122] Zhou LM, Xue B, Kogelschatz U, Eliasson B. Nonequilibrium plasma reforming of greenhouse gases to synthesis gas. *Energy Fuels* 1998; 12(6): 1191-1199.

[123] Song HK, Lee H, Choi JW, Na BK. Effect of electrical pulse forms on the CO_2 reforming of methane using atmospheric dielectric barrier discharge. *Plasma Chem Plasma Process* 2004; 24(1): 57-72.

[124] Goujard V, Tatibouët JM, Batiot-Dupeyrat C. Carbon dioxide reforming of methane using a dielectric barrier discharge reactor: effect of helium dilution and kinetic model. *Plasma Chem Plasma Process* 2011; 31: 315-325.

[125] Rueangjitt N, Sreethawong T, Chavadej S. Reforming of CO_2-containing natural gas using an AC gliding arc system: effects of operational parameters and oxygen addition in feed. *Plasma Chem Plasma Process* 2008; 28: 49–67.

[126] Tao X, Bai M, Li X, Long H, Shang S, Yin Y, Dai X. CH_4-CO_2 reforming by plasma – challenges and opportunities. *Prog Energy Combust Sci* 2011; 37: 113-124.

[127] Zhou LM, Xue B, Kogelschatz U, Eliasson B. Nonequilibrium plasma reforming of greenhouse gases to synthesis gas. *Energy Fuels* 1998; 12: 1191-1199.

[128] Gorbanzadeh AM, Modarresi H. Carbon dioxide reforming of methane by pulsed glow discharge at atmospheric pressure: the effect of pulse compression. *J Appl Phys* 2007; 101: 123303.

[129] Yang Y. Methane conversion and reforming by nonthermal plasma on pins. *Ind Eng Chem Res* 2002; 41(24): 5918-5926.

[130] Zhang Y, Li Y, Wang Y, Liu C, Eliasson B. Plasma methane conversion in the presence of carbon dioxide using dielectric-barrier discharge. *Fuel Process Technol* 2003; 83: 101-109.

[131] Bo Z, Yan J, Li X, Chi Y, Cen K. Plasma assisted dry methane reforming using gliding arc gas discharge: effect of feed gases proportion. *Int J Hydrogen Energy* 2009; 33(20): 5545-5553.

[132] Indarto A, Choi JW, Lee H, Song HK. Effect of additive gases on methane conversion using gliding ac discharge. *Energy* 2006; 31(14): 2986-2995

[133] Ghorbanzadeh AM, Lotfalipour R, Rezaei S. Carbon dioxide reforming of methane at near room temperature in low energy pulsed plasma. *Int J Hydrogen Energy* 2009; 34:293-298.

[134] Yan BH, Wang Q, Jin Y, Cheng Y. Dry reforming of methane with carbon dioxide using pulsed DC arc plasma at atmospheric pressure. *Plasma Chem Plasma Process* 2010; 30:257-266.

[135] Hong SW, Oh SM, Park DW, Kim GJ. The methane reforming with carbon dioxide on Ni-catalyst activated by a DC-pulsed corona discharge. *J Ind Eng Chem* 2001; 7(6): 410-416.

[136] Kado S, Urasaki K, Sekine Y, Fujimoto K. Low temperature reforming of methane to synthesis gas with direct current pulse discharge method. *Chem Commun* 2001; 415-416.

[137] Kraus M, Eliasson B, Kogelschatz U, Wokaun A. CO_2 reforming of methane by the combination of dielectric-barrier discharges and catalysis. *Phys Chem Chem Phys* 2001; 3(3): 294-300.

[138] Kraus M, Egli W, Haffner K, Eliasson B, Kogelschatz U, Wokaun A. Investigation of mechanistic aspects of the catalytic CO_2 reforming of methane in a dielectric-barrier discharge using optical emission spectroscopy and kinetic modeling. *Phys Chem Chem Phys* 2002; 4(4): 668-675.

[139] Song HK, Choi JW, Yue SH, Lee H, Na BK. Synthesis gas production via dielectric barrier discharge over Ni/gamma-Al_2O_3 catalyst. *Catal Today* 2004; 89: 27-33.

[140] Chavadej S, Supat K, Lobban LL, Mallinson RG. Partial oxidation of methane and carbon dioxide reforming with methane in corona discharge with/without Pt/KL catalyst. *J Chem Eng Jpn* 2005; 38(3): 163-170

[141] Li MW, Liu CP, Tian YL, Xu GH, Zhang FC, Wang YQ. Effects of catalysts in carbon dioxide reforming of methane via corona plasma reactions. *Energy Fuels* 2006; 20(3): 1033-1038.

[142] Futamura S, Kabashima H, Annadurai G. Roles of CO_2 and H_2O as oxidants in the plasma reforming of aliphatic hydrocarbons. *Catal Today* 2006; 115: 211-216.

[143] Lee H, Song HK, Min BR. Heating effect of plasma catalytic reaction on the CH_4 reforming of CO_2 over Ni/gamma-Al2O3 catalyst in dielectric barrier discharge reactor *Chem Lett* 2006; 35(6): 646-647.

[144] Long H, Shang SY, Tao XM, Yin YP, Dai XY. CO_2 reforming of CH_4 by combination of cold plasma jet and Ni/gamma-Al2O3 catalyst. *Int J Hydrogen Energy* 2008; 33: 5510-5515.

[145] Wang Q, Yan BH, Jin Y, Cheng Y. Dry reforming of methane in a dielectric barrier discharge reactor with Ni/Al_2O_3 catalyst: interaction of catalyst and plasma. *Energy Fuels* 2009; 23(8): 4196-4201.

[146] Goujard V, Tatibouët JM, Batiot-Dupeyrat C. Influence of the plasma power supply nature on the plasma-catalyst synergism for the carbon dioxide reforming of methane. *IEEE Trans Plasma Sci* 2009; 37(12): 2342-2346.

[147] Goujard V, Tatibouët JM, Batiot-Dupeyrat C. Use of a non-thermal plasma for the production of synthesis gas from biogas. *Appl Cat A: Gen* 2009; 353(2): 228-235.

[148] Gallon HJ, Tu X, Whitehead JC. Effects of reactor packing materials on H_2 production by CO_2 reforming of CH4 in a dielectric barrier discharge. *Plasma Process Polym* 2012; 9: 90-97.

[149] Tu X, Gallon HJ, Twigg MV, Gorry PA, Whitehead JC. Dry reforming of methane over a Ni/Al_2O_3 catalyst in a coaxial dielectric barrier discharge reactor. *J Phys D: Appl Phys* 2011; 44: 274007.

[150] Tu X, Whitehead JC. Plasma-catalytic dry reforming of methane in an atmospheric dielectric barrier discharge: understanding the synergistic effect at low temperature. *Appl Catal B: Environ* 2012; 125: 439-448.

[151] Kim HH. Nonthermal plasma processing for air-pollution control: a historical review, current issues, and future prospects. *Plasma Processes Polym* 2004; 1: 91-110.

[152] Schiorlin M, Marotta E, Rea M, Paradisi C. Comparison of toluene removal in air at atmospheric conditions by different corona discharges. *Environ Sci Technol* 200943: 9386–9392.

[153] Slater C, Douglas-Hamilton DH. Electron-beam-initiated destruction of low concentrations of vinyl chloride in carrier gases. *J Appl Phys* 1981; 52(9): 5820-5828.

[154] Marotta E, Schiorlin M, Rea M, Paradisi C. Products and mechanisms of the oxidation of organic compounds in atmospheric air plasmas. *J Phys D - Appl Phys* 2010; 43: 124011.

[155] Hansch C, Leo A, Taft RW. A survey of Hammett substituent constants and resonance and field parameters. *Chem Rev* 1991; 91: 165-195.

[156] Anbar M, Meyerstein D, Neta P. The reactivity of aromatic compounds toward hydroxyl radicals. *J Phys Chem* 1966; 70: 2660.

[157] Hoigné J, Bader H. Rate constants of reactions of ozone with organic and inorganic compounds in water. I. Non-dissociating organic compounds. *Water Res* 1983; 17: 173-183.

[158] von Gunten, U. Ozonation of drinking water: Part I. Oxidation kinetics and product formation. *Wat Res* 2003; 37(7): 1443-1467.

[159] Baker J, Arey J, Atkinson R. J Rate constants for the gas-phase reactions of OH radicals with a series of hydroxyaldehydes at 296 +/- 2 K. *Phys Chem A* 2004; 108(34): 7032-7037.

[160] Sotelo JL, Beltrán FJ, Benitez JF, Beltrán-Heredia J. Ozone decomposition in water: Kinetic study. *Ind Eng Chem Res* 1987; 26: 39-43.

[161] Von Gunten U. The basics of oxidants in water treatment. Part B: ozone reactions. *Water Sci Technol* 2007; 55: 25-29.

[162] Hoigné, J., Bader, H. “The role of hydroxyl radical reactions in ozonation processes in aqueous solutions”, *Wat Res* 1976; 10: 377-386.

[163] Leitzke A, von Stonnag C. Ozonolysis of unsaturated acids in aqueous solution: acrylic, metacrylic, maleic, fumaric and muconic acids. *Ozone Sci Eng* 2009; 31: 301-308.

[164] Malik M.A. Water purification by plasmas: which reactors are most energy efficient? *Plasma Chem Plasma Process* 2010; 30: 21–31.

[165] Gottschalk C, Libra JA, Saupe A. Ozonation of water and waste water. A practical guide to understanding ozone and its applications. 2nd Ed., *WILEY-VCH*, 2009; 378p.

[170] NIST Standard Reference Database – web link http://webbook.nist.gov/chemistry

[171] Zhu X, Huo P, Zhang YP, Cheng DG, Liu CG. Structure and reactivity of plasma treated Ni/Al_2O_3 catalyst for CO_2 reforming of methane. *Appl Cat B: Environ* 2008; 81: 132-140.

[172] Geiger R, Staack D. Analysis of solid products formed in atmospheric non-thermal carbon monoxide plasma. *J Phys D: Appl Phys* 2011: 44; 274005.

[173] Wang Q, Yan H, Jin Y, Cheng Y. Investigation of dry reforming of methane in a dielectric barrier discharge reactor. *Plasma Chem Plasma Process* 2009; 29: 217-228.

[174] Tu X, Whitehead JC. Plasma-catalytic dry reforming of methane in an atmospheric dielectric barrier discharge: understanding the synergistic effect at low temperature. *Appl Catal B: Environ* 2012; 125: 439-448.

[175] Pearse RWB, Gaydon AG. The identification of molecular spectra. 4th Ed. *Chapman and Hall*, London, 1962.

[176] Kiselman D. The 777 nm triplet oxygen in the sun and solar type stars. *Astron Astrophys* 1993; 275: 269-282.

[177] Konjevic, N. Plasma broadening and shifting of non-hydrogenic spectral lines; Present status and applications. *Phys Reports* 1999; 316(6): 339-401.

[178] Tao X, Qi F, Yin Y, Dai X. CO_2 reforming of CH_4 by combination of thermal plasma and catalyst. *Int J Hydrogen Energy* 2008; 33: 1262-1265.

ABBREVIATIONS

AC – Alternating Current

AOP – Advance Oxidation Processes

APGD – Atmospheric pressure Glow Discharge

CCD –Charge Coupled Device

CCS – Carbon Capture and Storage

DAD – Diode Array Detector

DBD – Dielectric Barrier Discharge

DC – Direct Current

FID – Flame Ionization Detector

FT-IR – Furrier Transform Infrared Spectroscopy

GC – Gas Chromatography

HPLC – High Performance Liquid Chromatography

HV – High Voltage

LTE – Local Thermodynamic Equilibrium.

MDR – Methane Dry Reforming

MFC – Mass Flow Controller

MFM – Mass Flow Meter

MPO – Methane Partial Oxidation

MS – Mass Spectrometry

MSD – Mass Spectrometer Detector

MSR – Steam Methane Reforming

NDIR – NonDispersive InfraRed (sensor)

NTP – Non Thermal Plasma

OES – Optical Emission Spectroscopy

PLOT - Porous Layer Open Tubular (column)

TCD – Thermal Conductivity Detector

TIC – Total Ion Current

TOC – Total Organic Carbon

UV-Vis – Ultraviolet-Visible range

ACKNOWLEDGEMENTS

At the end of this dissertation I would like sincerely acknowledge everybody who directly or not contributed on successful completion of this work.

I take this opportunity to express my profound gratitude and deep regards to my supervisor Dr. Ester Marotta for her exemplary guidance, monitoring and constant encouragement throughout the course of this Thesis.

I also would like to express the deep sense of gratitude to Prof. Cristina Paradisi for her cordial support, valuable information and guidance, which helped me in completing this task through various stages.

I would like to acknowledge the staff members of University of Padova Chemistry department and especially to my colleagues from laboratory, for the valuable information provided by them in their respective fields. I'm grateful for their cooperation during the period of my assignment and I strongly appreciate their valuable remarks and advices during my stay in the Department. I would like to acknowledge Dr. Erica Gazza, Dr Marco Scapinello, Elisa Ceriani, Dr. Milko Schiorlin, Eng. Claudio Ceretta, Prof Massimo Rea and also the members of technical services in the Department of Chemical Sciences: Mr. Stefano Mercanzin, Mr. Roberto Inilli, Mr. Vicenzo Afelbo, Mr Gianni Marin and Mr. Mauro Meneghetti for various technical supports.

I would like to express my sincere thanks to Prof. Valeriy Chernyak, Kiev National University, and Prof. Jerzy Mizeraczyk, Polish Academy of Sciences, for offering me their knowledge and qualifications and leading me working on diverse exciting projects in plasma chemistry.

My deepest thanks also to Dr. Illya Kulyk from Veneto Nanotech for the discussions on engineering aspects and technological applications of plasma chemical processes.

My sincere gratitude to Prof. Igor Anisimov, Kyiv National University, for exciting lectures on plasma physics and synergetics and all the lecturers of Radiophysical Department who gave me the excellent basis on fundamental and applied physics.

Also I would like to acknowledge the Cariparo Foundation for the doctoral fellowship.

Last but not the least, I thank almightily my parents, sister and friends for their constant encouragement and moral support.

Errata corrige of the Thesis titled “Atmospheric plasma processes for environmental applications”

Ph.D. student **Volodymyr Shapoval**

Page number	**Place**	**Written**	**Have to be**
2	Line 1	INDUCED BY AIR ATMOSPHERIPLASMA	INDUCED BY AIR ATMOSPHERIC PLASMA
81	Line 4 from the bottom	Fig. 3.2.8	Fig. 3.2.7
84	Figure number in the caption	Fig. 3.2.9.	Fig. 3.2.8.
110	Line 10 from the bottom	yielding a □ value of -0.48	yielding a ρ value of -0.48
151	Caption of Fig. 4.2.16	H_α and H_β emission lines of oxygen triplet acquired in pure CO_2 (black) and in 1:1 mixture of CO_2 and CH_4 (blue).	H_α and H_β emission lines in 1:1 mixture of CO_2 and CH_4 (blue) and spectra in pure CO_2 (black).